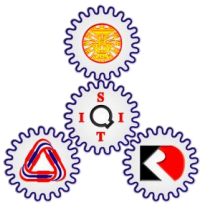

PREDICTION OF CRACKING IN MASS CONCRETE DUE TO HEAT OF HYDRATION AND SHRINKAGE

BY

JIRANUWAT BANJONGRAT

A THESIS SUBMITTED IN PARTIAL FULFILLMENT OF
THE REQUIREMENTS FOR THE DEGREE OF
MASTER OF SCIENCE (ENGINEERING)
SIRINDHORN INTERNATIONAL INSTITUTE OF TECHNOLOGY
THAMMASAT UNIVERSITY
ACADEMIC YEAR 2014

PREDICTION OF CRACKING IN MASS CONCRETE DUE TO HEAT OF HYDRATION AND SHRINKAGE

BY

JIRANUWAT BANJONGRAT

A THESIS SUBMITTED IN PARTIAL FULFILLMENT OF
THE REQUIREMENTS FOR THE DEGREE OF
MASTER OF SCIENCE (ENGINEERING)
SIRINDHORN INTERNATIONAL INSTITUTE OF TECHNOLOGY
THAMMASAT UNIVERSITY
ACADEMIC YEAR 2014

PREDICTION OF CRACKING IN MASS CONCRETE DUE TO HEAT OF HYDRATION AND SHRINKAGE

A Thesis Presented

By

JIRANUWAT BANJONGRAT

Submitted to

Sirindhorn International Institute of Technology

Thammasat University

In partial fulfillment of the requirements for the degree of

MASTER OF SCIENCE (ENGINEERING)

Approved as to style and content by

Advisor and Chairperson of
Thesis Committee _____
(Asst. Prof. Dr. Warangkana Saengsoy, Ph.D.)

Co-Advisor _____
(Prof. Dr. Somnuk Tangtermsirikul, D. Eng.)

Committee Member _____
(Assoc. Prof. Acting Major Dr. Ittiporn Sirisawat, Ph.D.)

Committee Member and Chairperson
of Examination Committee _____
(Assoc. Prof. Dr. Winyu Rattanapitikon, Ph.D.)

August 2015

Acknowledgements

First of all, the author would like to sincerely thank his advisor, Dr.Warangkana Saengsoy, for her guidance and continuous support. Her extensive advices have been very helpful for his thesis.

The author also wish to express his deepest acknowledgment to his co-advisor, Prof. Dr. Somnuk Tangtermsirikul, for his enthusiastic guidance, valuable advices, constructive suggestions and persistent supervision both direct and indirect ways. This thesis would not be achieved without his untiring advice and encouragement. The author is also truly grateful to Prof. Dr. Somnuk Tangtermsirikul for offering scholarship and providing him the opportunity to study at Sirindhorn International Institute of Technology.

The author would like to express his recognition to his former-advisor, Dr. Pongsak Choktaweekarn, who directly guides his study with kind discussion and suggestion which lead the author to see various aspects of his study.

The author gratefully thanks Assoc. Prof. Dr. Winyu Rattanapitikon, chairperson of examination committee, and Assoc. Prof. Acting Major Dr. Ittiporn Sirisawat, a thesis committee, for his constructive comments and advices which are valuable contributions to his academic progress.

The author also gives deepest appreciation to Sirindhorn International Institute of Technology and Construction and Maintenance Technology Research Center (CONTEC) for granting fully-funded scholarship to his study at Sirindhorn International Institute of Technology, Thammasat University.

His sincere thanks are also extended to Dr.Raktipong Sahamitmongkol, Dr.Krittiya Kaewmanee, Dr.Sontaya Tongaroonsri, Dr.Parnthep Julnipitawong, Ms.Pattanun Manachitrungrueng, Ms.Narumol Weerayangkul, Mrs.Aroonkamol Samanchuen as well as many students and staff in the School of Civil Engineering and Technology, SIIT, who kindly helps and support him during his study.

Finally, the author devotes this thesis to his beloved parents. He would like to express his gratitude to them for their continuous spiritual support and encouragement.

Abstract

PREDICTION OF CRACKING IN MASS CONCRETE DUE TO HEAT OF HYDRATION AND SHRINKAGE

by

JIRANUWAT BANJONGRAT

Bachelor of Engineering, Sirindhorn International Institute of Technology, 2009

The aim of this study is to simulate restrained strain of mass concrete at early age due to combined thermal effect and shrinkages. Firstly, restrained strain caused by differential thermal expansion as well as restrained strains caused by shrinkages are separately computed. Thermal properties such as specific heat, thermal conductivity and thermal expansion coefficient of concrete are estimated by the mathematical models developed by CONTEC. The previously proposed adiabatic temperature rise model is used to calculate heat of hydration. Heat of hydration obtained from the modified adiabatic temperature rise model and thermal properties derived from the proposed models are used as the input in a commercialized three-dimensional finite element program to calculate semi-adiabatic temperature and restrained strain.

The restrained strains caused by shrinkages are computed based on an existing mathematical models for estimating free shrinkages. Both autogenous and drying shrinkages are considered. The total restrained strain is subsequently computed by the supercomposition concept. From the analytical result which considered thermal expansion and autogenous shrinkage effect, it is found that autogenous shrinkage reduces the thermal cracking risk at early age during the insulation curing period. From the analytical result which considered thermal expansion and total shrinkage effect, drying shrinkage increases the risk of cracking on the exposed surface while after removal of insulation curing material.

Keywords: Mass concrete, Thermal cracking, Autogenous Shrinkage, Drying shrinkage, Self-restraint, Restrained strain

Table of Contents

List of Figures

List of Tables

Chapter 1

Introduction

1.1 General

Concrete is a one of the main construction materials that most widely used. The benefits of concrete are such as it is easily formed into shape, composed of common raw materials such as cement, aggregate and water, etc., low price and easily produced. Since concrete is man-made material, the design practice generally considers strength requirement. Not many engineers consider durability of concrete, which may result in premature deterioration. Unless durability is considered, concrete structures can't have a long service life leading to high cost of maintenance. It is not difficult to take care many small concrete members in a building such as columns, beams, slabs and walls, etc. While the damage of some concrete members such as piles and footings is a serious problem to solve. Footing is a very important and large member in a building. Any large volume of cast-in-place concrete with large dimension is called mass concrete.

In massive concrete structures, the temperature rise due to heat of hydration at the interior concrete is greater than the exterior portion. Excessive temperature gradients can induce thermal cracking especially at early age. Cracking of any massive concrete structure reduces load carrying capacity and service life of the structure. To avoid cracking due to heat of hydration, one approach is to control the hydration heat of concrete by reducing cement content. Fly ash is one of the pozzolanic materials which can be effectively used as a cement replacing material to reduce hydration heat of concrete.

Thermal cracking is not the only cause of cracking in mass concrete. In general, mass concrete encounters both stresses due to thermal effect and shrinkages. Shrinkage is also another cause of cracking. Then, the effect of shrinkage should be included in the cracking analysis of mass concrete. Total shrinkage of concrete is mainly composed of autogenous and drying shrinkages. Autogenous shrinkage occurs at early age during the progress of hydration reaction. Drying shrinkage is the volume change due to loss of water from the concrete to the surrounding environment. Shrinkage cracking can take place at either early or later ages. If shrinkage of concrete takes place without any restraint, concrete will not crack. Unfortunately, concrete structures are always subjected to some degrees of restraint. The compatibility between shrinkage and restraint induces restrained strain. When this restrained strain reaches the tensile strain capacity of the concrete, the concrete cracks. Development of a computerized program for predicting cracking of mass concrete is beneficial to design mix proportion and construction process. Many researchers proposed methods for predicting thermal cracking in mass concrete, however, the effect of shrinkage was rarely considered in their methods.

From this reason, this study incorporates the effect of autogenous and drying shrinkages, with the use of established free autogenous and drying shrinkage prediction models into the thermal cracking analysis to demonstrate their effects and to make the analysis more close to real. It is noted here that this study covers only the case of internally restrained thermal stress.

1.2 Statement of Problems

Nowadays, the effect of shrinkage is rarely included in the analysis of thermal cracking in mass concrete. As a result, the prediction of thermal cracking is not close to real. There are few studies that simulates cracking of mass concrete by combining thermal effect and shrinkage together.

Choktaweekarn and Tangtermsirikul (2008) proposed an analytical method to predict semi-adiabatic temperature rise and thermal crack in mass concrete. Even though this model can predict the occurrence of thermal crack, however, it is not realistic. This is because the effect of shrinkage was not considered in the analysis. From this reason, the effect of shrinkage should be included in the analysis. Figure 1.1 shows examples of thermal cracking.

(a) (b)

Figure 1.1 Cracking in mass concrete due to thermal stress

1.3 Objectives

The objective of this study is to propose and extend the analytical method of the research group of the author to be useful for the design to prevent cracking that occurs in massive concrete structures by modifying the existing method to predict thermal cracking in mass concrete. Effects of autogenous shrinkage and drying shrinkage are included into the analytical method which was proposed by Choktaweekarn in order to improve the prediction of cracking of mass concrete to be more realistic. The developed method will be useful for engineers to select the suitable mix proportion, percentage replacement of fly ash, dimension of casting volume, construction process and curing process for preventing cracking in mass concrete structures due to combined thermal and shrinkage effects.

1.4 Scope of Study

The scope of this study is focused on the self-restraint problem in mass concrete. The effect of creep and relaxation are still not included in the analysis. The computerized program is mainly developed by considering material properties especially cement and fly ash produced in Thailand. Only autogenous and drying shrinkages are considered.

Chapter 2

Theoretical Background and Literature Reviews

2.1 Thermal Cracking in Mass Concrete

Thermal cracking is one of the important problems for pouring massive concrete structures (Tangtermsirikul). In massive concrete structures such as dams and mat foundations, temperature gradients take place inside the concrete due to heat of hydration. The accumulated hydration heat with temperature gradient can induce cracks especially at early age of the concrete. The problems arise from the difference between the high temperature of the inner part of the concrete and the lower temperature near the surface of the mass concrete, causing self-restraining stress between the higher and the lower temperature portions of the concrete and then cracks can be generated. Cracks are formed at the early age state because heat is mostly generated and accumulated in the mass concrete causing maximum temperature at the early age state.

Thermal cracking reduces quality and durability of the concrete and affects serviceability of concrete structures in long term. Therefore, it is necessary to prevent the thermal cracking to ensure that the concrete structures can achieve their design service life.

2.1.1 Mechanisms of Thermal Cracking due to Self-restraint

The reactions between compounds in mass cement and water, or called hydration reactions, are exothermic reactions. The reactions generate heat and the rate of heat generation is rapid at a few hours after mixing the water with cement until a few days. As concrete has low thermal conductivity especially at the early ages, the generated heat slowly transfers to the outside environment and then accumulates in the concrete causing high temperature inside the mass concrete.

Usually concrete members having thin sections or small sizes are not subjective to temperature cracking because the heat can easily evacuate from the members, therefore temperature rise inside the members is usually not critical. On the other hand, in massive concrete, the generated heat can hardly evacuate out of the concrete. This makes the temperature inside the mass concrete, especially at the center, higher than the temperature at the surfaces that are exposed to the outside environment. Temperature gradient is then produced in the mass concrete. The temperature gradient will be more serious when rate of concrete placing is faster, the concrete section is larger and thicker, wind is stronger and relative humidity is lower. The temperature difference in the mass concrete will create differential volume change which results in self-equilibrating stresses within the mass concrete. The surface of concrete, which are lower in temperature, will be under tensile stress

whereas smaller tension and compression arise toward the inner part. If the developed tensile stress due to the self-restraint becomes higher than the tensile strength of the concrete, cracks will develop at the location of the highest temperature ingredient which is usually on or near the exposed surfaces. The self-restraint cracking usually happens in the mass concrete during the temperature-rising period. Figure 2.1 shows the mechanisms of thermal cracking.

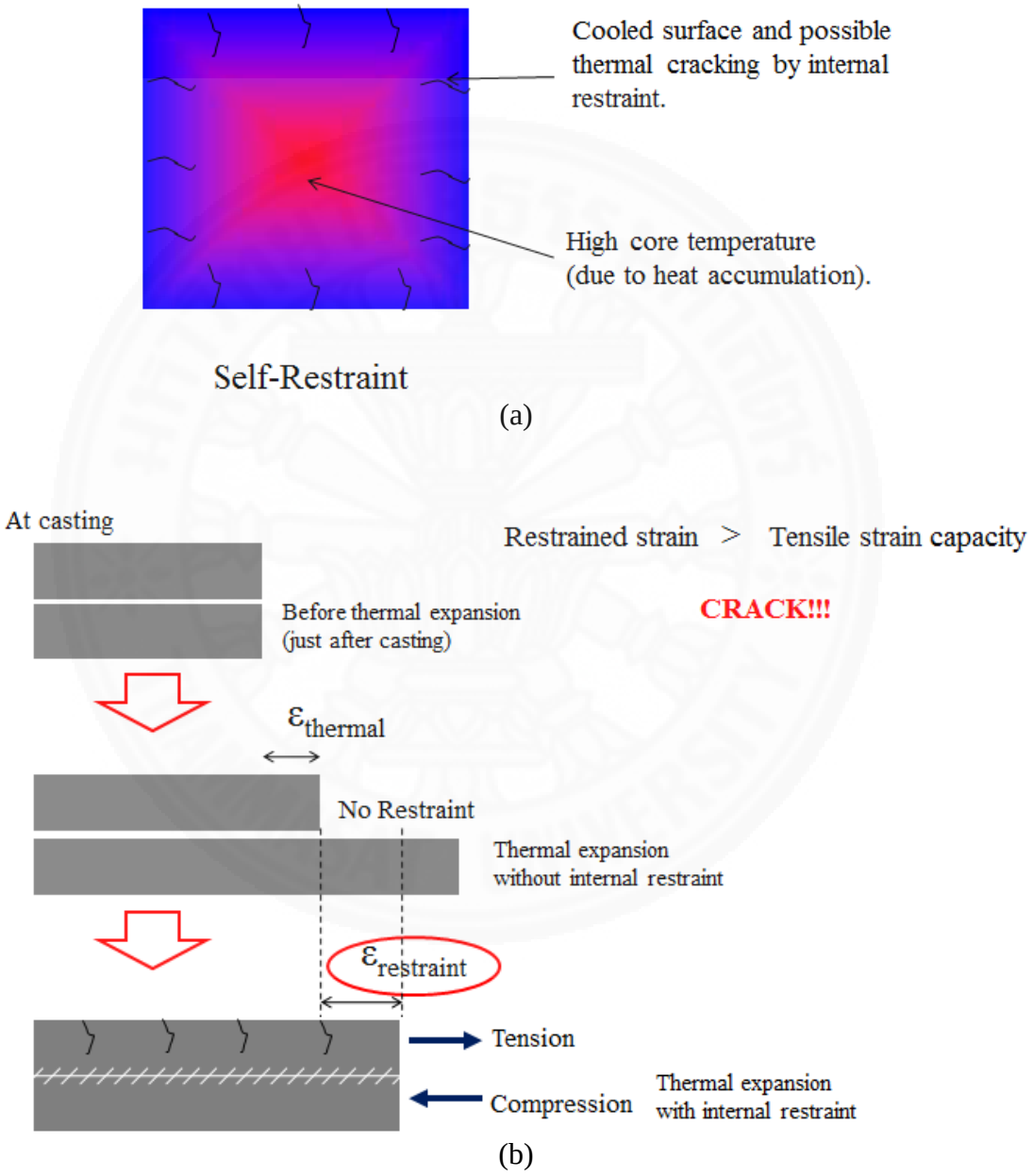

Figure 2.1 Mechanisms of thermal cracking

2.1.2 Preventions of thermal cracking

The prevention of the occurrence of thermal cracking can be practiced by one or more of the following means.

1) By mean of mix proportioning of concrete. The concept is to proportion the concrete to minimize the heat of hydration of the concrete mixture. In other words, it is to use a low-heat concrete. This method is considered cost effective but may have limitation if the mass concrete required high strength. In such case, combination of many methods may be used. Low-heat concrete can be produced by various methods as follows.

a) Minimizing the cement content such as to use chemical admixtures to improve workability or to optimize aggregate gradation or to use large maximum aggregate size, etc.

b) Using medium-heat cement (Type 2) or low-heat cement (Type 4).

c) Using cement-replacing materials like fly ash, limestone powder, etc.

2) By mean of construction methods. Some methods are aimed to reduce the initial temperature of the concrete whereas some are to maintain uniform temperature in the mass concrete. Some of the familiar methods are listed below.

a) By using insulators to control the evacuation of heat to the environment. Insulators are used to cover all surfaces of the concrete in order to make the concrete temperature uniform throughout the mass concrete. This method has limitation since excessively high temperature in the concrete may bring problems to the concrete.

b) Pipe-cooling method. The method involves the preparation of water cooling-pipes in the placing area before placing the concrete. Heat is then evacuated from mass concrete through the cooling water. After being used to cool the concrete, the cooling water then becomes hot. A part of hot water, after being used to cool the concrete, is utilized as curing water to maintain high temperature of the concrete surfaces to obtain uniform temperature throughout mass concrete

c) By dividing the placement into multi-layers or multi-sections. This method is time-consuming and produces construction joints within mass concrete.

d) By reducing temperature of the fresh concrete. Temperature of the fresh concrete can be reduced by many methods. For examples, the temperature of raw materials can be controlled by keeping the raw materials in the low-temperature area or by chilling the raw materials. Using liquid natural gas to freeze the surface

water of fine aggregate has been practiced. The use of ice and chilled water to mix concrete is also one of these methods. These methods may encounter some limitation on the production capacity and costs.

3) By mean of structural design. The temperature stress can be estimated and additional reinforcement can be provided to resist the temperature stress. Joints may be required in order to reduce the stress and to prevent cracking to occur in the undesirable location.

2.1.3 Literature Reviews

Koenders and Breugel (1994) defined the hydration curves in adiabatic condition. The hydration curves can be computed as a function of the cement composition and the concrete mix proportion. The adiabatic hydration curves of concrete were utilized as an input for computerizes models for calculating of the temperature distribution in hardening concrete. In their computations, the specific heat of the concrete was considered to be a function of the degree of hydration.

Wang and Dilger (1994) proposed a computerized program to predict temperature of concrete. A two-dimensional finite element thermal analysis was used to predict the transient heat transfer between the concrete and the surroundings as affected by the concrete mix, thermal properties and environmental conditions. They stated that the heat rate of cement hydration at 20°C and other temperature could be derived by the test results on adiabatic temperature rise with time dependent for the concrete mix.

Saengsoy and Tangtermsirikul (2003) proposed a computerized model to predict adiabatic temperature of mass concrete. The heat generation was computed based on the summation of the reaction of cement and the reaction of fly ash. The specific heat model considering time dependent properties was adopted for relating the heat generated in the concrete and its temperature rise to achieve more realistic temperature simulation especially during early age of mass concrete. The comparison between predicted temperature with the test results of temperature of cement only and fly ash concrete in adiabatic condition. It was found that the comparison between defined model and test result being satisfactory.

Buffo-Lacarrier et al. (2007) proposed a model to predict the hydration development and its consequences on temperature and water content. The hydration model can be applied for cement and pozzolanic materials. In this study, thermal properties of concrete were assumed to be constant. The model was tested on a 27 m^3 concrete block with temperature sensors in the core and near the exposes surface. The analytical results show good agreement with test results.

Schutter (2002) presented a model to demonstrate thermal cracking at early age due to the hydration heat. The model based on the degree of hydration reaction (for Portland cement). The cracking behavior was implemented using a smeared cracking approach with non-linear softening behavior with time dependent. With the increasing of degree of hydration, specific heat and thermal conductivity of hardening concrete decreases linearly. Properties of harden concrete such as compressive strength, tensile strength, modulus of elasticity, poisson's ratio, fracture energy and creep is intensively related with the degree of hydration. It was mentioned in this study that coefficient of thermal expansion was also developing during the hydration of concrete but by lack of test results, a constant value was used in this study. The analytical results were verified with the test results of a concrete with dimension 15 x 15 cm. This model was with a cracked armor unit concrete block. The demonstration results show good agreement with test results. A simulated concrete block with 25 hours stress was shown in Figure 2.2.

J. K. Kim et al. (2001) porposed a three-dimensional finite element program for thermal analysis of hydration heat in concrete structures with pipe cooling system. A line element was adopted for modeling of pipe. Internal flow theory was applied for computing the temperature variation of cooling water. In this study, the heat loss from cooling water was by convection process. The parameters used in this study were the convection coefficient of cooling water, the surface area of pipe, the distance between inlet and outlet, the temperatures of pipe and cooling water at inlet and outlet. The convection coefficient of cooling water (h_w) used in this study was obtained from the equations recommended by JCI. The convection coefficient of cooling water depends on the velocity of cooling water. The predicted results were verified with the test result from the spread concrete footing of the Seo-Hae Bridge in Korea. From the comparison between the predicted and test results in the spread footing with pipe cooling system, the developed three-dimensional finite element program was effectively predicted the temperature history of the footing. The verification also showed that the temperature variation of cooling water is efficiently obtained by introducing internal flow theory and line element. The developed program was able to be used in thermal analysis of hydration heat with pipe cooling system regardless of the pipe layout, the cooling water velocity and inlet temperature, and the thermal properties of concrete and cooling pipe. Figure 2.3 shows thermal analysis with pipe-cooling system.

J. Noorzaei et al. (2006) presented application and verification of a two-dimensional finite element code developed for the thermal and structural analysis of the Kinta RCC gravity dams. The parameters used in the analysis are hydration heat, foundation temperature, RCC placing temperature, ingredient temperature, solar radiation and wind speed. The temperature of Kinta RCC dam was predicted and used to calculate the tensile stress at the time t. The crack occurrence over time has been predicted by the crack index which is the ratio of tensile strength to tensile stress in order to check the dam's safety against cracking. If the RCC tensile strength is greater than the tensile stress or crack index is higher than 1 then the RCC dam is predicted to be no crack. The crack index variation can give a good indication of the probability of a crack occurring. The predicted temperature was compared with actual

monitoring temperatures recorded by thermocouples installed in the dam. The comparisons of the predicted temperatures are in good agreement with the measured temperatures. This analytical is useful for study the possibility of RCC dam construction. The actual climatic conditions and thermal properties of the materials were considered in the analysis. The predicted temperatures are found to be in good agreement with measured temperatures in the construction site using thermocouples installed within the dam. Figure 2.4 shows thermal stress analysis of Kinta RCC dam.

Choktaweekarn (2009) proposed a computerized program for predicting a semi-adiabatic temperature and thermal cracking of mass concrete using fly ash. The computerized program proposed by Saengsoy and Tangtermsirikul (2003) was modified to be used for semi-adiabatic temperature rise. A three-dimensional finite element analysis is used for calculating temperature and restrained strain in mass concrete. The model considered time, material properties, and mix proportion dependent behavior of concrete. The hydration heat and thermal properties used in the finite element analysis are obtained from our previously proposed adiabatic temperature rise model (Saengsoy, 2003) and are used as the input in the analysis. This model can compute the temperature rise of fly ash concrete with variation of dimension of structure, ambient temperature, boundary conditions and convection heat transfer coefficient at the exposed surface. Temperature gradient between center and surface of concrete was used to compute restrained strain by thermal. Restrained strain was compared with tensile strain capacity, if restrain strain is greater than tensile strain capacity, concrete will crack. The proposed model was proved to be satisfactory to predict thermal cracking of mass concrete.

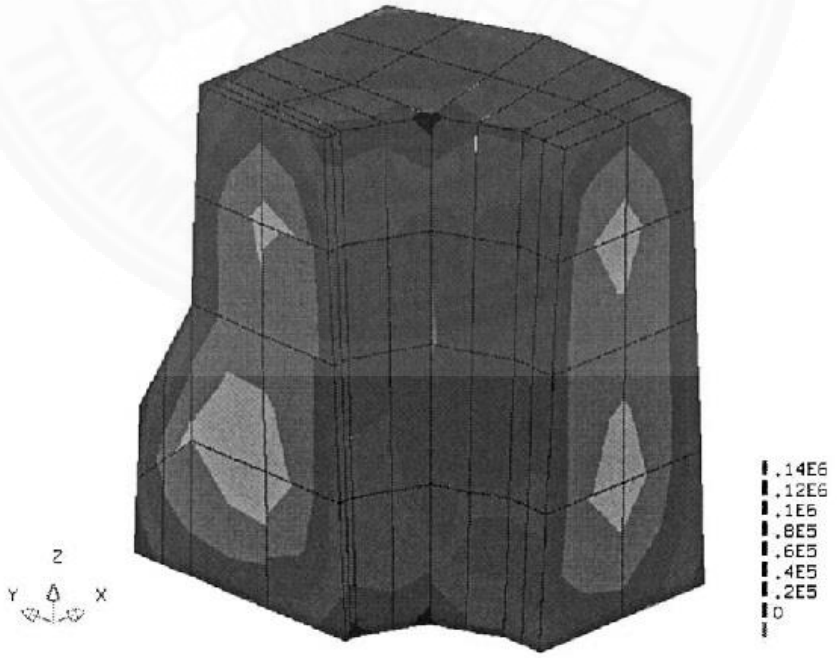

Stresses after 25 h (darker zone means higher tensile stress).

Figure 2.2 A simulated concrete block with 25 hours stress (Schutter, 2002)

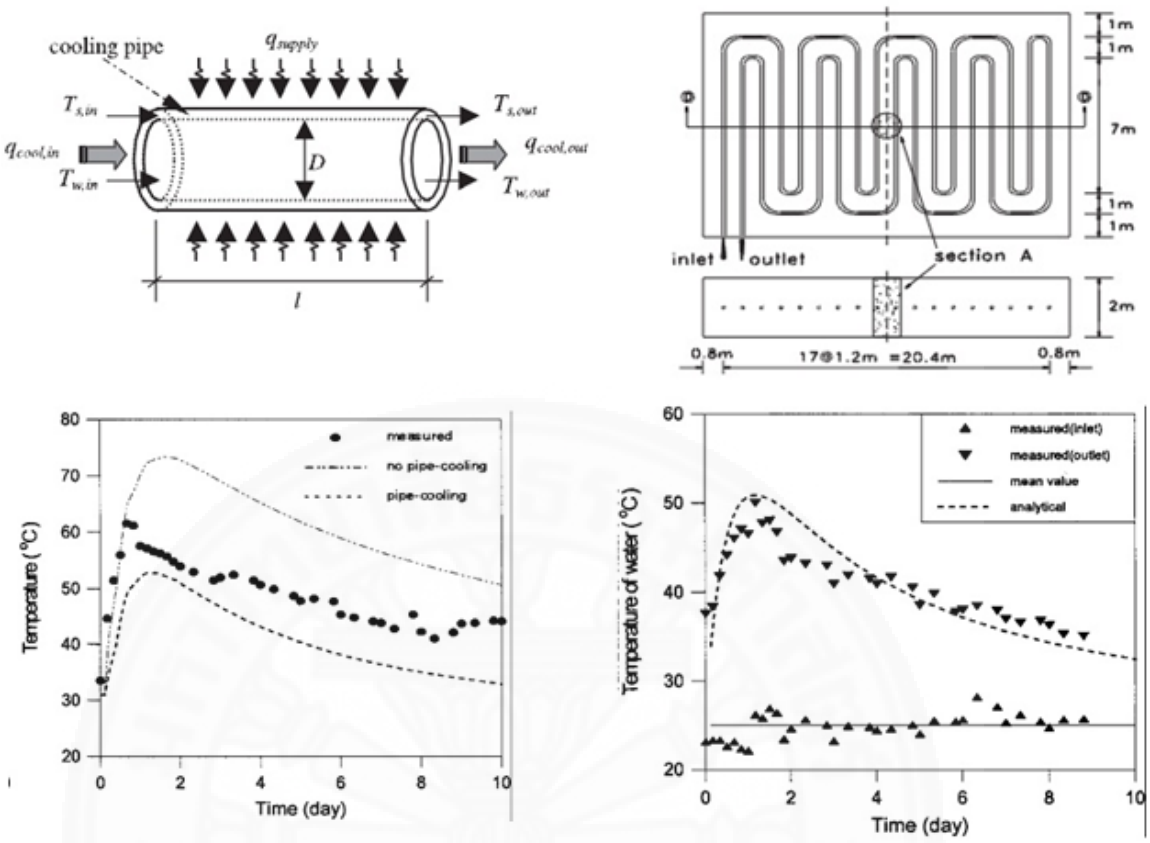

Figure 2.3 Thermal analysis with pipe-cooling system (J. K. Kim et al., 2001)

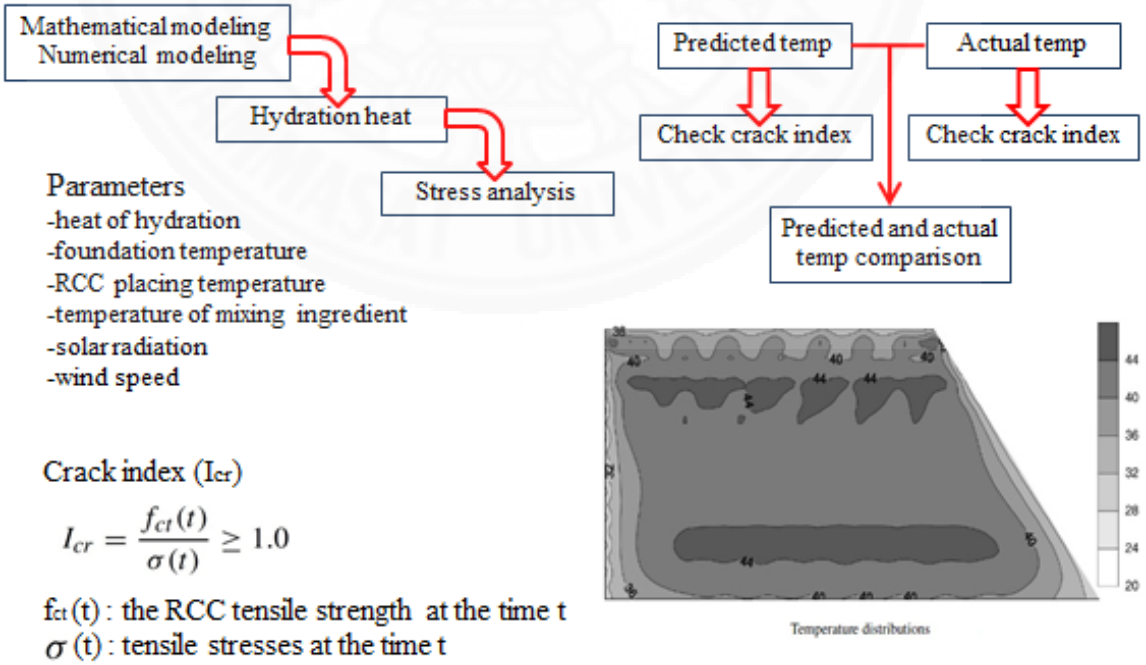

Figure 2.4 Thermal stress analysis of Kinta RCC dam (Noorzaei J. et al., 2006)

2.2 Shrinkage

Shrinkage of concrete can be separated into two main groups; thermal and moisture related shrinkage. Thermal shrinkage is a serious problem in mass concrete structures in which thermal strain or stress develops as a result of hydration reaction. The temperature change can also cause temperature shrinkage. Moisture related shrinkage includes the response of concrete to internal and external moisture variation condition. The moisture related shrinkage is the most significant in thin concrete member (large surface area to volume ratio) due to the faster loss of water to surrounding environment. Pavements, wall and slabs are examples of thin concrete member that may be sensitive to drying shrinkage cracking. Although autogenous shrinkage is depended on internal moisture loss, it can also cause thin concrete member to crack especially in high strength concrete. The moisture related shrinkages consist of plastic shrinkage, autogenous shrinkage and drying shrinkage.

Shrinkage in concrete is not a problem if the concrete is not under restraint. However, all concrete structures normally are restrained by internal or external restraint, thus cracking may occur. Restrained shrinkage in concrete can be classified into three different scales: macroscopic, mesoscopic and microscopic (Bisschop, 2002). The macroscopic scale defines the confinement such as subgrade, formwork or other connecting parts of the structures, or by the steel reinforcement embedded in the concrete. The macroscopic scale of restrained shrinkage may also be mentioned to as external restraint. The mesoscopic scale of restraint refers to restraint brought about by the aggregate or self-restraint due to the moisture gradient within the cement-paste matrix. Mesoscopic scale is also mentioned to as self-restraint. Self-restraint is developed by the difference between shrinkage near the surface and shrinkage of the interior concrete. Since drying shrinkage is always larger at the exposed surface, the interior portion restrains the shrinkage of the surface concrete, thus developing non-uniform stress distribution along the depth of the concrete. This will cause cracking on the surface. The microscopic level of restraint describes the hard phases in the cement paste such as hydrated cement grains or calcium hydroxide crystals.

Restrained shrinkage can induce tensile stresses or restrained strain which if it exceeds the tensile strength or tensile strain capacity of concrete, will cause the concrete to crack. The magnitude of tensile stress or restrained strain developed from restrained shrinkage of concrete is influenced by a combination of parameters, such as amount and rate of shrinkage, creep and relaxation, modulus of elasticity, tensile strain capacity or tensile strength and degree of restraint of concrete. Thus, the amount of shrinkage is only one factor governing the cracking.

2.2.1 Autogenous Shrinkage

Autogenous shrinkage is the macroscopic volume reduction due to chemical shrinkage that happens after the final set of concrete together with the volume reduction due to self-desiccation. The latter happens due to water consumption of the unhydrated cement that results in reducing humidity in the capillary pores and then self-equilibrating stresses are created by capillary tension in the capillary pore water and compression in hydrated products, which is called self-desiccation. The matrix of hydrated products then shrinks due to the introduced compressive stress. Autogenous shrinkage is different from drying shrinkage in the sense that there is no water loss to the environment in the case of autogenous shrinkage. The loss of water happens inside the concrete due to consumption of moisture by the unhydrated cement and the still non-reacted cementitious materials (Tangtermsirikul).

Volume reduction happens immediately after the concrete is mixed, however, the volume reduction will be essential when the concrete has already been placed. The volume reduction will generate stress when the concrete has achieved its final setting time because stress is not generated before the concrete has gained some strength. Autogenous shrinkage is therefore defined as the shrinkage that is measurable after the final setting time of the concrete. Autogenous shrinkage was not paid much attention in the past because low water to binder concrete was not extensively used at that time. Concrete with high water-to-binder ratio have large and more continuous capillary pores. Water cured can be more easily reached, by the unhydrated cement, in concrete with high water-to-binder ratio too. Capillary tension is then not generated much, causing negligible autogenous shrinkage in high water-to-binder concrete. On the other hand, at present days many kinds of advanced concrete are designed to have lower water to binder ratio and sometimes with large paste volume. Figure 2.5 shows mechanisms of autogenous shrinkage of paste.

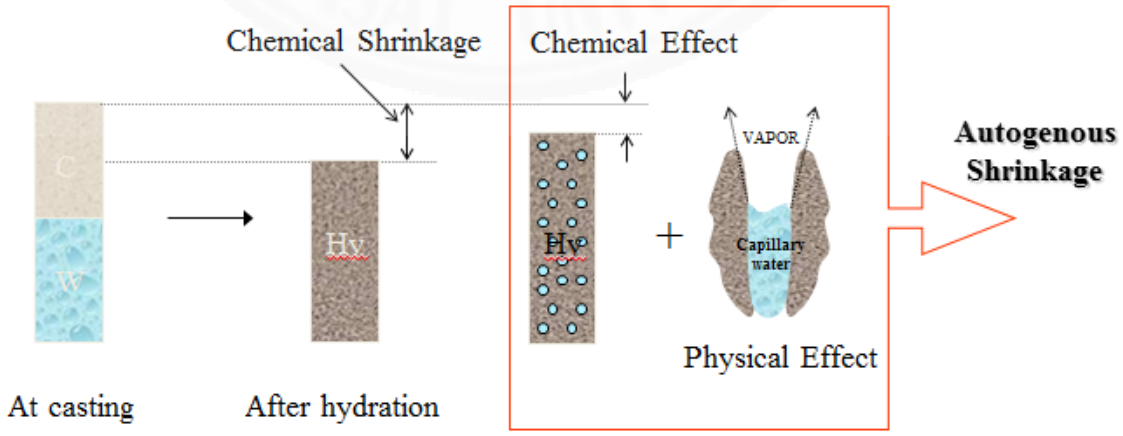

Figure 2.5 Mechanisms of autogenous shrinkage of paste

2.2.1.1 Recommended methods to reduce autogenous shrinkage

Some solutions are listed below.

1) Using fly ash. Fly ash is effective in reducing autogenous shrinkage. Fly ash with higher SO_3 content seems to have better performance, however, the SO_3 content of fly ash should not be too much since it may contribute to a long term volume stability problem such as problem due to delayed ettringite formation.

2) Use of expansive agent to compensate the shrinkage.

3) Use low C_3A but high C_2S cements such as type 2 or type 4 cement.

4) Avoid using concrete with too low water to binder ratio or too large paste volume.

5) Reduce paste content or increase aggregate content.

2.2.2 Drying shrinkage

The process of drying begins when the relative humidity of the environment is lower than that in the concrete pores (usually capillary pores). Free water in the capillary pores then evaporates from the pores into the drier environment (Tangtermsirikul). The rate of drying depends on the pore structure, i.e. pore size and pore volume, and the condition of the environment such as humidity, temperature and wind speed. When capillary pores lose some of their free water, volume reduction takes place due to the loss of water together with the occurrences of self-equilibrating stress condition which makes the concrete crack on the surface due to its self-restraint. Figure 2.6-2.7 show drying shrinkage of concrete and drying shrinkage stress distribution of concrete, respectively.

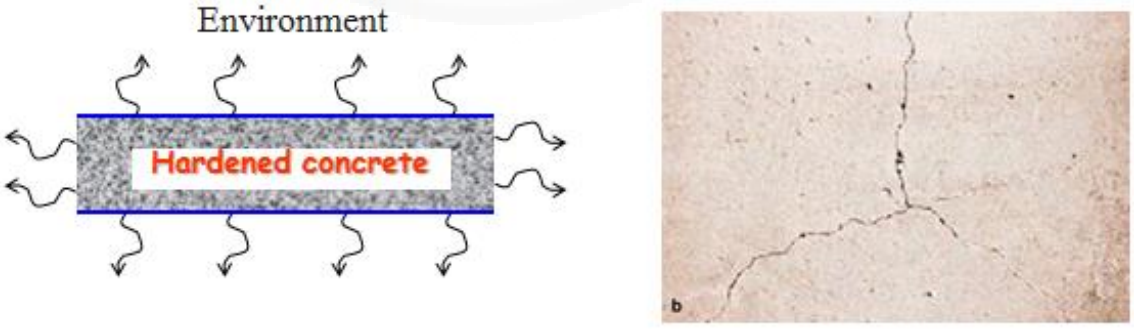

Figure 2.6 Drying shrinkage of concrete

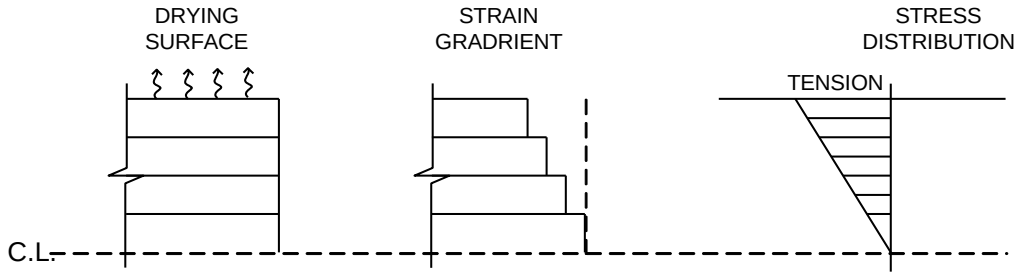

Figure 2.7 Drying shrinkage stress distribution of concrete

2.2.2.1 Recommended methods to reduce drying shrinkage

The methods for preventing cracking due to drying shrinkage may be done by various means as follows.

1) Provide additional reinforcement to resist the tensile stress induced by the drying shrinkage. This method is effective in the cases of continuous structures like pavement, slab of walls in which tensile stress is almost uniform across the section of the members.

2) Proportion the concrete to have low shrinkage. This can be done in many ways as follows.

a) Minimizing the unit water content and water-to-cement ratio of the concrete which is possibly done through the use of water reducing admixtures or superplasticizers.

b) Minimizing the paste content of the concrete or in other words, maximizing the aggregate content.

c) Using appropriate types of mineral admixtures such as fly ash, silica fume, limestone powder, etc. The decision should be made based on consideration of other required performances of the concrete and cost of expansiveness too.

d) Using expansive agent. This method is usually costly.

e) Avoid using aggregate with too high absorption or poor gradation.

3) Sufficiently cure the concrete especially when high content of pozzolans are used in the concrete. Longer curing period results in smaller drying shrinkage.

4) Apply painting or coating or adhering tiles on the exposed surface of the concrete. These materials can reduce or even inhibit the evaporation of water from the concrete surface and the drying shrinkage can be reduced or may even be almost perfectly prevented.

2.2.3 Literature Reviews

Tazawa and Miyazawa (1993) proposed a model of autogenous shrinkage by considering the influence of each parameter. Autogenous shrinkage of cement is influenced by its mineral compositions and their hydration reaction. The model is derived from an analysis of autogenous shrinkage as a function of the degree of hydration of minerals for various types of cement with a fixed water-to-cement ratio (0.3). It was found that the C_3A and C_4AF are the major influencer of autogenous shrinkage.

Justnes et al. (1998) studied the influence of cement characteristics on chemical shrinkage. The total and external chemical shrinkage were defined for 10 different Portland cements with a wide range of fineness and mineral composition. Increasing of fineness and content of C_3S and C_3A clearly contribute to increase shrinkage at early age. It is important to note that the chemical shrinkage of the C_3A reaction is about 5 times greater than the C_3S reaction.

Mak et al. (1998) studied effects of temperature on autogenous shrinkage at early age of high strength concretes. The results were obtained from measured free autogenous shrinkage with and without silica fume. The dual effects of hydration induced autogenous shrinkage and the counteracting thermally induced expansion significantly influences the early age free autogenous movements in a range of high strength concretes with low water-to-binder ratio. Even a moderate temperature rise of 15 °C has a significant impact in reducing the early age autogenous shrinkage in some concretes during 25 to 50%.

Tazawa and Miyazawa (1998) experimentally investigated various factors influencing autogenous shrinkage of concrete, such as cement type, water-to-cement ratio and amount of aggregate for establishing a prediction model. It has been proved that the influence of aggregate on autogenous shrinkage after 24 hours can be evaluated with Hobbs' model for mortar and concrete with dissimilar amount of aggregate. Autogenous shrinkage of concrete is quite a lot depended on water-to-cement ratio. It was found that the ultimate value of autogenous shrinkage increases with decrease in water-to-cement ratio.

Tangtermsirikul (1998) studied the effect of fly ashes with various particle sizes, chemical composition, and replacement ratios on autogenous shrinkage of pastes. It was found that for the effect of particle size, paste with fly ash having smaller average size than cement presented larger autogenous shrinkage whereas pastes with fly ash having bigger size than cement presented smaller autogenous shrinkage than that of cement paste. For the effect of chemical composition, fly ash with higher SO_3 content resulted in lower autogenous shrinkage. For the effect of fly ash content, non-classified and classified fly ash having larger average size than cement showed the same tendency i.e. larger autogenous shrinkage in 20% fly ash paste than in 50% fly ash paste when non-classified fly ash was used. On the other hand, smaller autogenous shrinkage in 20% fly ash paste than in 50% fly ash paste was found in case of pastes with classified fly ash having smaller average size than

cement. It could be concluded that not only chemical composition which affects rate of hardening and volume change of pastes with fly ash but also particle size which affects the pore structure of the paste, has to be considered for predicting autogenous shrinkage of pastes with fly ash replacement.

Fujiwara (1989) studied the drying shrinkage relation between mix proportion of hardened cement paste, mortar and concrete. Test results showed that more water content leads the larger drying shrinkage will be in the case of the medium and wet consistency. In order to prevent large drying shrinkage and the occurrence of cracking, it is very significant to reduce water content. On the other hand, mix proportion with high stiff consistency shows shrinkage greater than the expectation, even though its low water content. The relationship between paste content and drying shrinkage was indicated by some investigation. The higher cement content is, the larger drying shrinkage will be when water-to-cement ratio is fixed, except for in a very lean mixture, which shows comparatively large shrinkage.

Bissonnette et al. (1999) evaluated the influences of different key parameters such as relative humidity, specimen size, water-to-cement ratio and paste volume. Test results showed that between 48 and 100% relative humidity, shrinkage of cement paste was approximately inversely proportional to relative humidity. Results also showed that the ultimate shrinkage of paste and mortars measured on 50x50x400 mm specimens did not differ much from the "real" shrinkage measured on 4x8x32 mm specimens. Thus for the specimen dimensions investigated in this study, the existence of humidity gradient did not affect to a large extent the ultimate shrinkage strain. The influence of the water-to-cement ratio within the investigated range (0.35-0.50) was found to be relatively small. On the other hand, paste volume was noted to be a very strong influencer.

Akkaya et al. (2007) studied the autogenous and drying shrinkage of Portland cement concrete, and binary and ternary binder concretes. The binary and ternary binder concretes were formed by replacing fly ash and silica fume. Restrained shrinkage test was also performed to evaluate the effect of binder type on early age cracking. After the cracking of the restrained ring samples, crack widths were measured and compared with the results of an R-curve based model, which takes post-peak elastic and creep strains into account. It was found that the incorporation of fly ash decreased the autogenous shrinkage strain but increased the drying shrinkage strain. Since the total shrinkage strains of both the ternary and the binary concrete mixtures were similar. The strength development of the concrete became an important factor in the cracking. The lower strength of the concrete with ternary binders led to earlier cracking compared to the binary binder concrete. Portland cement concrete cracked the earliest and had the biggest crack width.

Tangtermsirikul et al. (1992) proposed a model for predicting water transportation due to drying with considering carbonation effect. The model was based on Fick's law of diffusion by the assumption that when concrete was exposed to surrounding environment, water in the concrete moved through the pore structure according to the gradient of vapor pressure regarded to vary with relative humidity in

the pores of concrete. It can be concluded that for saturated concrete, amount of evaporable water was smaller in the carbonation portion than in non-carbonated portion due to the reduction of pore volume in the carbonated area.

Kim and Lee (1999) calculated the internal relative humidity in drying concrete specimens at early ages. The variation of relative humidity due to self-desiccation of sealed specimens. It was found that moisture distribution in low-strength concrete (high water-to-cement ratio) was mostly influenced by moisture diffusion due to drying rather than self-desiccation. On the other hand, for high-strength concrete (low water-to-cement ratio), self-desiccation had a considerable influence on moisture distribution.

Rico (2000) studied moisture transport properties. Measurements of weight loss were made due to the difficulties in measuring the relative humidity within concrete. A three-dimensional finite element formulation in terms of the relative humidity in the pores was employed in order to solve the governing non-linear diffusion equation, which was described along with the physical mechanisms involving the moisture diffusion. The weight losses of the specimens were calculated using the desorption isotherm that related the humidity in the pores to the water content. The evolution of the weight loss of the mortar specimens was compared to test data and the parameters that led to an acceptable global fit were determined in his study.

Y. Yuan and Z.L. Wan (2000) predict potential early-age cracking after concrete placing and the relationship of relative humidity in concrete and drying shrinkage strain inside concrete. A numerical simulation procedure has been completed based on a micromechanical model and empirical formulas on the property development of young concrete. The numerical model could account for the effects of hydration, moisture transport and creep. Environmental influences, such as removal of formworks, curing conditions and variations of surrounding temperature and relative humidity have been investigated. The concrete specimens with 300x300x150 millimeters were tested by varied water-to-cement ratio and gauge locations. Water-to-cement ratios were 0.4 and 0.65. The gauges were installed at 2, 5, 8 and 12 centimeters from the exposed surface. The test result shows that for water-to-cement ratio equal to 0.4 and 0.65, there are no drying shrinkage strain at 12 centimeters from the exposed surface because there are no losing water to the surrounding environment. The highest shrinkage strain is at 2 centimeters from the exposed surface because there is maximum loss of water to surrounding environment (the lowest relative humidity). The good agreement between analytical results and tests shows that the modelling of pore structure within concrete is adequate in predicting the drying shrinkage behavior. Significant variances of the internal drying shrinkage strain according to the depth from drying surface result in large tensile stress directly, even surface cracking. Figure 2.8 shows cracking due to shrinkage behavior

Tongaroonsri (2008) presented the prediction of autogenous and drying shrinkage and shrinkage cracking in fly ash concrete. The predicting model consists of parameters such as water to cement ratio, paste content, cementitious materials,

cement type, curing type/period and maximum size of aggregate and proposed by the result of the experiment. Total shrinkage of concrete is the summation of autogenous and drying shrinkage. The verification models showed that the model is satisfactory to predict shrinkage of concrete.

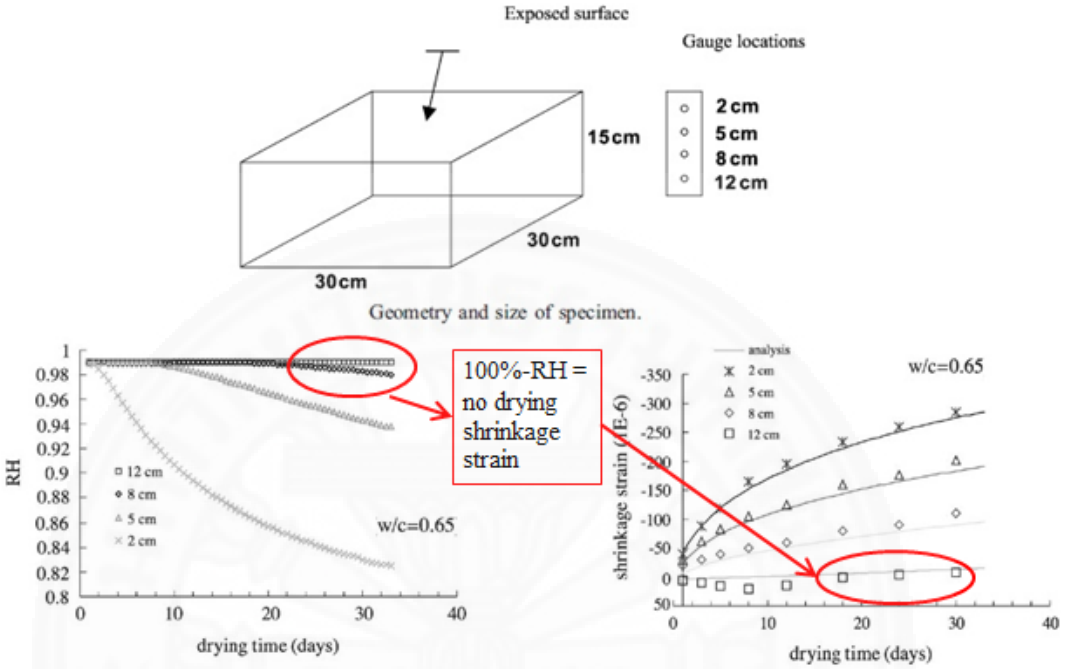

Figure 2.8 Cracking due to shrinkage behavior (Y. Yuan and Z.L. Wan, 2000)

2.3 Combination of effect of thermal expansion and shrinkage

G. Kim et al. (2009) evaluated autogenous shrinkage of high-strength mass concrete with the consideration of the specimen size and hydration delay effects. The thermal deformation was computed by using coefficient of thermal expansion corrected by the maturity method. The autogenous shrinkage was the thermal deformation subtracted from measured total deformation. The properties and relations of hydration heat and autogenous shrinkage at early ages were numerically analyzed. The analytical results showed that hydration temperature is affected by specimen conditions such as size and admixture, and change of hydration temperature could affect autogenous shrinkage. The higher hydration temperature leads the greater autogenous shrinkage. There is a close relationship between hydration temperature and autogenous shrinkage at early ages, especially between hydration heating velocity and autogenous shrinking velocity. The higher hydration heating velocity leads the higher autogenous shrinking velocity and the greater ultimate autogenous shrinkage. Figure 2.9 shows hydration heat and autogenous shrinkage deformation.

Faria et al. (2006) proposed a thermo-mechanical model based on the framework of finite element techniques with the consideration of various factors such as the heat of hydration, the evolving properties of concrete during hydration period and early age. A numerical application was proposed by focusing on the thermo-mechanical behaviour of a slab that was restrained by piles. The thermal problem was calculated by the cement hydration reaction included an Arrhenius law for the internal heat source. The model finite element spatial discretization and a backward-Euler time integration scheme were used in the analysis. The mechanical problem that was arisen from the non-uniform thermal field was solved by the finite element method, taking into consideration the changes in the mechanical properties of concrete due to aging, creep and shrinkage phenomena. Thermo-mechanical model provided results that were well correlated with the observed in situ measurements of temperatures and strains. Figure 2.10 shows verification of modeling of restrained slab at early age.

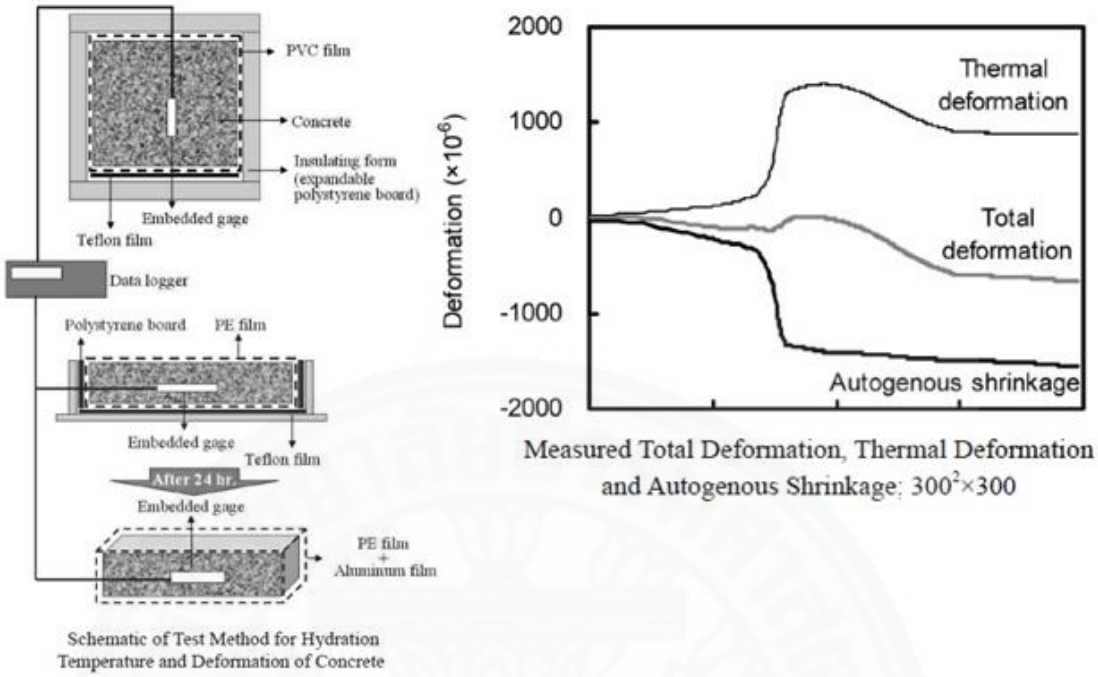

Figure 2.9 Hydration heat and autogenous shrinkage deformation (G. Kim et al., 2009)

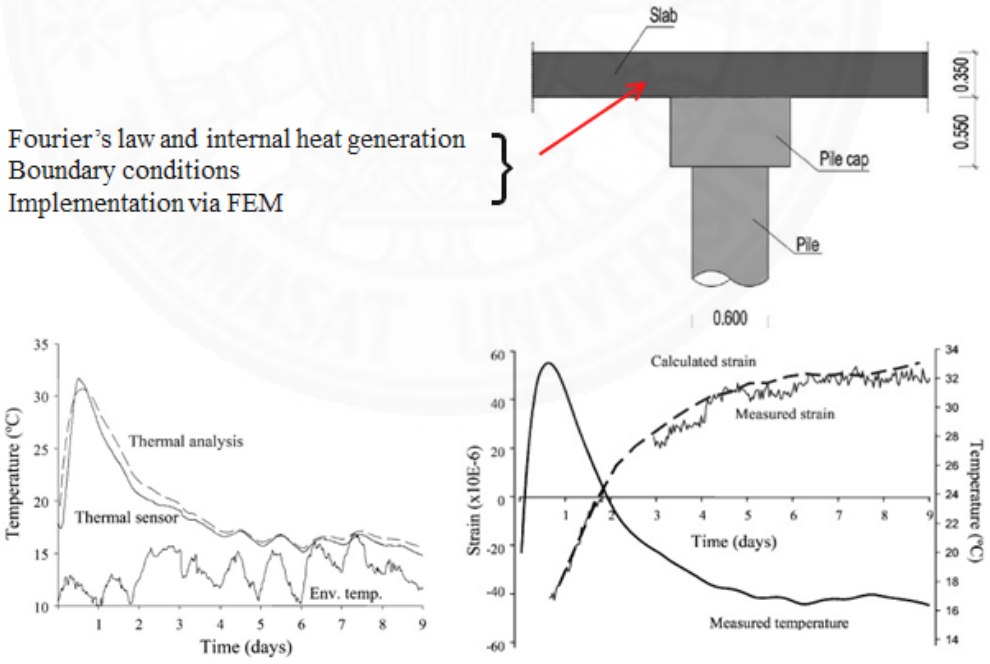

Figure 2.10 Verification of modeling of restrained slab at early age (Faria et al., 2006)

Chapter 3

Details of Existing Models

3.1 Semi-adiabatic temperature rise and thermal cracking model

A flow chart of the existing model for simulating thermal cracking of mass concrete is shown in Figure 3.1. Heat of hydration and heat produced by pozzolanic reaction, which were obtained from the models proposed by Saengsoy and Tangtermsirikul (2003) were used as the input for a commercial FEM program. Thermal properties such as specific heat, thermal conductivity and coefficient of thermal expansion (CTE) are obtained from thermal properties' models proposed by Choktaweekarn, et.al. (2009). An FEM program was used to analyze the semi-adiabatic temperature rise of concrete. A three-dimensional eight node brick element was used in the analysis. The couple thermo-mechanical problem was used in the analysis in which heat transfer analysis is firstly solved. The temperature obtained from the heat transfer analysis is used as the input for the computation of the restrained strain. More details are mentioned below.

3.1.1 Heat Transfer Analysis

By the use of the common heat transfer analysis which was mentioned by many researchers together with the derived heat of hydration and pozzolanic reactions and thermal properties from the existing models developed at SIIT, the semi-adiabatic temperature can be analyzed.

The governing equation of heat transfer for temperature prediction of mass concrete with consideration of heat of hydration is shown in Eq. (1).

$$\rho c \frac{\partial T}{\partial t} = q_{hy} + \frac{\partial}{\partial x}\left(k_x \frac{\partial T}{\partial x}\right) + \frac{\partial}{\partial y}\left(k_y \frac{\partial T}{\partial y}\right) + \frac{\partial}{\partial z}\left(k_z \frac{\partial T}{\partial z}\right) \qquad (1)$$

Where: k_x, k_y, k_z are thermal conductivities of concrete in x, y and z directions, respectively (kcal/m hr ^oC). ρ is density ofconcrete (kg/m^3), c is specific heat of concrete (kcal/ kg ^oC), q_{hy} is heat of hydration and pozzolanic reaction (kcal). t is age of concrete (hr.). T is temperature of concrete (^oC).

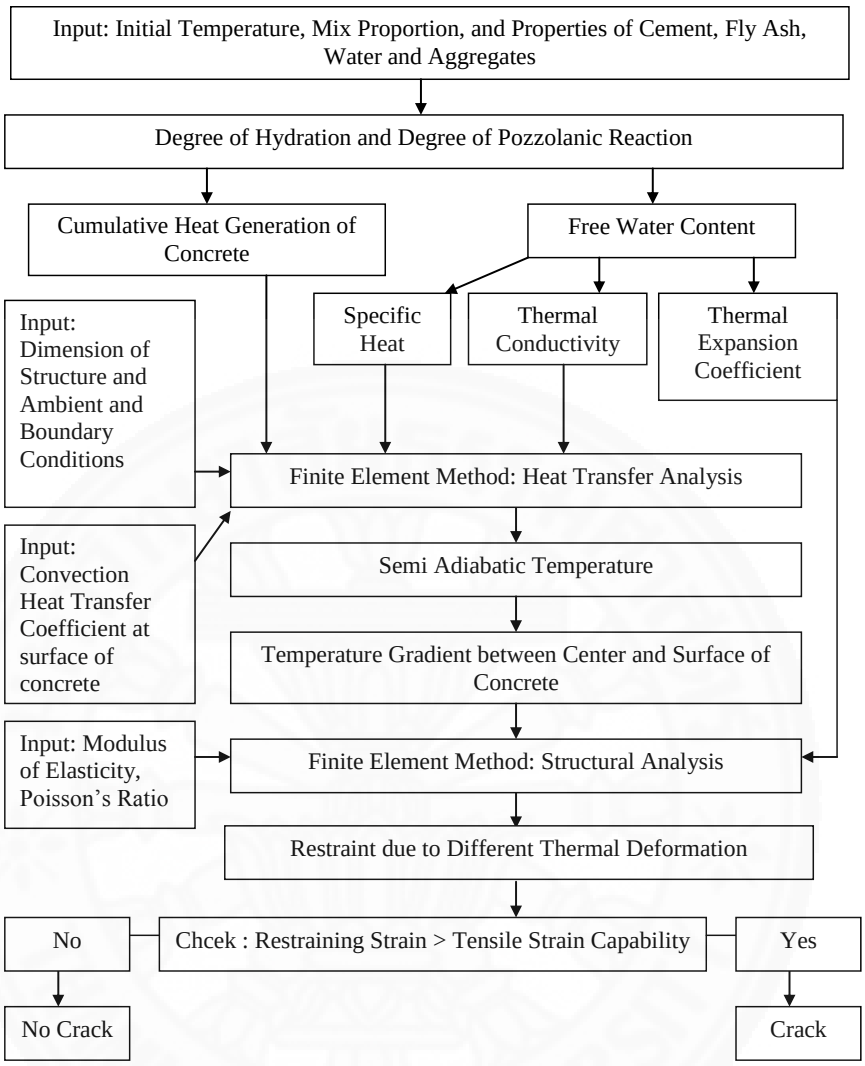

Figure 3.1 A flow chart of the proposed model for simulating thermal cracking of mass concrete

Total heat generation of concrete was calculated from summation of the heat liberated due to the reaction of each cement compound, including the formation of ettringite and monosulphate and the reaction of fly ash as

$$Q(t) = Q_{C_3S}(t) + Q_{C_2S}(t) + Q_{C_3A}(t) + Q_{C_4AF}(t) + Q_{C_3AET}(t) + Q_{C_4AFET}(t) + Q_{FA}(t) \quad (2)$$

Where: Q(t) is the total heat generation of concrete at the considered age (kcal/kg of concrete). $Q_{C3S}(t)$, $Q_{C2S}(t)$, $Q_{C3A}(t)$, $Q_{C4AF}(t)$ and $Q_{FA}(t)$ are the cumulative heat generation of C_3S, C_2S, C_3A, C_4AF, and fly ash, respectively, at the considered age (kcal/kg of concrete). $Q_{C3AET}(t)$ and $Q_{C4AFET}(t)$ are cumulative heat generation of the ettringite and monosulphate formation by C_3A, and C_4AF reacting with gypsum, respectively, at the considered age (kcal/kg of concrete).

Some details for calculation of heat generation are briefly mentioned below. More details can be found in Saengsoy and Tangtermsirikul (2003). The cumulative heat generation of each cement compound was considered to be linearly related to its degree of reaction and its content in the concrete as shown in Eq. (3). The cumulative heat generation of fly ash was computed based on the degree of pozzolanic reaction and fly ash content in concrete as shown in Eq. (4).

$$Q_i(t) = \frac{\alpha_i(t)}{100} \times Q_{i,max} \times w_i \qquad (3)$$

$$Q_{FA}(t) = \frac{\alpha_{poz}(t)}{100} \times Q_{FA,max} \times w_{fa} \qquad (4)$$

Where: $Q_i(t)$ is the cumulative heat generation of each cement compound i and $Q_{FA}(t)$ is the cumulative heat generation of fly ash at the considered age (kcal/kg of concrete). $\alpha_i(t)$ and $\alpha_{poz}(t)$ are the degree of hydration of each cement compound i and the degree of pozzolanic reaction at the considered age (%). $Q_{i,max}(t)$ and $Q_{FA,max}(t)$ are the cumulative heat generation of each cement compound i and fly ash at their complete reaction at the considered age (kcal/kg). w_i and w_{fa} are the effective weight ratio of each cement compound i and fly ash available to generate heat in 1 m^3 of concrete to the unit weight of concrete.

Figure 3.2a shows the cumulative heat generation of C_3S, C_2S, C_3A, and C_4AF at different degrees of hydration. The cumulative heat generation of fly ash at its maximum pozzolanic reaction degree ($Q_{FA,max}$) is assumed to be the function of calcium oxide content in fly ash as can be seen in Figure 3.2b.

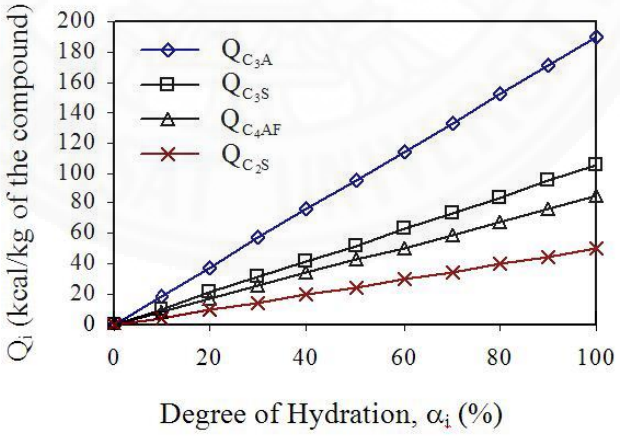

(a)

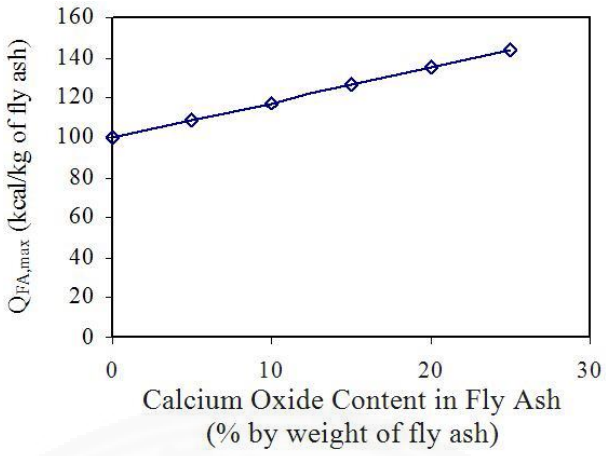

(b)

Figure 3.2 Cumulative heat generation of (a) C_3S, C_2S, C_3A, and C_4AF at different degree of hydration, (b) fly ash at the maximum pozzolanic reaction with various calcium oxide content in fly ash

Specific heat and thermal conductivity used in the analysis were obtained from Choktaweekarn *et al.* (2009a) and Choktaweekarn *et al.* (2009b) as shown in Eqs (5) and (6).

$$c(t) = w_g c_g + w_s c_s + w_{ra} c_{ra} + w_{fw}(t) c_w + w_{uc}(t) c_c + w_{ufa}(t) c_{fa} + w_{hp}(t) c_{hp} \quad (5)$$

$$k(t) = n_g k_g + n_s k_s + n_{fw}(t) k_w + n_{uc}(t) k_c + n_{ufa}(t) k_{fa} + n_{ra} k_{ra} + n_{hp}(t) k_{hp} \quad (6)$$

Where: c(t) is the specific heat of concrete at the considered age (kcal/kg °C). w_{ra}, w_g, and w_s are the weight ratio of air, coarse aggregate, and sand per unit weight of concrete, respectively (kg / kg of concrete). $w_{fw}(t)$, $w_{uc}(t)$, $w_{ufa}(t)$, and $w_{hp}(t)$ are the weight ratio of free water, unhydrated cement, non-reacted fly ash, and the hydration and pozzolanic products, respectively, at the considered age (kg / kg of concrete). c_g, c_s, c_w, c_c, c_{fa}, c_{ra} and c_{hp} are the values of specific heat of coarse aggregate, sand, water, cement, fly ash, air and the hydration and pozzolanic products, respectively (kcal/kg °C). k(t) is thermal conductivity of concrete at any age (kcal/m.hr °C), k_g, k_s, k_w, k_c, k_{fa}, k_{ra}, k_{hp} are thermal conductivity of coarse aggregate, sand, water, cement, fly ash, air and the hydrated product, respectively (kcal/m.hr °C). $n_{fw}(t)$, $n_{uc}(t)$, $n_{ufa}(t)$, $n_{hp}(t)$ are volumetric ratio of free water, non-reacted cement, unhydrated fly ash and the hydrated product, respectively, at the time considered (m^3/m^3 of concrete). n_g, ns, n_{ra} are volumetric ratio of coarse aggregate, sand and air, respectively (m^3/m^3 of concrete). Specific heat and thermal conductivity of each ingredient of concrete are shown in Table 1. Equations for predicting these two thermal properties of concrete were proposed as time, material and mix proportion dependent functions.

The equations were verified with various experimental results and the verification results were satisfactory. The details of the model are not mentioned here but are elsewhere (Choktaweekarn *et al.*, 2009a; Choktaweekarn *et al.*, 2009b).

Table 3.1 Thermal properties of the ingredients in concrete

Thermal Coefficients	Limestone	Quartz Sand	Air	Water	Cement	Fly Ash	Hydrated Product
k (kcal/m hr °C)	2.2	3.0	0.022	0.51	1.33	0.65	1.0
c (kcal/kg °C)	0.2	0.19	0.24	1.0	0.18	0.17	0.1
CTE (micron/°C)	4.5	10.4	-	-	14.4	6.45	20

*Remark: k, c, CTE are thermal conductivity, specific heat and coefficient of thermal expansion, respectively

The heat transfer inside the mass concrete is governed by Eq. (1), however, the condition at the concrete surface is different. Conduction process plays an important role in transferring heat within the interior elements. However, for exterior elements, convection is the major phenomenon role in transferring heat at the concrete surface. The presence of wind and solar radiation affect the temperature profile significantly and must be considered. The convective heat transfer is involved in transferring heat between surface of mass concrete and surrounding environment. The amount of heat transfer at the surface of concrete can be pomputed using Newton's cooling law. For simplicity, radiation is taken into account together with the convection, through a single convection-radiation coefficient (Faria, et.al, 2006). The convective heat transfer at concrete surface can be expressed as

$$q = h(T_s - T_a) \qquad (7)$$

Where: q is the convective heat flux per unit area, h is the combined convection-radiation heat transfer coefficient (kcal/m^2 hr ^{o}C), T_s and T_a are the exposed surface and air temperature.

In a real mass concrete footing, heat loss to surrounding environment is processed by convection. Normally, the side and bottom faces of the footing are covered by subsoil and heat dissipates from concrete to the surrounding soil by conduction process. However, the problem can be simplified by assuming that the amount of heat loss to the surrounding subsoil is assumed to be done by the convection process. This kind of assumption and boundary condition was used in a previous study of Faria, et.al, (2006).

The model was verified with the test results conducted in the lab and the measured results of many real footings. Their verifications were shown in the previous studies (Choktaweekarn, 2008). The verifications show that the model is satisfactory for predicting temperature of the measured footings.

3.1.2 Restrained Strain Analysis

At each time step, the temperature at each position in the mass concrete, obtained from heat transfer analysis, is used as the input for the restrained strain analysis. The internal deformation and stress in each element are related by Hooke's law as shown in Eq. (8).

$$\{\Delta\sigma(t)\} = E(t)\left[\overline{D}\right]\{\Delta\varepsilon_{res}(t)\} \qquad (8)$$

Where: $\Delta\sigma$ (t) is the change of stress at the considered age (MPa), $\Delta\varepsilon_{res}$(t) is the restrained strain at the considered age (micron). $E(t)$ is the modulus of elasticity at the considered age (MPa). $\left[\overline{D}\right]$ is the material properties matrix and t is the considered age.

In case of the absence of external loading, the stresses that cause cracking at the early age of concrete are induced by restraint of deformations. In the existing model, the restrained strain in mass concrete is caused mainly from the thermal strain due to the temperature variation of concrete. The free thermal strain of concrete element subjected to thermal expansion can be calculated from Eq. (9).

$$\Delta\varepsilon_{th}(t) = CTE(t)\Delta T(t) \qquad (9)$$

Where: $\Delta\varepsilon_{th}$(t) is the free thermal expansion strain. CTE(t) is the coefficient of thermal expansion coefficient (micron/ ^{o}C) and ΔT(t) is the temperature change at the considered age (^{o}C).

CTE of concrete is obtained from Choktaweekarn and Tangtermsirikul (2006) as shown in Eq. (10).

$$CTE(t) = \frac{n_p CTE_p(t) E_p(t) + n_s CTE_s E_s + n_g CTE_g E_g}{n_p E_p(t) + n_s E_s + n_g E_g} \qquad (10)$$

Where: *CTE*(t) is the coefficient of thermal expansion of mortar or concrete at the considered age (micron/°C). CTE_p (t), CTE_s, and CTE_g are the values of coefficient of thermal expansion of paste, fine aggregate and coarse aggregate, respectively (micron/°C). n_p, n_s, and n_g are the volumetric ratios of paste, fine aggregate, and coarse aggregate, respectively (m^3/m^3 of concrete). E_p(t), E_s, and E_g are the modulus of elasticity of paste, fine aggregate, and coarse aggregate, respectively, (MPa), t is the considered age (day).

3.1.3 Verification of the Model to predict thermal cracking of mass concrete

The model was verified with a real concrete footing. Figure 3.3 shows a thermal crack at one side of the footing. The size of the footing was 14 x 63 x 1.4 m. The footing was cured by insulation curing for 4.6 days. Cracks were found right after the removal of the insulation materials. This means that cracks might have occurred since early age before the removal of the insulation material.

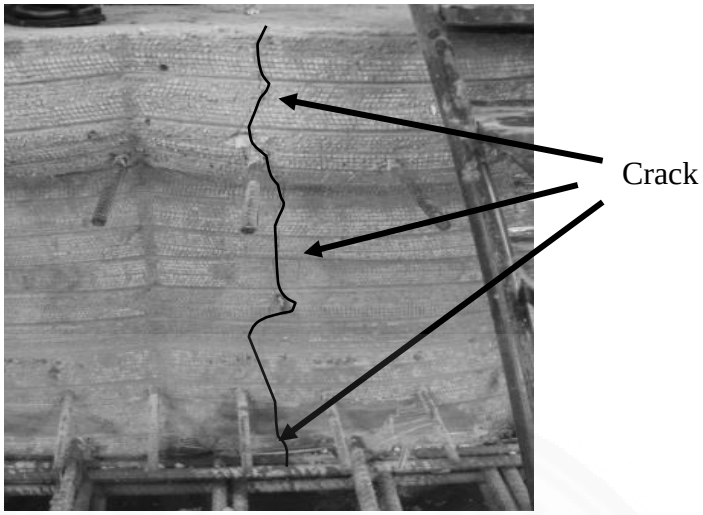

Figure 3.3 Crack on side surface of a mass concrete footing

The analytical results of temperature and restrained strain in the core zone at top surface, mid-depth and bottom surface of the footing are shown in Figure 3.4 and Figure 3.5. The rapid change of temperature and restrained strain after 4.6 days occurs due to the removal of insulation material. In case of temperature, top surface shows the lowest but mid-depth shows the highest temperature. The different expansion between the mid-depth and surface causes internal restraint between the mid-depth and the surface of the structure. The surface is restrained in tension and the mid-depth part is restrained in compression. The analytical results show the same tendency as that occurs in mass concrete as shown in Figure 3.5. The restrained strain in tension ($\varepsilon_{res,\ ten}$) at the top surface is the highest. The $\varepsilon_{res,\ ten}$ at the top surface obtained from the analysis is compared with the tested tensile strain capacity of concrete (TSC) by Tongaroonsri (2009) and if the $\varepsilon_{res,\ ten}$ is higher than tensile strain capacity then the mass concrete structure is predicted crack. Figure 3.5 shows the comparison between the predicted $\varepsilon_{res,\ ten}$ on top surface and TSC of the concrete. By comparing the analyzed restrained strain with the test results of TSC by Tongaroonsri (2009), the footing was predicted to crack since early age before the removal of the insulation material. From the comparison using the proposed model and tested TSC, it can be concluded that the model was satisfactory to predict thermal cracking of the footing.

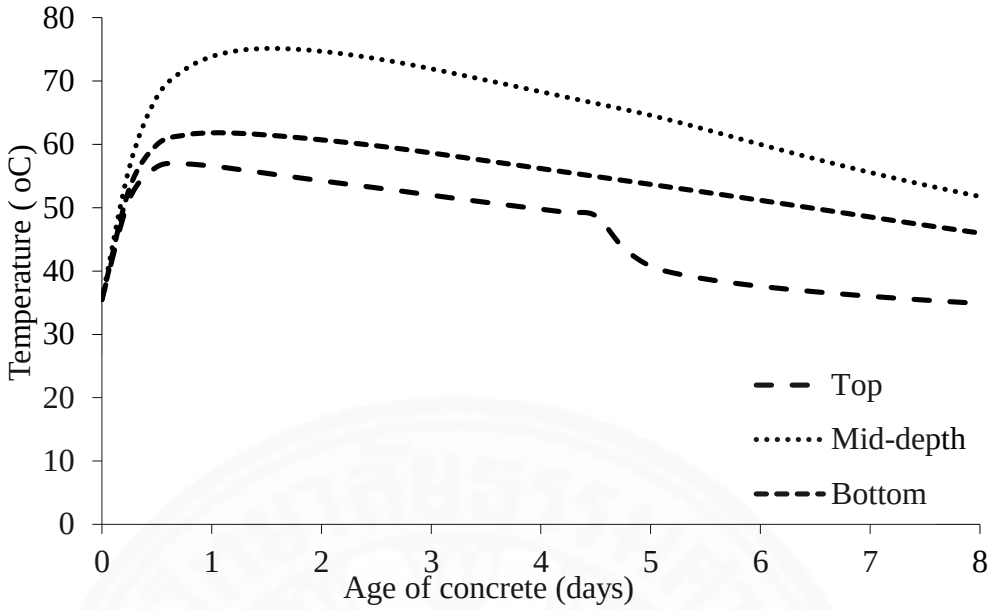

Figure 3.4 Predicted temperatures at top, center and bottom parts (Choktaweekarn,2008)

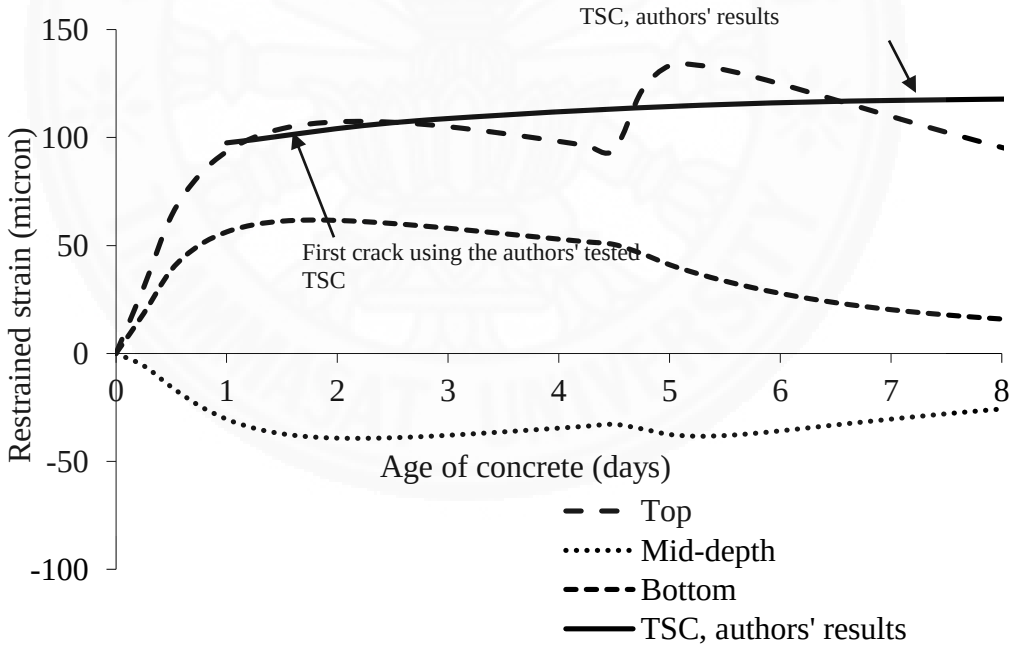

Figure 3.5 Comparison between tensile strain capacity and predicted restrained strain in lateral direction (Choktaweekarn,2008)

3.2 Shrinkage Model

In this study, the previously proposed models for predicting free shrinkage of concrete is used in the analysis. Details of the models are given by Tongaroonsri (2009). Total shrinkage of concrete is the summation of autogenous shrinkage and drying shrinkage which can be calculated by using Eq. (11).

$$\varepsilon_{TS}(t,t_0) = \varepsilon_{as}(t,t_0) + \varepsilon_{ds}(t,t_0) \qquad (11)$$

Where: $\varepsilon_{TS}(t,t_0)$ is total shrinkage strain from age of t_0 to t (micron), $\varepsilon_{as}(t,t_0)$ is autogenous shrinkage strain from age of t_0 to t (micron), $\varepsilon_{ds}(t,t_0)$ is drying shrinkage strain from age of t_0 to t(micron), T is age of concrete (days) and t_0 is age at start of drying of concrete (days)

When calculating the total shrinkage, curing period (t_0) and type of curing must be considered because they affect values of autogenous shrinkage and drying shrinkage. In case of water curing, water can continuously penetrate into the concrete, resulting in insignificant autogenous shrinkage and drying shrinkage during the water curing period especially for thin concrete members. In case of seal-cured concrete or moist-cured concrete (wet burlap), there is no water or insufficient water, respectively, supplied into the concrete, so autogenous shrinkage can occur during the seal curing or moist curing period while there is no drying shrinkage because of no drying can occur on the concrete surface. In this condition, the total shrinkage includes the autogenous shrinkage from the time of final setting to the time considered. More details of the autogenous shrinkage model and drying shrinkage model are mentioned in sections 3.2.1 and 3.2.2, respectively.

3.2.1 Autogenous Shrinkage Model

Unrestrained autogeneous shrinkage was calculated by using a two-phase model concept, as shown in Eq. (12), for calculating concrete autogeneous shrinkage strain. Shrinkage occurs only in paste phase whereas the aggregate phase is considered to restrain the paste shrinkage by their particle interaction. A two-phase material model shown in Eq. (13), taking into account the restrained shrinkage due to aggregate particle interaction proposed by Tatong, 2001, was adopted in this analysis. This model involved the stiffness, equilibrium condition and strain compatibility of paste phase and aggregate phase.

$$\varepsilon_{as}(t,t_0) = \varepsilon_{as}(t) - \varepsilon_{as}(t_0) \qquad (12)$$

$$\varepsilon_{as}(t) = \frac{\varepsilon_{po}(t)\cdot E_p(t)\cdot(1-n_a)}{E_p(t)+E_a} \qquad (13)$$

Where: $\varepsilon_{as}(t,t_0)$ is the autogenous shrinkage strain from age t_0 to t (micron), $\varepsilon_{po}(t)$ is the free shrinkage of paste in concrete at the considered age (micron). n_a is the volume concentration of aggregate. E_p (t) is stiffness of paste phase at considered age (kg/cm^2). E_a is stiffness of aggregate phase (kg/cm^2). t_0 is the age at start of drying of concrete (days). t is the considered age (days).

3.2.2 Drying Shrinkage Model

Unrestrained drying shrinkage was calculated by using Eqs. (14) - (17).

$$\varepsilon_{ds}(t,t_0) = \varepsilon_{dsm} \cdot \beta(t,t_0) \cdot \beta(h) \quad (14)$$

$$\varepsilon_{dsm} = \left(663 - 291\exp\left(-7.26\left(\frac{w}{b}\right)^{5.26}\right)\right) \cdot K_1 \cdot K_2 \cdot K_3 \cdot K_4 \quad (15)$$

$$\beta(h) = 1.73\left(1 - \left(\frac{RH}{100}\right)^3\right) \quad (16)$$

$$\beta(t,t_0) = \left[\frac{(t-t_0) \cdot B \cdot P}{(t-t_0) + A \cdot G \cdot N \cdot F}\right] \quad (17)$$

Where: $\varepsilon_{ds}(t,t_0)$ is the drying shrinkage strain of concrete from age t_0 to t (micron). ε_{dsm} is drying shrinkage strain of concrete at 150 days of age (micron). $\beta(h)$ is a factors for considering the effect of relative humidity. $\beta(t,t_0)$ is the time-dependent function component. K_1, K_3 and K_4 are factors considering the effect of the volume concentration of aggregate, fly ash content, and curing condition (curing type and curing period), respectively. K_2 and P are coefficients for cement type. A and B are factors considering the effect of strength of concrete. G is a factor considering the effect of volume to surface ratio. N and F are factors considering the effect of aggregate content and fly ash content. RH is relative humidity (%).t_0 is the age at start of drying of concrete (days). t is the considered age (days).

The drying shrinkage model takes into account the effect of cement type, fly ash, water to binder ratio, paste content, curing condition, ambient relative humidity and volume to surface area ratio (Tatong,2001). All of these parameters significantly affect the drying shrinkage of concrete.

Verification of the total shrinkage model was performed on concrete specimens exposed to drying condition. Experiments were conducted on concrete with different water to binder ratios, fly ash content, paste content, curing period and curing type. The results obtained from total shrinkage tests by the authors' research group and data obtained from various researchers were compared with the model of total shrinkage of concrete. An example of verification is shown in Figure 3.6. It was found that the results obtained from the model were in good agreement with the test results (Tongaroonsri,2009).

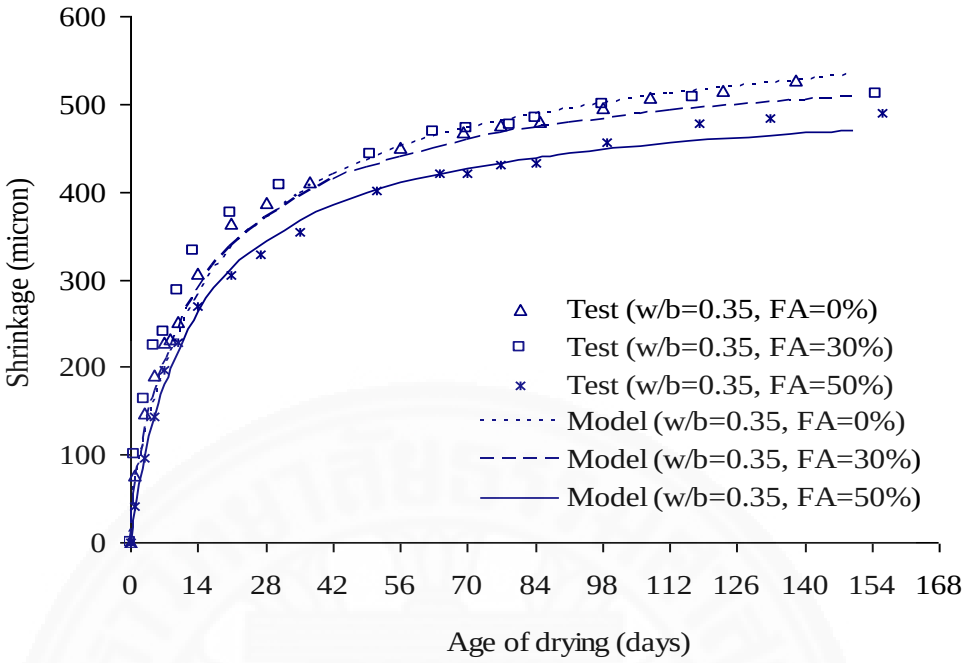

Figure 3.6 Comparisons between test results of total shrinkage of concrete and the computed results from the model of concrete with various replacement percentage of fly ash with w/b of 0.35, n_a=0.676, temperature= 28ºC, RH=75% (water curing=7 days) ,(Tongaroonsri,2009).

Chapter 4

Modification of Existing Analytic Method

4.1 Mechanisms of cracking due to heat of hydration and shrinkage in mass concrete

As shown in Figures 4.1 and 4.2, for internal restraint, the restrained strain of mass concrete is contributed from the thermal strain and shrinkage strain. The restrained strain caused by thermal strain in mass concrete is in compression at the inner core and in tension at the surface, leading to risk of thermal cracking near the surface. The restrained strain caused by shrinkage strain was separated into two parts. In the first part, autogenous shrinkage strain is the strain that occurs in the whole body of the mass concrete. Based on degree of hydration, the highest autogenous shrinkage strain occurs in the center part which has the highest degree of hydration reaction. The second part is the drying shrinkage strain that takes place on the exposed surfaces of the mass concrete. The effect of drying shrinkage exists up to a depth that has no moisture loss. The resulting restrained strain in mass concrete is derived by superimposing the thermal and shrinkage strains as shown in Eqs. (18) and (19).

$$\varepsilon_{res}(t) = \varepsilon_{res,sh}(t) + \varepsilon_{res,th}(t) \qquad (18)$$

$$\varepsilon_{res,sh}(t) = \varepsilon_{res,as}(t) + \varepsilon_{res,ds}(t) \qquad (19)$$

Where: $\varepsilon_{res}(t)$ is the restrained strain resulted from combined thermal and shrinkage effects, while $\varepsilon_{res,th}(t), \varepsilon_{res,sh}(t), \varepsilon_{res,as}(t)$ and $\varepsilon_{res,ds}(t)$ are the restrained strains of concrete caused by thermal effect, by total shrinkage, by autugenous shrinkage and by drying shrinkage at the considered age, respectively (micron) and t is the considered age (days).

In general, at early age, insulation curing is recommended to be used for mass concrete for the benefit of thermal crack control. During the stage of insulation curing, there is no loss of water to the surrounding. In other word, drying shrinkage is insignificant during this stage and it is neglected during the insulation curing period. After the removal of insulation materials, there is loss of water at the concrete surface due to evaporation if the exposed surface is not protected from drying. As a result both autogenous shrinkage and drying shrinkage are considered.

An existing analytical method to predict semi-adiabatic temperature and thermal cracking in mass concrete proposed by Choktaweekarn (2008) was used in this study. It was modified in this study to take into account the effect of autogenous and drying shrinkages in mass concrete. The free shrinkage strain used in the analysis is calculated by using the model proposed by Tongaroonsri (2009), as shown in Eqs. (12) to (13). The calculated temperature of concrete at each position is used as the

input in the shrinkage model to calculate the autogenous shrinkage at each position. As shown in Figure 4.1, the autogenous shrinkage at the mid-depth of mass concrete is higher than that at the top surface. This is because the temperature at the mid-depth of mass concrete is higher than that at the surface, then the degree of hydration at mid-depth is higher. From this reason, based on degree of hydration, autogenous shrinkage strain at the mid-depth is higher than that at the concrete surface. The free shrinkage strain at each position was input into the FEM program in the form of temperature change as shown in Eq. (20).

$$\Delta T_{sh}(t) = \varepsilon_{sh}(t) / CTE(t) \qquad (20)$$

Where: $\varepsilon_{sh}(t)$ is the input free shrinkage strain at the considered age (micron). CTE(t) is the coefficient of thermal expansion coefficient at the considered age (micron/°C) and ΔT_{sh} (t) is the shrinkage equivalent temperature change at the considered age (°C) and t is the considered age (days).

In the restrained strain analysis, the restrains from thermal and shrinkage effects are analyzed separately. At the end of the analysis, both restrained strains are superimposed as illustrated in Figure 4.1 and Figure 4.2.

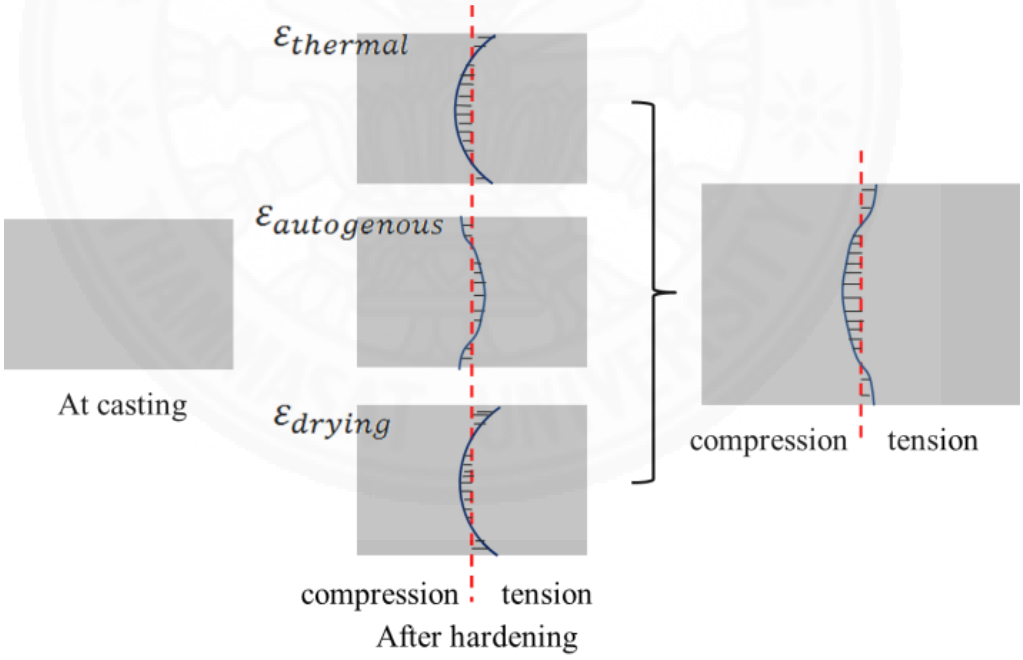

Figure 4.1 Strain distributions caused by thermal effect, autogenous shrinkage and drying shrinkage in mass concrete

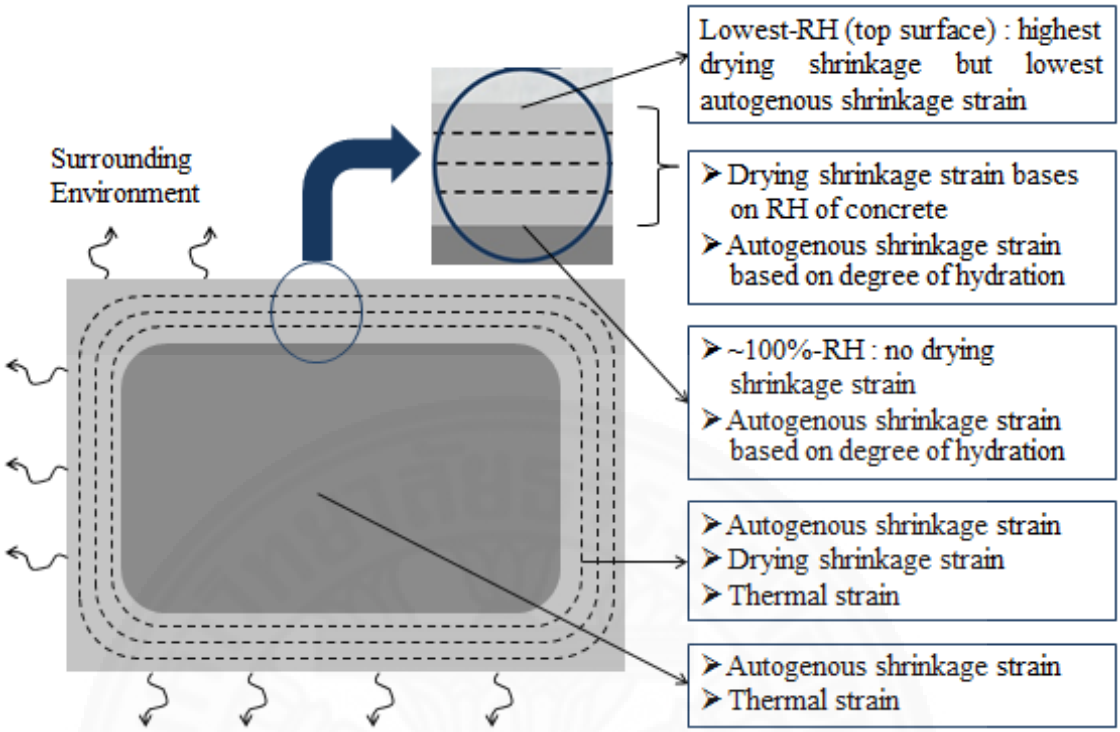

Figure 4.2 Type of restrained strain in different parts of the mass concrete

Chapter 5

Analytical Results and Discussion

5.1 Thermal and Shrinkage Analysis of Mass Concrete Footing

A concrete block with a size of 5.5 x 11 x 2.5 m was used as an example to simulate the effect of shrinkage on mass concrete. A concrete block is shown in Figure 5.1. This concrete block was assumed to be cured by insulation curing for 7 days. The insulation curing profiles are steel formwork and 2-inch thick foam as shown in Figure 5.2. Mix proportion and 28-day compressive strength of the concrete used in the analysis are shown in Table 5.1. Environment conditions used in the analysis are shown in Table 5.2.

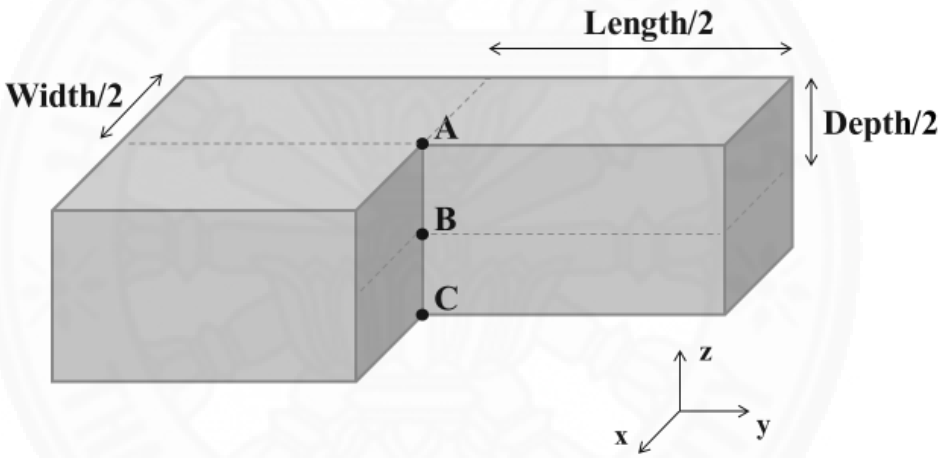

Figure 5.1 An example of concrete block used in the analysis

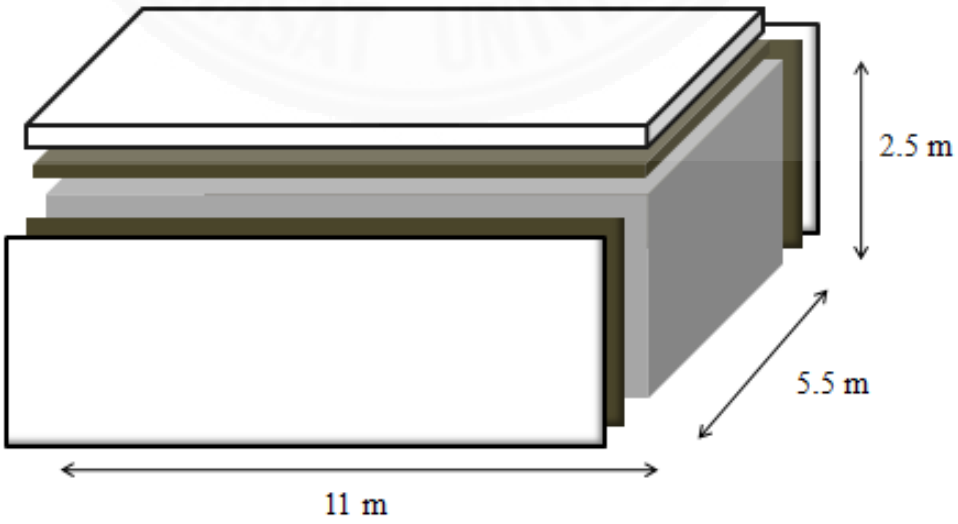

Figure 5.2 An example of concrete block with insulation curing formworks

Table 5.1 Mix proportion of concrete (in kg/m^3)

Cement	Water	Sand	Gravel	28 days Compressive Strength (MPa)
294	150	860	1123	25.8

Table 5.2 Environmental conditions

Ambient temperature	32°C
Initial temperature of concrete	32°C
Wind speed	4 m/s

A flow chart of the analytical process for simulating cracking of mass concrete is shown in Figure 5.3. The adiabatic temperature of the mixture was obtained when knowing mix proportion. Concrete mix proportion and properties of cementitious materials were used for calculating adiabatic temperature. Predicted adiabatic temperature is shown in Figure 5.4.

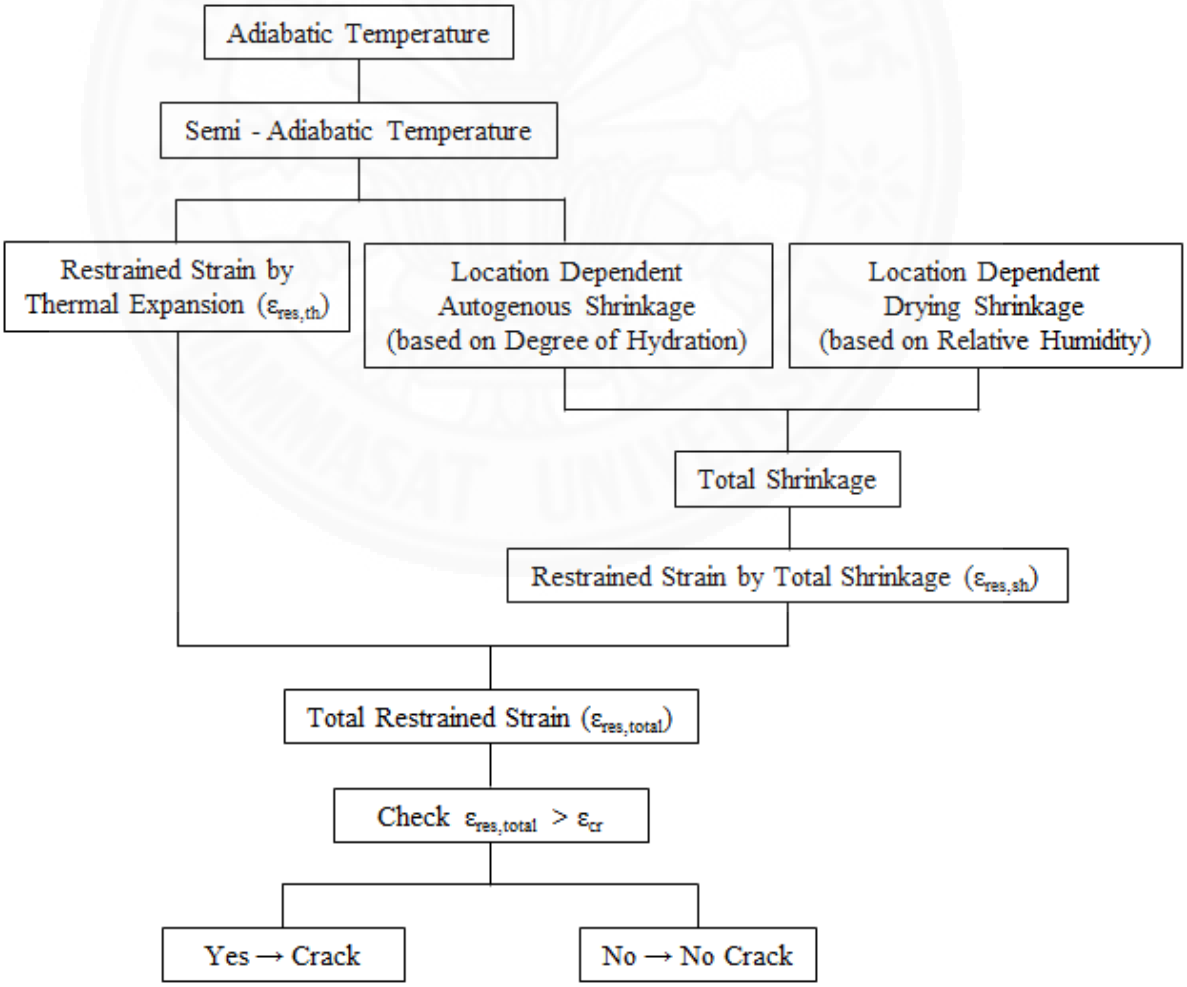

Figure 5.3 A flow chart of the analysis for simulating cracking of mass concrete

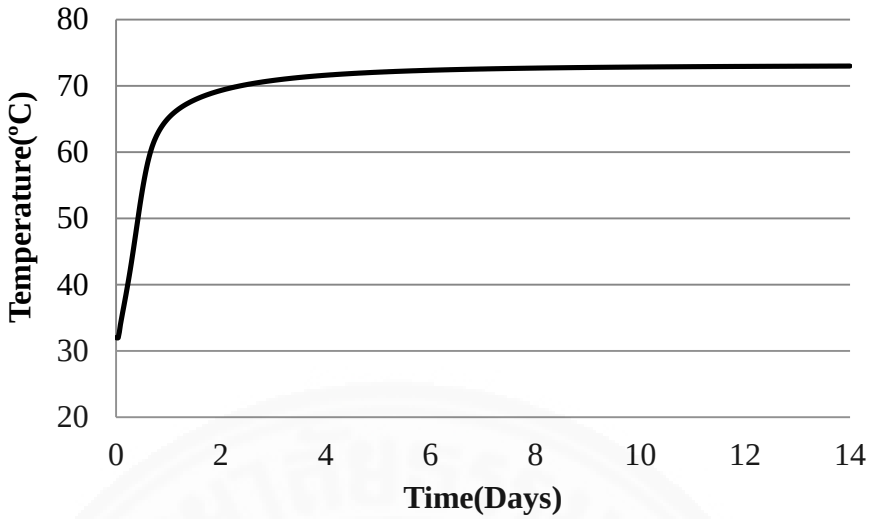

Figure 5.4 Predicted adiabatic temperature of the sample mixture

Thermal properties of concrete such as specific heat, thermal conductivity and cumulative heat generation, dimension of structure, ambient temperature, boundary conditions and convection heat transfer coefficient were used as the inputs to analyze the semi-adiabatic temperature rise of concrete. Thermal properties of concrete used in the analysis are shown in Table 5.3.

Predicted semi-adiabatic temperatures are shown in Figures 5.5 and 5.6. Different colors mean different temperature of each layer. The results in Figure 5.6 show that the temperature at location B (mid-depth as shown in Figure 5.1) is higher than that at location A and C (the top and the bottom surfaces, respectively).

Table 5.3 Thermal properties of concrete

Specific heat	0.2134	kcal/kg °C
Thermal conductivity	2.1139	kcal/m.hr °C
Coefficient of Thermal Expansion	7	micron
Heat transfer coefficient	6.469	kcal/m^2.hr °C (before insulation removal)
	18.4	kcal/m^2.hr °C (after insulation removal)
Modulus of Elasticity	24000	MPa
Poisson's ratio	0.2	

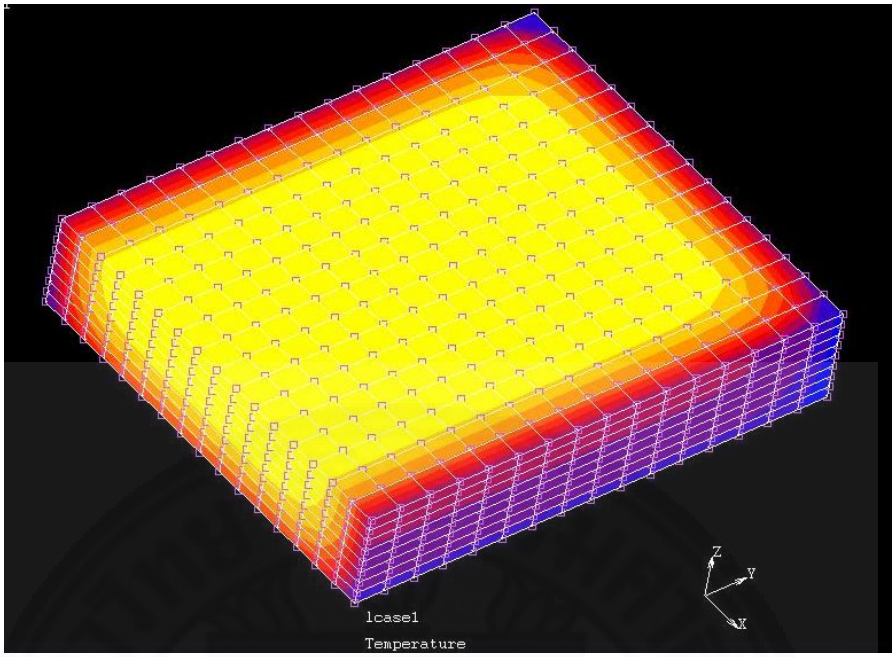

Figure 5.5 Predicted semi-adiabatic temperatures

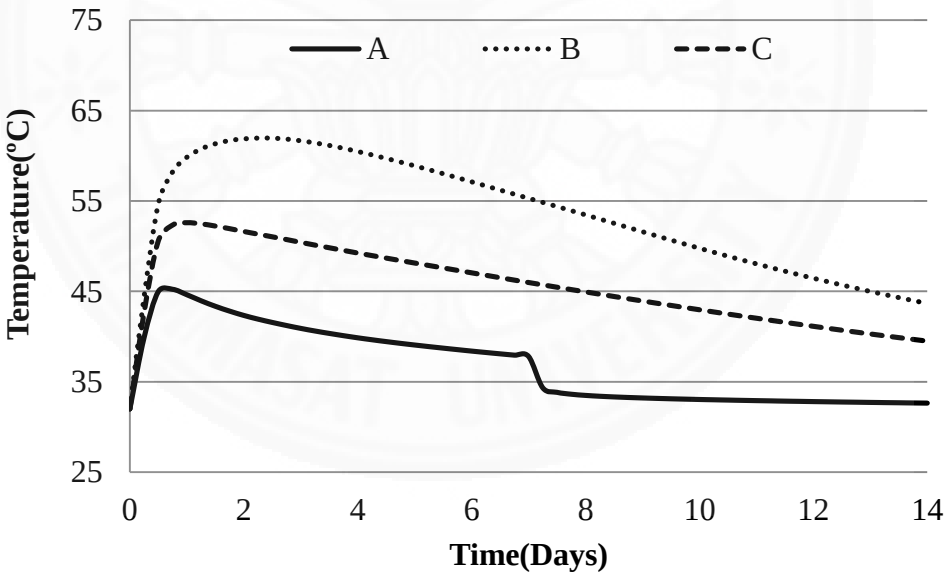

Figure 5.6 Predicted semi-adiabatic temperatures at location A, B and C (top surface, mid-depth and bottom surface, respectively)

From Figure 5.6, the temperature gradients between the mid-depth and the surface of the concrete were used to analyze the restrained strain due to differential thermal deformation where modulus of elasticity, Poisson's ratio and coefficient of thermal expansion were used as the input of the computation.

Restrained thermal strains at locations A, B and C in Figure 5.1 of concrete are shown in Figure 5.7.

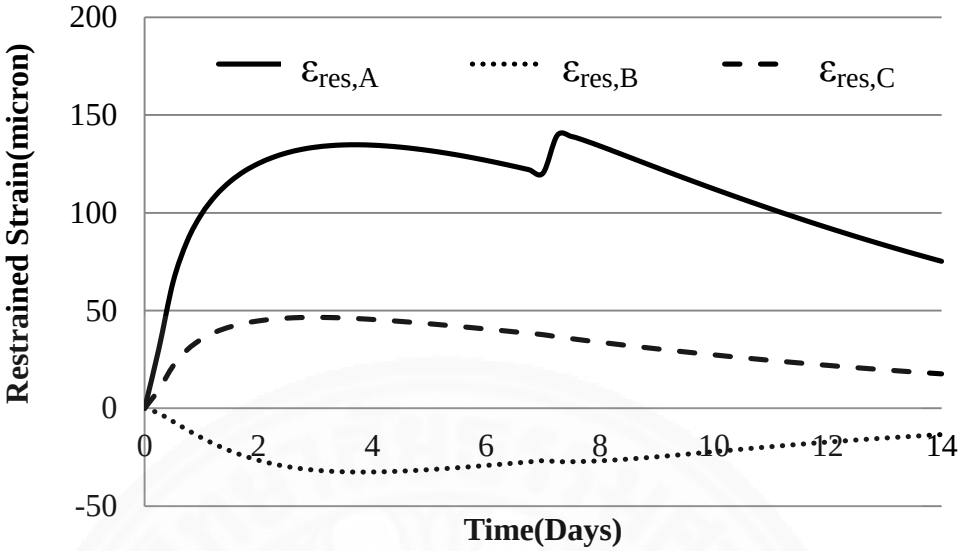

Figure 5.7 Restrained thermal strain at in the concrete

Figure 5.7 shows the restrained strain without effect of shrinkage consideration. While $\varepsilon_{res,A}$, $\varepsilon_{res,B}$ and $\varepsilon_{res,C}$ are restrained thermal strains at locations A, B and C, respectively. The restrained strain by thermal effect at the surface of concrete shows two peak values, one at early age and another at the day the insulation curing material is removed (7 days), and after that decreases continuously. It should be noted that the effect of shrinkages in the 2nd peak (at the time of insulation material removal) is not discussed. The target is to demonstrate effect of autogenous shrinkage at the early age (before insulation material removal) and drying shrinkage after drying exposure (after removing the insulation material). At the point of insulation material removal, the effect of autogenous shrinkage is smaller than that at the earlier age. Also, the effect of drying shrinkage is still not seen at that time since the concrete surface is just exposed to drying.

To consider effect of restrained strain by shrinkage, free shrinkage strains were used as input at each location. Firstly, the differential autogenous shrinkage came from the effect of temperature gradient in Figure 5.6. These temperatures were used to compute the degree of hydration, and degree of hydration affects autogenous shrinkage as shown in Figure 5.7. It can be seen that the inner portion (B) is in tension while the near surface portions (A and C) are in compression because the inner portion with higher temperature has higher autogenous shrinkage. The inner portion is in self-equilibrium with the lower autogenous shrinkage portions near the surfaces.

The analytical results of restrained strain at mid- depth (B) and surface (A) are shown in Figure 5.8. Figure 5.9 shows that autogenous shrinkage strain at the mid- depth is higher than that near the top surface due to higher temperature and degree of hydration, while the lowest autogenous shrinkage at the top surface is due to lower temperature and moisture content (due to drying near the exposed surface), leading to lower degree of hydration reaction, especially at the early age.

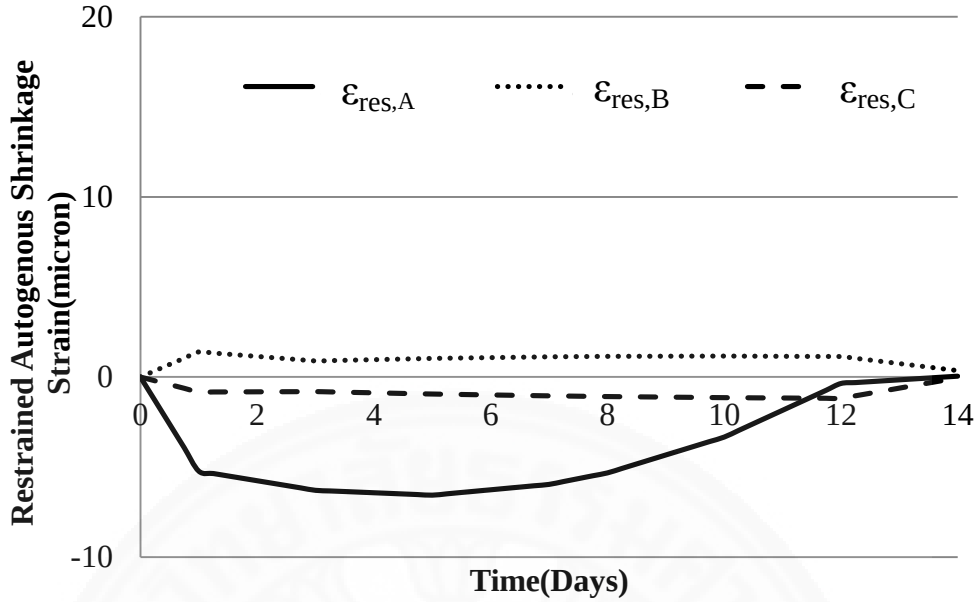

Figure 5.8 Restrained autogenous shrinkage strains

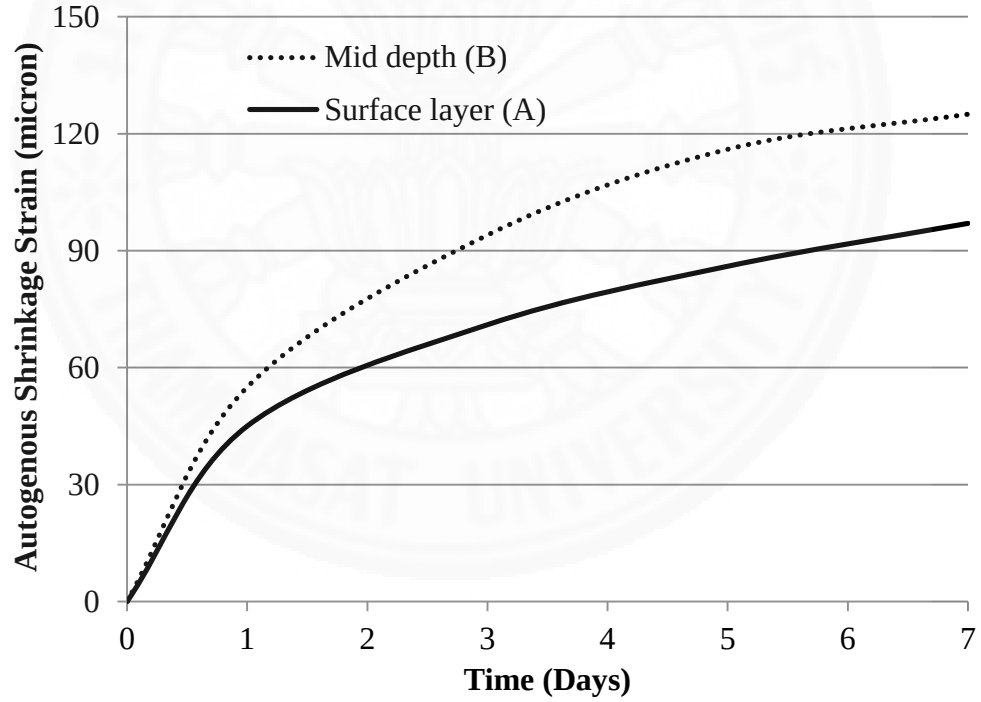

Figure 5.9 Different autogenous shrinkage at mid-depth (location B) and surface layer (location A) due to different degree of hydration

The analytical results at mid-depth and top surface at the center axis of the mass concrete were used in the discussions. The free shrinkage strain at each position was input into the FEM program in the form of temperature change as shown in Eq. (20). The restrained autogenous shrinkage strain was computed separately as shown in Figure 5.8 and the summation of the restrained strains by thermal and autogenous shrinkage effects are shown in Figure 5.10.

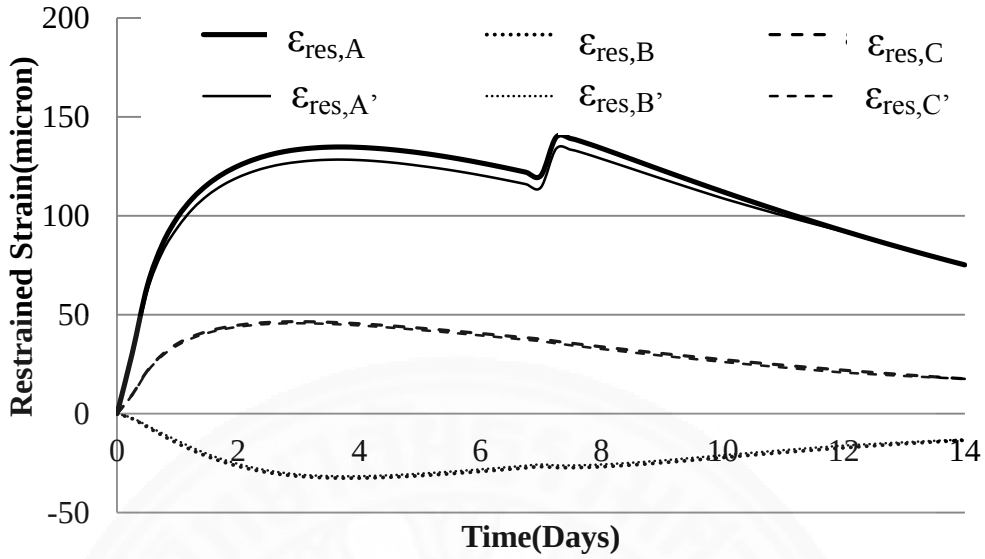

Figure 5.10 Combined restrained thermal and autogenous shrinkage strains

$\varepsilon_{res,A'}$, $\varepsilon_{res,B'}$ and $\varepsilon_{res,C'}$ are the combined restrained thermal-autogenous shrinkage strain at locations A, B and C, respectively. It can be seen from Figure 5.10 that the combination of the autogenous shrinkage strain with thermal strain results in reduction of restrained strain near the top surface of the concrete (comparing $\varepsilon_{res,A}$ 9with $\varepsilon_{res,A'}$). The restrained strain by only thermal strain ($\varepsilon_{res,A}$) is reduced by about 10 micron by the restrained autogenous shrinkage strain.

The restrained total shrinkage strain was also computed separately, the results as shown in Figure 5.11. Free total shrinkage strain in Figure 5.12 was used as input at each location.

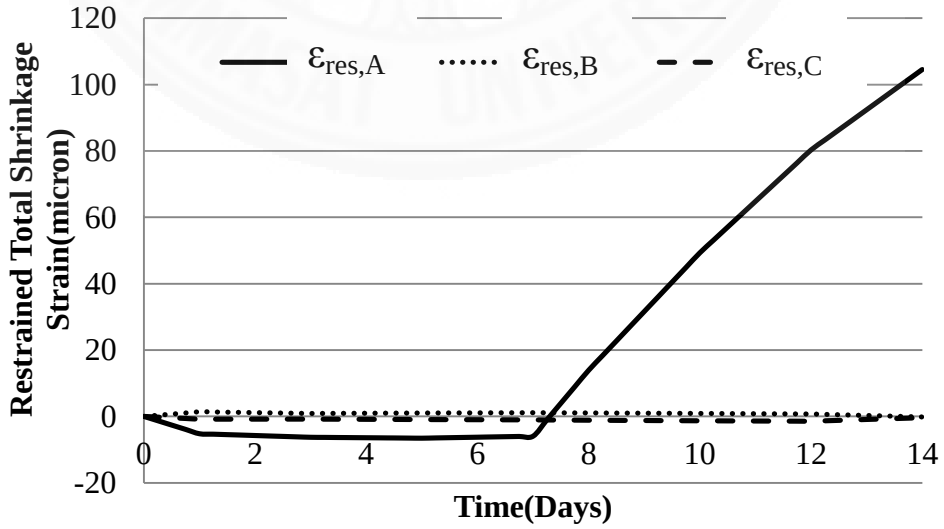

Figure 5.11 Restrained total shrinkage strains

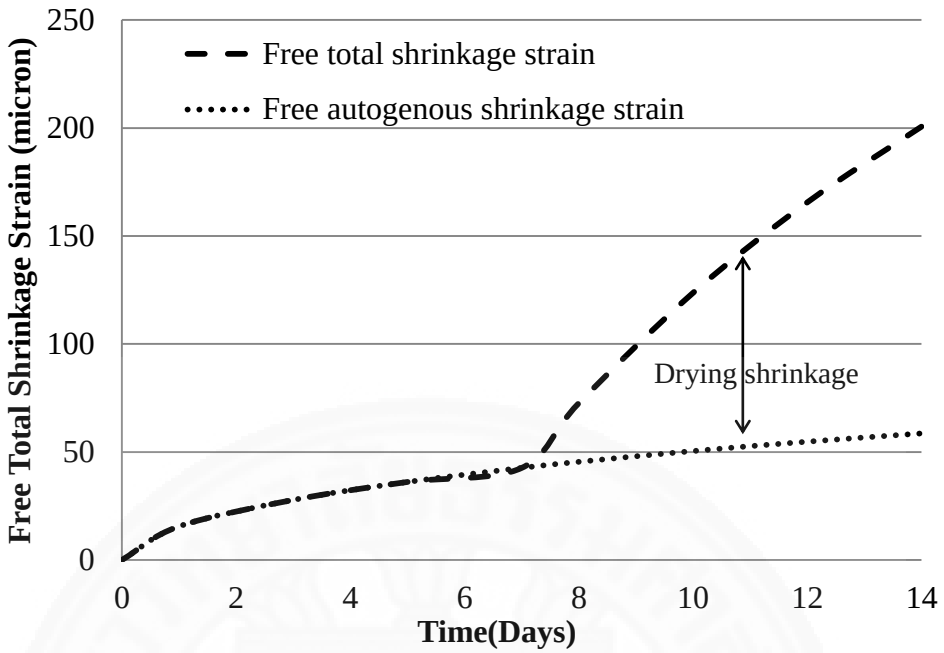

Figure 5.12 Free total shrinkage strains at the top surface of concrete

Figure 5.12 shows the free total shrinkage strain caused by summation of autogenous and drying shrinkages. Autogenous shrinkage reduces restrained strain during the insulation curing period but drying shrinkage increases restrained strain of the mass concrete after the insulation curing period. It was assumed that there was no drying shrinkage during the insulation curing period.

After combining restrained strain due to total shrinkage with thermal restrained strain, the net restrained strains in Figure 5.13 decrease at early age by the effect of autogenous shrinkage. After insulation curing material is removed (7 days), restrained drying shrinkage strain shows great effect on tension zone and leads to cracking at the mass concrete top surface when the net restrained strain is greater than tensile strain capacity (TSC) as shown in Figure 5.13. It is therefore recommended not to let the exposed surface of concrete dry immediately after the removal of insulation.

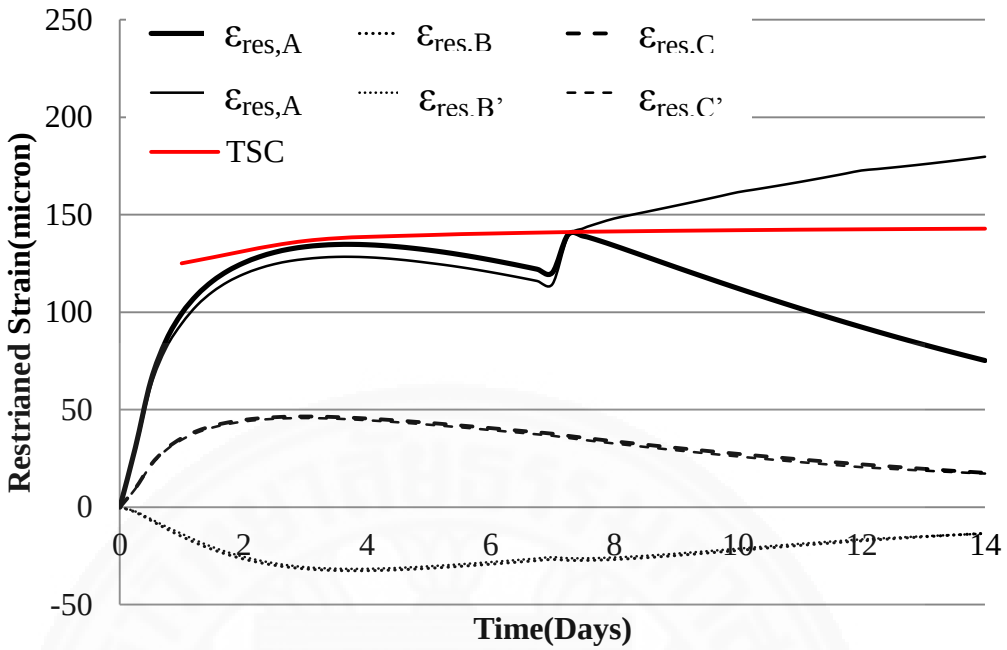

Figure 5.13 The net restrained strains

5.2 Thermal and Shrinkage Analysis of a Water Storage Structure

The scope of this work is to conduct the analysis of thermal and shrinkage strains of structure components of a water storage structure which may have potentials of thermal and shrinkage cracking as an example of real application. The restrained strains caused by temperature gradient and shrinkage are computed. If the restrained strain at any location is higher than tensile strain capacity, that location of the structure is evaluated to crack. Finally, the proper concrete mix proportion, construction method and curing method are recommended. In the case that the structure has possibility to crack, an appropriate amount of reinforcement will be recommended in order to control the crack width to be within the acceptable value. The scope of this work also includes other important works which are the recommendation for formwork design and material. The drawing of water storage is shown in Figure 5.14 and water storage elements used for the analysis are shown in Figure 5.15.

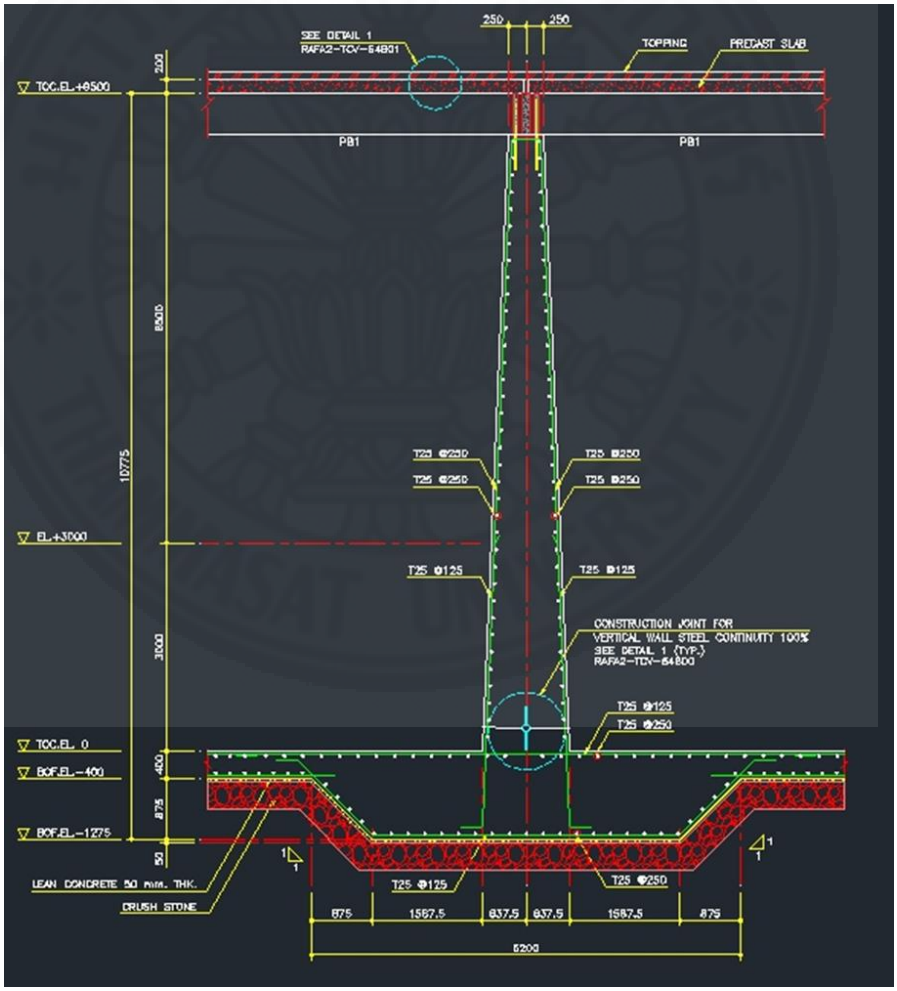

Figure 5.14 Drawing details of the water storage structure

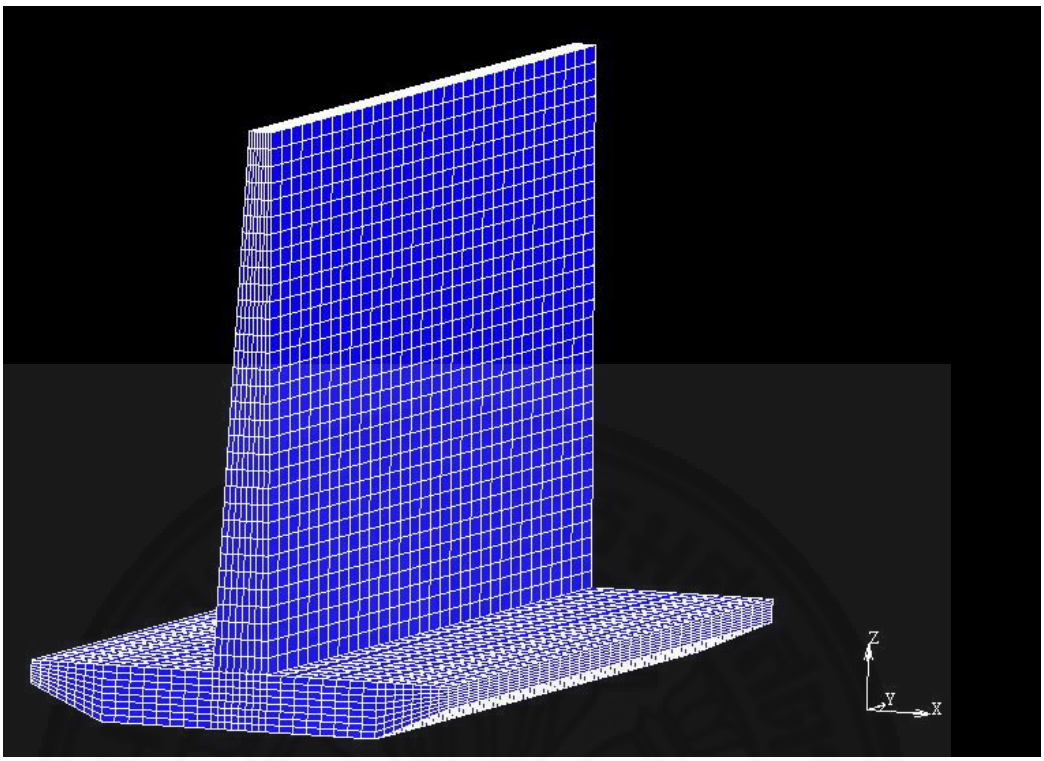

Figure 5.15 Water storage elements used for the FEM analysis

The environmental data used in the thermal and shrinkage analysis of bottom slab and wall are shown in Table 5.4

Table 5.4 Environmental conditions

Ambient temperature	38°C
Initial temperature of concrete	32°C
Wind speed	10 m/s

Insulation curing is used in the analysis. It is assumed that all surfaces of the bottom slab and wall are insulated immediately after casting until the end of the curing period.

5.2.1 Bottom slab Temperature and restrained strain analysis

Table 5.5 shows the recommended mix proportion for the bottom slab. Table 5.6 shows the thermal properties and mechanical properties used in the analysis of the bottom slab. The temperature and restrained strain of bottom slab are analyzed as follows.

Table 5.5 Recommended mix proportion for bottom slab (in kg/m^3)

Cement	Fly Ash	Water	Sand	Gravel	28 days Compressive Strength (MPa)
228	152	137	838	1098	38

Table 5.6 Thermal properties and mechanical properties of the concrete used in the analysis of the bottom slab

Specific heat	0.2148	kcal/kg °C
Thermal conductivity	2.0626	kcal/m.hr °C
Coefficient of Thermal Expansion	7	micron
Heat transfer coefficient	7.96	kcal/m^2.hr °C (before insulation removal)
	39.38	kcal/m^2.hr °C (after insulation removal)
Modulus of Elasticity	24000	MPa
Poisson's ratio	0.2	

Figure 5.16 shows the analysis of temperatures and restrained strains at different locations of bottom slab, i.e. the center of bottom slab (Point A), the top of the side face of the bottom slab (Point B), the mid depth of the side face of the bottom slab (Point C) and the bottom surface of the side face of the bottom slab (Point D). For an initial temperature of concrete (T_{ini}) of 32^{o}C, the predicted temperatures and restrained strain are shown in Figure 5.17.

From the analytical results, Point A shows the highest temperature with the peak value lower than 60^{o}C (Figure 5.17). The restrained strain in tension at Point B was the highest (see Figure 5.18), then the result of the top surface was used to describe the maximum restrained strain in tension (ε_{res}) in this analysis. The predicted ε_{res} of bottom slab was compared with tensile strain capacity (TSC) of the concrete and it can be seen that ε_{res} is lower than TSC (Figure 5.18) then the bottom slab is evaluated safe when using the proposed mix proportion (T_{ini} of 32^{o}C with 4-day insulation curing). In this case the insulation curing is done by using 2-in thick foam.

However, after removal of insulation material at 4 days of insulation curing (Figure 5.18), the temperature at the surfaces of Point A, B and C decrease rapidly and this causes the increase of temperature gradient of the mass concrete. It also causes the restrained strains on their surfaces to increase rapidly due to the increase of temperature gradient in the concrete.

It is also recommended not to let the surface of concrete dry after the removal of the insulation material to prevent cracking due to drying shrinkage. It is not recommended to use cold water in the curing process after insulation curing.

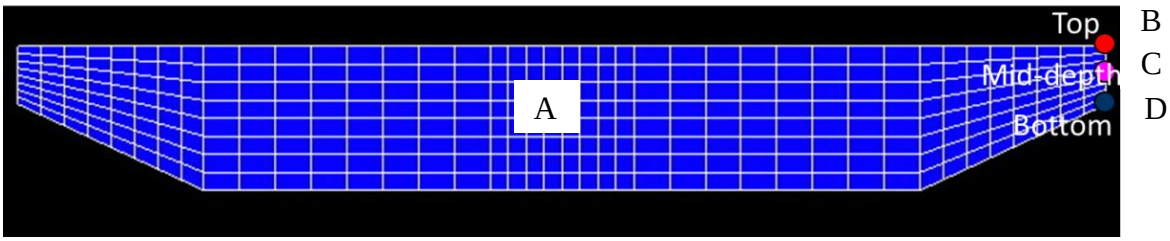

Figure 5.16 Locations of temperature and restrained strain analysis of bottom slab

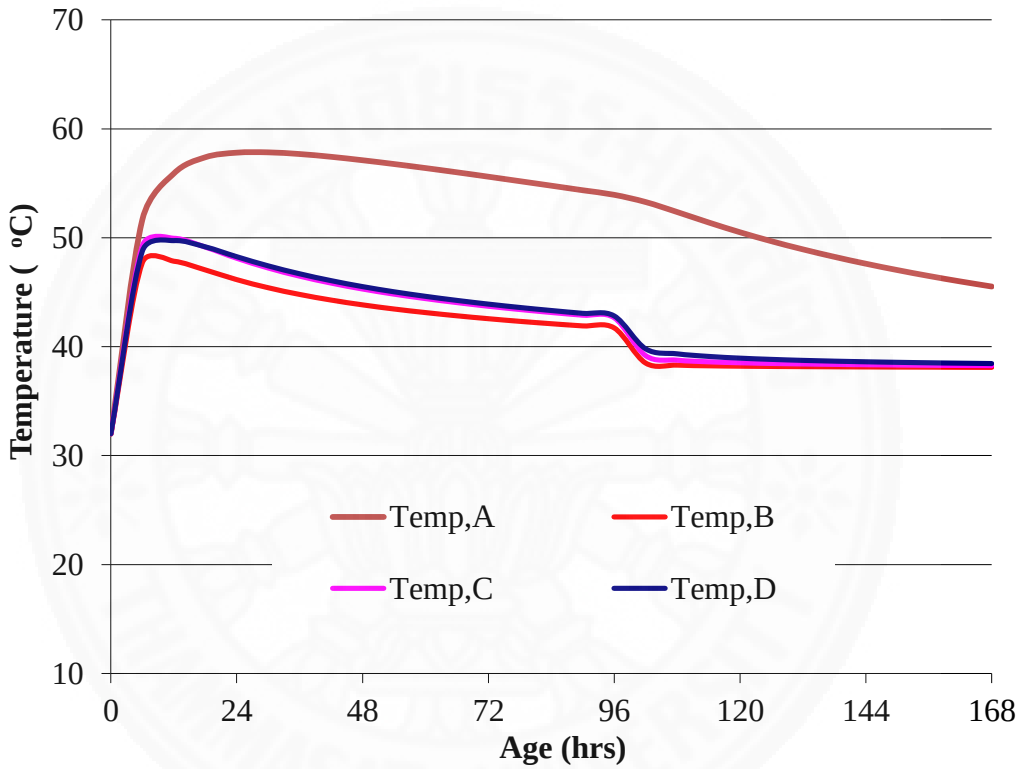

Figure 5.17 Predicted temperature of bottom slab using the proposed mix proportion, T_{ini} = 32°C

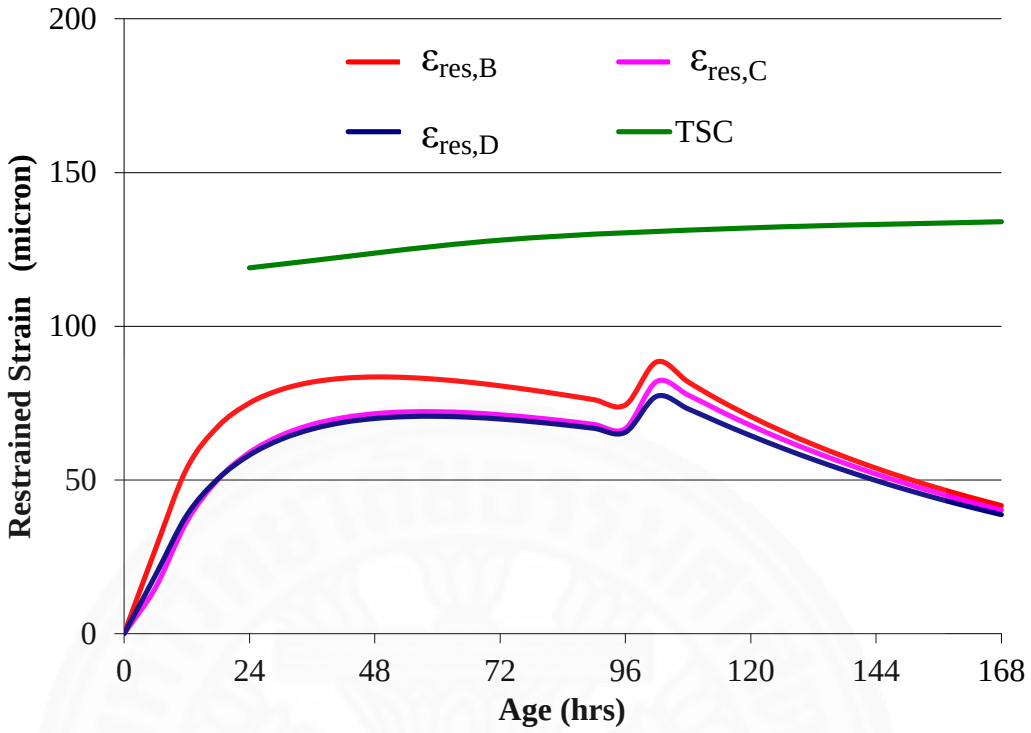

Figure 5.18 Predicted restrained strain of bottom slab using the proposed mix proportion, T_{ini} = 32°C

5.2.2 Wall – Temperature and restrained strain analysis

Table 5.7 shows the recommended mix proportion for wall. Table 5.8 shows the thermal properties and mechanical properties used for the analysis of the wall. The restrained strain of wall cast by using this mix proportion was analyzed.

Table 5.7 Recommended mix proportion for wall (in kg/m^3)

Cement	Fly Ash	Water	Sand	Gravel	28 days Compressive Strength (MPa)
266	114	152	838	1098	38

Table 5.8 Thermal properties and mechanical properties used in the analysis of the concrete wall

Specific heat	0.2151	kcal/kg °C
Thermal conductivity	2.0656	kcal/m.hr °C
Coefficient of Thermal Expansion	7	micron
Heat transfer coefficient	7.96	kcal/m^2.hr °C (before insulation removal)
	39.38	kcal/m^2.hr °C (after insulation removal)
Modulus of Elasticity	24000	MPa
Poisson's ratio	0.2	

The finite element meshes of wall and bottom slab are shown in Figure 5.19. For initial temperature of concrete (T_{ini}) of 32°C, the restrained strains due to thermal expansion of the different nodes (Point A, B, C) on the wall are shown in Figure 5.20. It can be seen that all restrained strains of those nodes are lower than the tensile strain capacity (TSC).

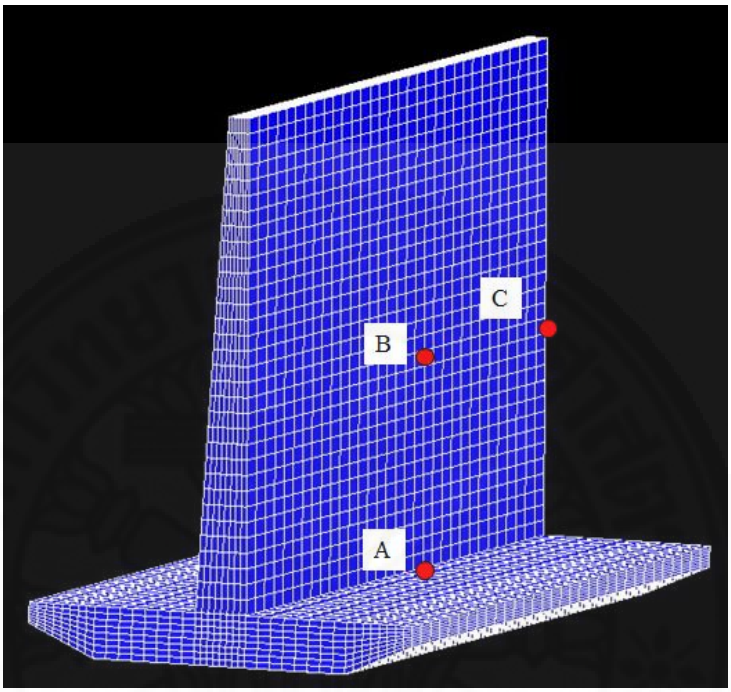

Figure 5.19 Finite element meshes of wall and bottom slab

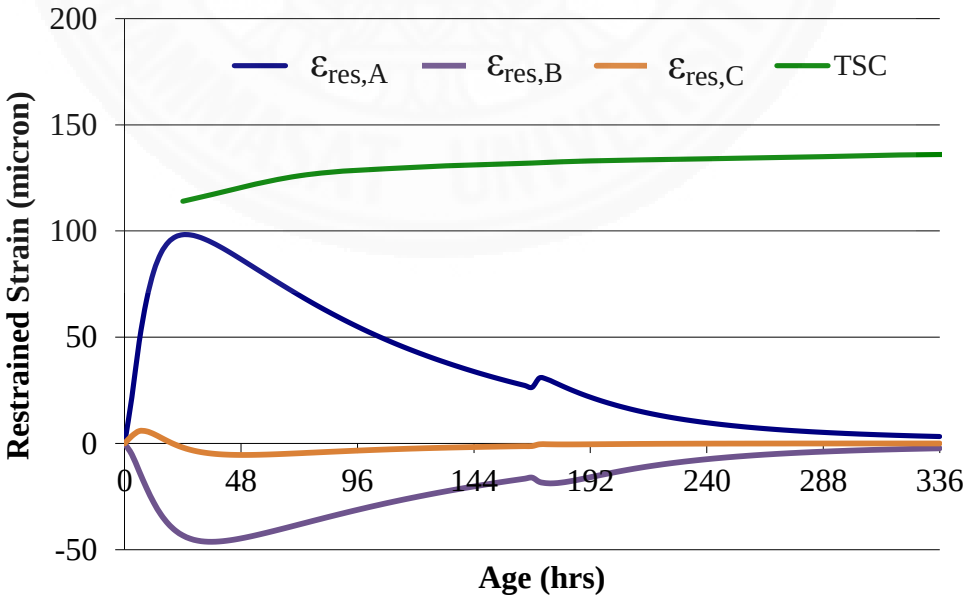

Figure 5.20 Restrained strain (ε_{res}) due to thermal expansion of different nodes on the wall compared with tensile strain capacity (TSC)

Besides the restrained strain analysis due to thermal expansion, the restrained strain analysis due to shrinkage has to be taken into account since the wall structure is restrained by the bottom slab. Figure 5.21 shows the finite element meshing of wall and bottom slab used in this analysis and the illustration of the possible shrinkage crack location.

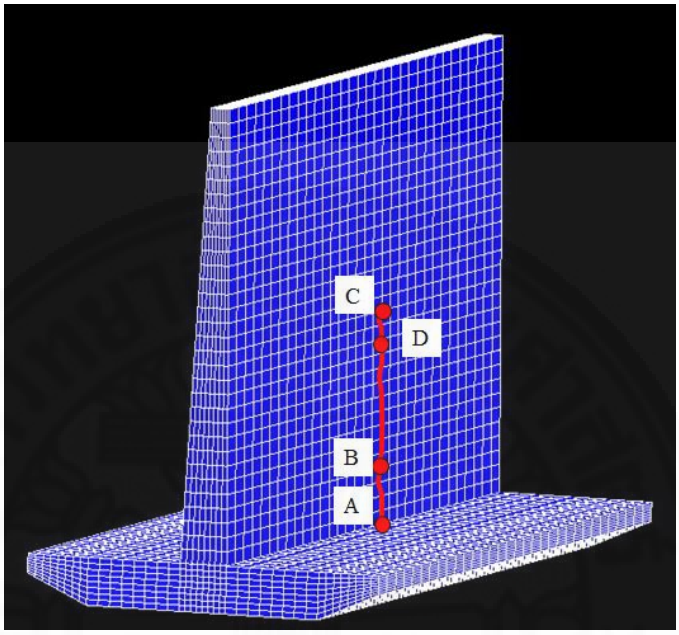

Figure 5.21 Finite element meshes of wall and bottom slab and the possible shrinkage crack location

Figure 5.22 shows the results of the analysis of restrained strain of wall at ultimate shrinkage at possible location of shrinkage crack at various nodes (Point A, B, C) compared with tensile strain capacity (TSC), it can be seen that the restrained strains of Point A, B and C are higher than the tensile capacity. However, the wall structure is restrained by the bottom slab, only considering ultimate shrinkage of wall is not sufficient. As the wall structure is restrained by the bottom slab, the differential shrinkage between wall and bottom slab should be included in the analysis. The results of the analysis taking into account the differential shrinkage are shown in Figure 5.23. This analysis was conducted based on the assumption that the wall structure was cast 30 days after finishing casting the bottom slab. From the calculation, it appears that the restrained strains of Point B and D on potential cracking location are lower than tensile strain capacity but the restrained strain of Point A is closed to tensile capacity. Therefore, additional shrinkage reinforcement is recommended. The details of location and the size of the additional reinforcements are provided as shown in Figure 5.24.

Therefore, the wall is evaluated safe when using the proposed mix proportion with T_{ini} of 32^{o}C with 7-day insulation curing. In this case the wall is insulated along its height of 10-m by using 2-in thick foam for 3-m above the bottom slab, followed by 1.5-in thick foam for another 3-m, and followed by 1-in thick foam for 4-m.

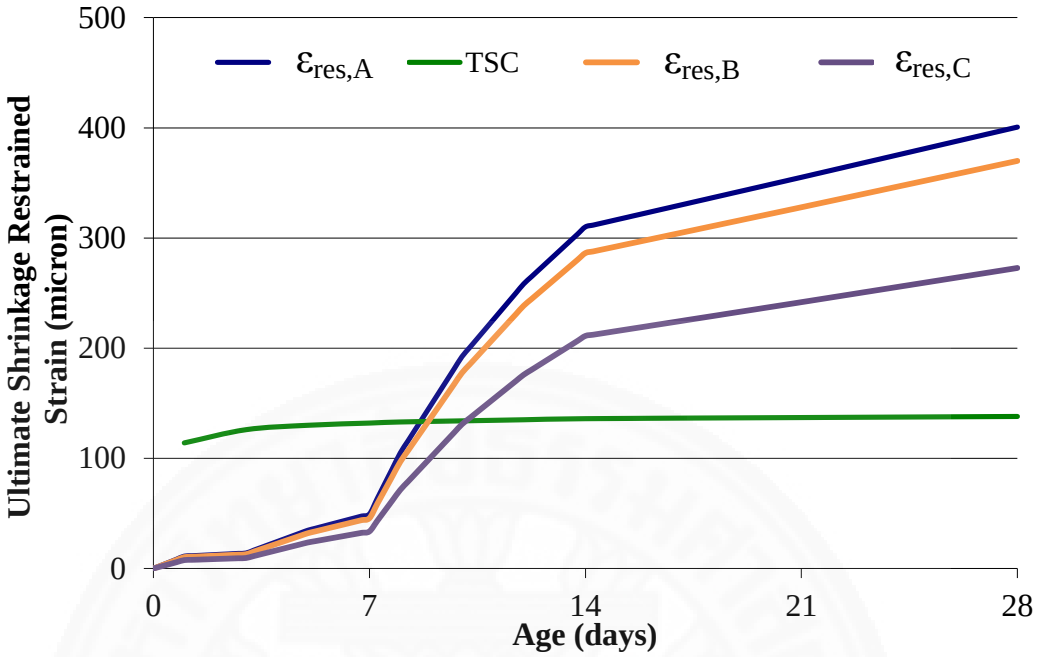

Figure 5.22 Restrained strain due to ultimate shrinkage at the possible location of shrinkage crack of wall with 7 days insulation curing

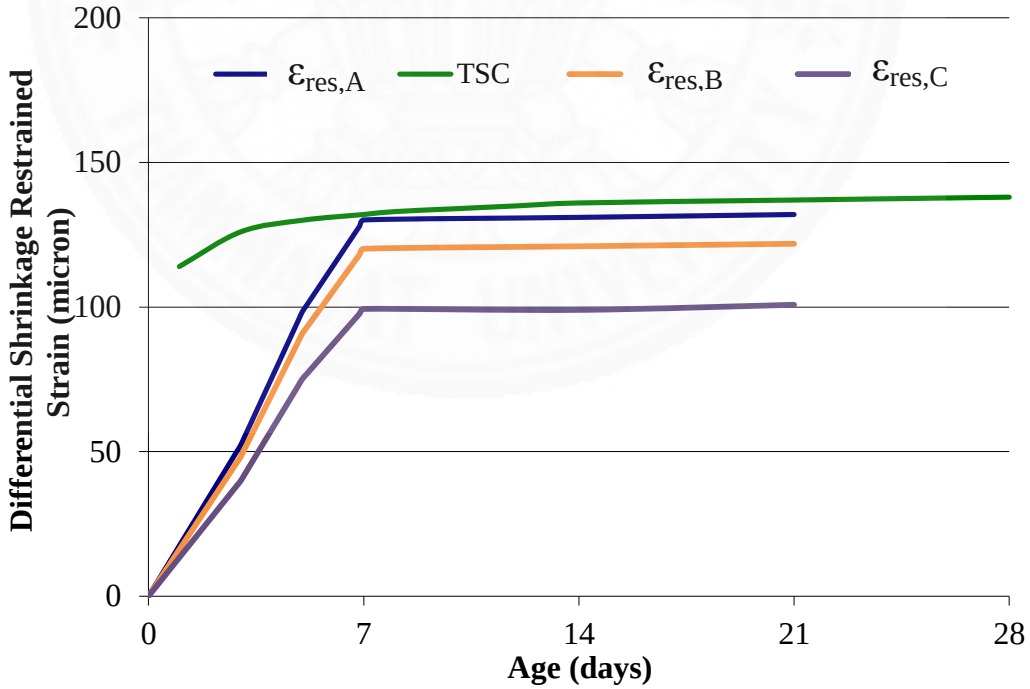

Figure 5.23 Restrained strain due to differential shrinkage at the possible location of shrinkage crack of wall with 7 days insulation curing

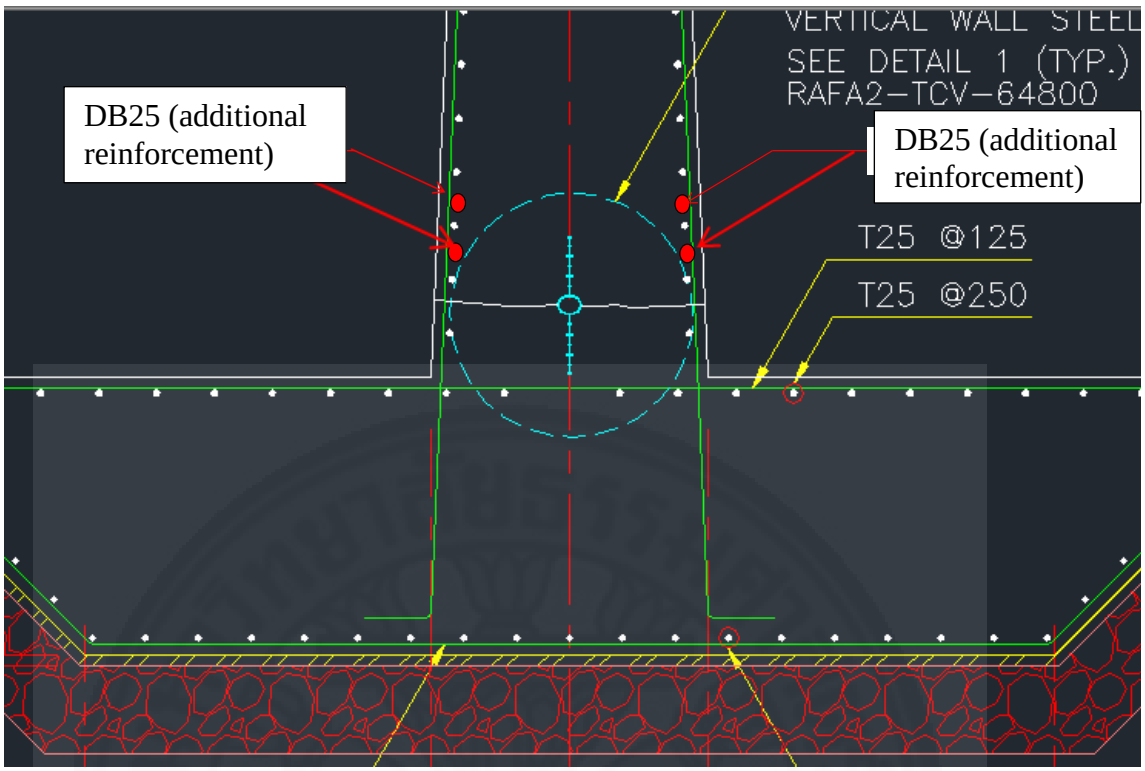

Figure 5.24 Placing locations of additional reinforcements to prevent shrinkage crack

The consideration of autogenous and drying shrinkages will result in a more realistic prediction of cracking in mass concrete footings. It was found that the effect of drying shrinkage is more significant than the effect of autogenous shrinkage for the internally restrained thermal stress. However, in the case of external restraint, both autogenous and drying shrinkages are supposed to increase the tensile restrained strain and then cracking risk of mass concrete. It is noted that creep and relaxation are not included in this study.

Chapter 6

Conclusion and Recommendation for Future Studies

6.1 Conclusion

From the analytical results, it was found that for the internally restrained thermal cracking risk, autogenous shrinkage reduces the risk of cracking especially at the early age before the removal of insulation curing material in the condition of internal restrained strain. However mass concrete can be at risk by the effect of drying shrinkage after the removal of the insulation curing material. Care must be taken to prevent excessive loss of moisture to surrounding environment after the removal of insulation material.

6.2 Recommendation for Future Studies

For future study, the effect of creep and relaxation of concrete should be included to the computation for more precise prediction. The use of other cement replacing materials such as blast furnace slag, silica fume, limestone powder, etc. should also be included.

References

ACI committee 207. (1996). *Mass concrete.* ACI 207.1-96, *ACI Manual of Concrete Practice Part 1*. Detroit, Michigan, USA.

ACI Committee 224. (1994). *Control of cracking in concrete structure* ACI 224R-90, *ACI Manual of Concrete Practice Part 3*. Detroit, Michigan, USA.

Akkaya, Y., Ouyang, C., & Shah, S.P. (2007). *Effect of supplementary cementitious material on shrinkage and crack development in concrete. Cement and Concrete Composites 29*: 117-123.

Bisschop, J. (2002). *Drying Shrinkage Microcracking in Cement-Based Materials*. Delft University Press., Netherlands

Bissonnette, B., Pierre, P., & Pigeon, M. (1999). *Influence of key parameters on drying shrinkage of cementitious material. Cement and Concrete Research 29*: 1655-1662.

Buffo-Lacarriere, L., Sellier, A., Escadeillas, G. & Turatsinze, A. (2007). *Multiphasic finite element modeling of concrete hydration*. *Cement and Concrete Research 37*, 2: 131-138

Choktaweekarn. P. (2008). *Thermal Properties and Model for Predicting Temperature and Thermal Cracking in Mass Concrete*. Doctoral Thesis, Sirindhorn International Institute of Technology, Thammasat University, Thailand.

Choktaweekarn. P. & Tangtermsirikul. S. (2010). Effect of aggregate type, casting, thickness and curing condition on restrained strain of mass concrete [Electronic version]. *Songklanakarin Journal of Science and Technology, 32*(4), 391-402.

Coefficient of thermal expansion, http://www.supercivilcd.com/THERMAL.htm, 2006.

Cusson, D. & Hoogeveen, T. (2007). *An experimental approach for the analysis of early age behavior of high performance concrete structures under restrained shrinkage. Cement and Concrete Research* 37: 200-209.

Faria, R., Azenha, M., & Figueiras, J.A. (2006). *Modeling of concrete at early ages: application to an externally restrained slab*. *Cement and Concrete Composites* 28, 6: 572-585

Fujiwara, T. (1989). *Relation between mix proportion and drying shrinkage of hardened cement paste, mortar and concrete. Concrete Libibrary of JSCE,* 13, June.

Justnes, H., et al. (1998). *The Influence of Cement Characteristics on Chemical Shrinkage*. Proceeding of the International Workshop organized by JCI (Japan Concrete Institute) on Autogenous Shrinkage of Concrete, Hiroshima, Japan, 71-80.

Kim, G., Lee., E., & Koo, K. (2009). *Hydration heat and autogenous shrinkage of high-strength mass concrete*. Journal of Asian architecture and building engineering, 509-516.

Kim, J.K., Kim, K.H. & Yang, J.K. (2001). *Thermal analysis of hydration heat in concrete structures with pipe-cooling system.* Computers and Structures 79, 163-171

Kim, J.K., & Lee, C.S. (1999). *Moisture diffusion of concrete considering self-desiccation at early ages. Cement and Concrete Research* 29: 1921-1927.

Koenders, E. A. B. & Breugel, K. V. (1994). *Numerical and experimental adiabatic hydration curve determination. The Proceeding of the International RILEM Symposium on Thermal Cracking in Concrete at Early Ages.,* Munich, 1:3-10.

Kwak, H.G., Ha S.J. & Kim J.K. (2006) *Non-structural cracking in RC walls: Part I. Finite element formulation*. Cement and Concrete Research, Vol. 36 No. 4, pp 749-760.

Maekawa K., Chaube R. & Kishi T. (1999). *Modelling of Concrete Performance.* E & FN Spon, London,

Mak, S.L., Ritchie, D., Taylor, A., & Diggins, R. (1998). *Temperature Effects on Early Age Autogenous Shrinkage in High Performance Concretes.* Proceeding of the International Workshop organized by JCI (Japan Concrete Institute) on Autogenous Shrinkage of Concrete, Hiroshima, Japan, 155-166.

Maruyama I., & Igarashi G. (2014). *Cement Reaction and Resultant Physical Properties of Cement Paste*. Journal of Advanced Concrete Technology Vol.12, 200-213.

Neville, A.M. (1995). *Properties of Concrete*: Fourth Edition, Longman Singapore Publishers Pte. Ltd., Singapore.

Noorzaei J., Bayagoob K.H., Thanoon W.A. & Jaafar M.S. (2006). *Thermal and stress analysis of Kinta RCC dam*. Engineering Structures 28, 1795–1802

Portland Cement Association. (2003). *Design and Control of Concrete Admixtures*, 14th ed-CD Version, CD100.1.

Rico, J.R. (2000). *Effect of Superplasticizers on The Behavior of Concrete in The Fresh and Hardened States*: Implication for High Performance Concretes, Doctoral Thesis, Universitat Politechnica de Catalunya, Barcelona, June.

Saengsoy, W. & Tangtermsirikul, S. (2003). *Model for predicting temperature of mass concrete*. Proceedings of the 1st National Concrete Conference, Engineering Institute of Thailand, Kanchanaburi, 211-218

Sarker P.K., Jitvutikrai P., Tangtermsirikul S. & Kishi T. (1999) *Modeling of temperature rise in concrete using fly ash*. Concrete Model Code for Asia IABSE Collo-quium, Phuket, Thailand, pp. 126-132

Schutter, G.D. (2002). *Finite element simulation of thermal cracking in massive hardening concrete elements using degree of hydration based material laws. Computers and Structures*, 80, 27-30: 2035–2042

Sicat, E., Gong, F., Zhang, D., & Ueda, T. (2013) *Change of the Coefficient of Thermal Expansion of Mortar Due to Damage by Freeze Thaw Cycles*. Journal of Advanced Concrete Technology Vol.11, 333-346.

Suzuki, K., Ohno, Y. & Nakagawa, T. (1993). *Test method for cracking of concrete due to drying shrinkage*: Zdenek P. Bazant (Ed.), *Creep and shrinkage of concrete*, E & FN Spon, London, pp.63-70.

Tao, Z. & Weizu, Q. (2006). *Tensile creep due to restraining stresses in high-strength concrete at early ages. Cement and concrete Research* 36: 584-591.

Tangtermsirikul, S. (2003). *Durability and Mix Design of Concrete*. 1st Edition Handbook, Thailand, Printing House of Thammasat University.

Tangtermsirikul, S. (1998). *Effect of Chemical Composition and Particle Size of Fly Ash on Autogenous Shrinkage of Paste*. Proceeding of the International Workshop organized by JCI (Japan Concrete Institute) on Autogenous Shrinkage of Concrete, Hiroshima, Japan, 175-186.

Tangtermsirikul, S., Maruya, T., & Matsuoka, Y. (1992). *Improvement of Model for Simulating Water Movement in Harden Concrete*: *Taking into Account Effect of Carbonation. Taisei Technical Research Report* 25: 239-242.

Tatong S., &Tangtermsirikul S. (2001). *Modeling of aggregate stiffness and its effect on shrinkage of concrete*. Science Asia, Vol. 27, No. 3, pp 185-192.

Tazawa, E., & Miyazawa, S. (1993). *Autogenous Shrinkage of Concrete and Its Importance in Concrete Technology.* Proceedings of the Fifth International RILEM Symposium, Barcelona, Spain, 189-168.

Tazawa, E., & Miyazawa, S. (1998). *Effect of Constituents and Curing Condition on Autogenous Shrinkage of Concrete*. Proceeding of the International Workshop Organized by JCI (Japan Concrete Institute) on Autogenous Shrinkage of Concrete, Hiroshima, Japan, 269-280.

Tongaroonsri, S. (2009). *Prediction of Autogenous Shrinkage, Drying Shrinkage and Shrinkage Cracking in Concrete*. Doctoral Thesis, Sirindhorn International Institute of Technology, Thammasat University, Thailand, May.

Wang, C. & Dilger, W.H. (1994). *Prediction of temperature distribution in hardening concrete*, in : Springenschmid R. (Ed.), *Thermal Cracking in Concrete at Early Ages*, E & FN Spon, London, UK, pp. 21-28

Whittier, S., Olyniec, J. & Mcglohn, R. (2004). *Minimizing Temperature Differentials in Mass Concrete*. *Concrete International*, 42-45

Wiegrink, K., Marikunte, S., & Shah, S.P. (1993). *Shrinkage cracking of high-strength concrete. ACI Material Journal* 93(5): 409-415.

Yuan Y. & Wan Z.L. (2000). *Prediction of cracking within early-age concrete due to thermal, drying and creep behavior.* Cement and Concrete Research 32, 1053–1059.

Appendices

Appendix A

Analytical Results of Mass Concrete Footing

Table A.1 Predicted semi-adiabatic temperatures at location A

Curve	**A**	
X	:	Time
Y	:	Temperature

X (Days)	X (Hours)	Y (°C)	X (Days)	X (Hours)	Y (°C)
0.00	0.00	32.00	7.25	174.00	34.33
0.25	6.00	39.90	7.50	180.00	33.84
0.50	12.00	44.99	7.75	186.00	33.62
0.75	18.00	45.23	8.00	192.00	33.50
1.00	24.00	44.63	8.25	198.00	33.40
1.25	30.00	43.96	8.50	204.00	33.33
1.50	36.00	43.35	8.75	210.00	33.27
1.75	42.00	42.82	9.00	216.00	33.21
2.00	48.00	42.34	9.25	222.00	33.17
2.25	54.00	41.93	9.50	228.00	33.12
2.50	60.00	41.57	9.75	234.00	33.08
2.75	66.00	41.23	10.00	240.00	33.05
3.00	72.00	40.91	10.25	246.00	33.01
3.25	78.00	40.62	10.50	252.00	32.98
3.50	84.00	40.35	10.75	258.00	32.95
3.75	90.00	40.10	11.00	264.00	32.92
4.00	96.00	39.87	11.25	270.00	32.89
4.25	102.00	39.65	11.50	276.00	32.86
4.50	108.00	39.45	11.75	282.00	32.84
4.75	114.00	39.25	12.00	288.00	32.81
5.00	120.00	39.07	12.25	294.00	32.79
5.25	126.00	38.89	12.50	300.00	32.76
5.50	132.00	38.72	12.75	306.00	32.74
5.75	138.00	38.56	13.00	312.00	32.72
6.00	144.00	38.40	13.25	318.00	32.70
6.25	150.00	38.24	13.50	324.00	32.68
6.50	156.00	38.09	13.75	330.00	32.66
6.75	162.00	37.95	14.00	336.00	32.64
7.00	168.00	37.81			

Table A.2 Predicted semi-adiabatic temperatures at location B

Curve	**B**	
X	:	Time
Y	:	Temperature

X (Days)	X (Hours)	Y (°C)	X (Days)	X (Hours)	Y (°C)
0.00	0.00	32.00	7.25	174.00	54.84
0.25	6.00	44.42	7.50	180.00	54.39
0.50	12.00	54.68	7.75	186.00	53.93
0.75	18.00	58.22	8.00	192.00	53.47
1.00	24.00	59.83	8.25	198.00	53.00
1.25	30.00	60.75	8.50	204.00	52.53
1.50	36.00	61.33	8.75	210.00	52.07
1.75	42.00	61.69	9.00	216.00	51.60
2.00	48.00	61.87	9.25	222.00	51.14
2.25	54.00	61.96	9.50	228.00	50.68
2.50	60.00	61.95	9.75	234.00	50.22
2.75	66.00	61.85	10.00	240.00	49.77
3.00	72.00	61.66	10.25	246.00	49.33
3.25	78.00	61.42	10.50	252.00	48.89
3.50	84.00	61.14	10.75	258.00	48.47
3.75	90.00	60.83	11.00	264.00	48.05
4.00	96.00	60.47	11.25	270.00	47.64
4.25	102.00	60.10	11.50	276.00	47.24
4.50	108.00	59.71	11.75	282.00	46.84
4.75	114.00	59.30	12.00	288.00	46.46
5.00	120.00	58.89	12.25	294.00	46.08
5.25	126.00	58.46	12.50	300.00	45.71
5.50	132.00	58.02	12.75	306.00	45.35
5.75	138.00	57.58	13.00	312.00	45.00
6.00	144.00	57.12	13.25	318.00	44.65
6.25	150.00	56.67	13.50	324.00	44.32
6.50	156.00	56.21	13.75	330.00	43.99
6.75	162.00	55.75	14.00	336.00	43.67
7.00	168.00	55.30			

Table A.3 Predicted semi-adiabatic temperatures at location C

Curve	**C**	
X	:	Time
Y	:	Temperature

X (Days)	X (Hours)	Y (°C)	X (Days)	X (Hours)	Y (°C)
0.00	0.00	32.00	7.25	174.00	45.72
0.25	6.00	42.68	7.50	180.00	45.46
0.50	12.00	50.60	7.75	186.00	45.20
0.75	18.00	52.34	8.00	192.00	44.95
1.00	24.00	52.60	8.25	198.00	44.69
1.25	30.00	52.47	8.50	204.00	44.44
1.50	36.00	52.23	8.75	210.00	44.19
1.75	42.00	51.94	9.00	216.00	43.94
2.00	48.00	51.63	9.25	222.00	43.69
2.25	54.00	51.33	9.50	228.00	43.45
2.50	60.00	51.04	9.75	234.00	43.21
2.75	66.00	50.74	10.00	240.00	42.97
3.00	72.00	50.42	10.25	246.00	42.73
3.25	78.00	50.12	10.50	252.00	42.49
3.50	84.00	49.83	10.75	258.00	42.26
3.75	90.00	49.54	11.00	264.00	42.03
4.00	96.00	49.24	11.25	270.00	41.80
4.25	102.00	48.96	11.50	276.00	41.58
4.50	108.00	48.68	11.75	282.00	41.36
4.75	114.00	48.41	12.00	288.00	41.14
5.00	120.00	48.14	12.25	294.00	40.92
5.25	126.00	47.87	12.50	300.00	40.71
5.50	132.00	47.60	12.75	306.00	40.50
5.75	138.00	47.33	13.00	312.00	40.29
6.00	144.00	47.05	13.25	318.00	40.09
6.25	150.00	46.78	13.50	324.00	39.89
6.50	156.00	46.52	13.75	330.00	39.69
6.75	162.00	46.25	14.00	336.00	39.50
7.00	168.00	45.98			

Table A.4 Restrained thermal strain at location A

Curve	**A**	
X	:	Time
Y	:	Restrained Strain

X (Days)	X (Hours)	Y (micron)	X (Days)	X (Hours)	Y (micron)
0.00	0.00	0.00	7.25	174.00	139.66
0.25	6.00	30.42	7.50	180.00	139.02
0.50	12.00	64.64	7.75	186.00	136.76
0.75	18.00	85.67	8.00	192.00	134.13
1.00	24.00	99.34	8.25	198.00	131.39
1.25	30.00	108.92	8.50	204.00	128.60
1.50	36.00	115.93	8.75	210.00	125.81
1.75	42.00	121.22	9.00	216.00	123.04
2.00	48.00	125.22	9.25	222.00	120.29
2.25	54.00	128.31	9.50	228.00	117.57
2.50	60.00	130.67	9.75	234.00	114.88
2.75	66.00	132.39	10.00	240.00	112.23
3.00	72.00	133.56	10.25	246.00	109.61
3.25	78.00	134.31	10.50	252.00	107.03
3.50	84.00	134.71	10.75	258.00	104.48
3.75	90.00	134.79	11.00	264.00	101.98
4.00	96.00	134.59	11.25	270.00	99.52
4.25	102.00	134.17	11.50	276.00	97.09
4.50	108.00	133.55	11.75	282.00	94.71
4.75	114.00	132.77	12.00	288.00	92.37
5.00	120.00	131.82	12.25	294.00	90.08
5.25	126.00	130.74	12.50	300.00	87.82
5.50	132.00	129.54	12.75	306.00	85.61
5.75	138.00	128.22	13.00	312.00	83.44
6.00	144.00	126.79	13.25	318.00	81.32
6.25	150.00	125.28	13.50	324.00	79.23
6.50	156.00	123.70	13.75	330.00	77.19
6.75	162.00	122.05	14.00	336.00	75.20
7.00	168.00	120.34			

Table A.5 Restrained thermal strain at location B

Curve	**B**	
X	:	Time
Y	:	Restrained Strain

X (Days)	X (Hours)	Y (micron)	X (Days)	X (Hours)	Y (micron)
0.00	0.00	0.00	7.25	174.00	-27.26
0.25	6.00	-2.55	7.50	180.00	-27.30
0.50	12.00	-6.76	7.75	186.00	-27.14
0.75	18.00	-11.05	8.00	192.00	-26.84
1.00	24.00	-15.04	8.25	198.00	-26.43
1.25	30.00	-18.61	8.50	204.00	-25.95
1.50	36.00	-21.73	8.75	210.00	-25.40
1.75	42.00	-24.38	9.00	216.00	-24.80
2.00	48.00	-26.58	9.25	222.00	-24.17
2.25	54.00	-28.37	9.50	228.00	-23.52
2.50	60.00	-29.78	9.75	234.00	-22.86
2.75	66.00	-30.86	10.00	240.00	-22.20
3.00	72.00	-31.64	10.25	246.00	-21.54
3.25	78.00	-32.16	10.50	252.00	-20.88
3.50	84.00	-32.47	10.75	258.00	-20.24
3.75	90.00	-32.59	11.00	264.00	-19.61
4.00	96.00	-32.56	11.25	270.00	-19.00
4.25	102.00	-32.40	11.50	276.00	-18.41
4.50	108.00	-32.13	11.75	282.00	-17.83
4.75	114.00	-31.78	12.00	288.00	-17.27
5.00	120.00	-31.36	12.25	294.00	-16.73
5.25	126.00	-30.88	12.50	300.00	-16.21
5.50	132.00	-30.36	12.75	306.00	-15.70
5.75	138.00	-29.81	13.00	312.00	-15.21
6.00	144.00	-29.23	13.25	318.00	-14.74
6.25	150.00	-28.63	13.50	324.00	-14.29
6.50	156.00	-28.02	13.75	330.00	-13.85
6.75	162.00	-27.40	14.00	336.00	-13.43
7.00	168.00	-26.78			

Table A.6 Restrained thermal strain at location C

Curve	**C**	
X	:	Time
Y	:	Restrained Strain

X (Days)	X (Hours)	Y (micron)	X (Days)	X (Hours)	Y (micron)
0.00	0.00	0.00	7.25	174.00	36.59
0.25	6.00	9.61	7.50	180.00	35.62
0.50	12.00	21.68	7.75	186.00	34.69
0.75	18.00	29.96	8.00	192.00	33.79
1.00	24.00	35.40	8.25	198.00	32.92
1.25	30.00	39.08	8.50	204.00	32.07
1.50	36.00	41.65	8.75	210.00	31.24
1.75	42.00	43.46	9.00	216.00	30.42
2.00	48.00	44.72	9.25	222.00	29.62
2.25	54.00	45.58	9.50	228.00	28.84
2.50	60.00	46.13	9.75	234.00	28.08
2.75	66.00	46.42	10.00	240.00	27.33
3.00	72.00	46.50	10.25	246.00	26.60
3.25	78.00	46.41	10.50	252.00	25.89
3.50	84.00	46.20	10.75	258.00	25.19
3.75	90.00	45.87	11.00	264.00	24.51
4.00	96.00	45.46	11.25	270.00	23.85
4.25	102.00	44.97	11.50	276.00	23.21
4.50	108.00	44.43	11.75	282.00	22.58
4.75	114.00	43.86	12.00	288.00	21.97
5.00	120.00	43.24	12.25	294.00	21.37
5.25	126.00	42.60	12.50	300.00	20.79
5.50	132.00	41.93	12.75	306.00	20.23
5.75	138.00	41.24	13.00	312.00	19.67
6.00	144.00	40.54	13.25	318.00	19.14
6.25	150.00	39.83	13.50	324.00	18.62
6.50	156.00	39.11	13.75	330.00	18.11
6.75	162.00	38.39	14.00	336.00	17.61
7.00	168.00	37.67			

Table A.7 Restrained autogenous shrinkage strain at location A

Curve	**A**	
X	:	Time
Y	:	Restrained Strain

X (Days)	X (Hours)	Y (micron)	X (Days)	X (Hours)	Y (micron)
0.00	0.00	0.00	7.25	174.00	-5.80
0.25	6.00	-1.31	7.50	180.00	-5.64
0.50	12.00	-2.61	7.75	186.00	-5.48
0.75	18.00	-3.92	8.00	192.00	-5.32
1.00	24.00	-5.23	8.25	198.00	-5.07
1.25	30.00	-5.36	8.50	204.00	-4.83
1.50	36.00	-5.49	8.75	210.00	-4.58
1.75	42.00	-5.62	9.00	216.00	-4.33
2.00	48.00	-5.76	9.25	222.00	-4.08
2.25	54.00	-5.89	9.50	228.00	-3.83
2.50	60.00	-6.02	9.75	234.00	-3.58
2.75	66.00	-6.16	10.00	240.00	-3.33
3.00	72.00	-6.29	10.25	246.00	-2.96
3.25	78.00	-6.32	10.50	252.00	-2.59
3.50	84.00	-6.36	10.75	258.00	-2.22
3.75	90.00	-6.39	11.00	264.00	-1.85
4.00	96.00	-6.43	11.25	270.00	-1.47
4.25	102.00	-6.46	11.50	276.00	-1.10
4.50	108.00	-6.49	11.75	282.00	-0.73
4.75	114.00	-6.53	12.00	288.00	-0.36
5.00	120.00	-6.56	12.25	294.00	-0.31
5.25	126.00	-6.48	12.50	300.00	-0.26
5.50	132.00	-6.41	12.75	306.00	-0.21
5.75	138.00	-6.34	13.00	312.00	-0.16
6.00	144.00	-6.26	13.25	318.00	-0.10
6.25	150.00	-6.19	13.50	324.00	-0.05
6.50	156.00	-6.11	13.75	330.00	0.00
6.75	162.00	-6.04	14.00	336.00	0.05
7.00	168.00	-5.96			

Table A.8 Restrained autogenous shrinkage strain at location B

Curve	**B**	
X	:	Time
Y	:	Restrained Strain

X (Days)	X (Hours)	Y (micron)	X (Days)	X (Hours)	Y (micron)
0.00	0.00	0.00	7.25	174.00	1.13
0.25	6.00	0.35	7.50	180.00	1.14
0.50	12.00	0.70	7.75	186.00	1.14
0.75	18.00	1.05	8.00	192.00	1.15
1.00	24.00	1.39	8.25	198.00	1.15
1.25	30.00	1.33	8.50	204.00	1.15
1.50	36.00	1.27	8.75	210.00	1.15
1.75	42.00	1.21	9.00	216.00	1.16
2.00	48.00	1.14	9.25	222.00	1.16
2.25	54.00	1.08	9.50	228.00	1.16
2.50	60.00	1.02	9.75	234.00	1.16
2.75	66.00	0.96	10.00	240.00	1.16
3.00	72.00	0.89	10.25	246.00	1.16
3.25	78.00	0.91	10.50	252.00	1.16
3.50	84.00	0.93	10.75	258.00	1.15
3.75	90.00	0.95	11.00	264.00	1.15
4.00	96.00	0.96	11.25	270.00	1.15
4.25	102.00	0.98	11.50	276.00	1.14
4.50	108.00	1.00	11.75	282.00	1.14
4.75	114.00	1.02	12.00	288.00	1.14
5.00	120.00	1.03	12.25	294.00	1.04
5.25	126.00	1.05	12.50	300.00	0.94
5.50	132.00	1.06	12.75	306.00	0.84
5.75	138.00	1.07	13.00	312.00	0.75
6.00	144.00	1.08	13.25	318.00	0.65
6.25	150.00	1.09	13.50	324.00	0.55
6.50	156.00	1.10	13.75	330.00	0.45
6.75	162.00	1.11	14.00	336.00	0.36
7.00	168.00	1.12			

Table A.9 Restrained autogenous shrinkage strain at location C

Curve	**C**	
X	:	Time
Y	:	Restrained Strain

X (Days)	X (Hours)	Y (micron)	X (Days)	X (Hours)	Y (micron)
0.00	0.00	0.00	7.25	174.00	-1.05
0.25	6.00	-0.21	7.50	180.00	-1.06
0.50	12.00	-0.42	7.75	186.00	-1.07
0.75	18.00	-0.62	8.00	192.00	-1.08
1.00	24.00	-0.83	8.25	198.00	-1.09
1.25	30.00	-0.83	8.50	204.00	-1.10
1.50	36.00	-0.83	8.75	210.00	-1.11
1.75	42.00	-0.82	9.00	216.00	-1.11
2.00	48.00	-0.82	9.25	222.00	-1.12
2.25	54.00	-0.82	9.50	228.00	-1.13
2.50	60.00	-0.82	9.75	234.00	-1.14
2.75	66.00	-0.81	10.00	240.00	-1.14
3.00	72.00	-0.81	10.25	246.00	-1.15
3.25	78.00	-0.83	10.50	252.00	-1.15
3.50	84.00	-0.84	10.75	258.00	-1.16
3.75	90.00	-0.86	11.00	264.00	-1.16
4.00	96.00	-0.88	11.25	270.00	-1.17
4.25	102.00	-0.89	11.50	276.00	-1.17
4.50	108.00	-0.91	11.75	282.00	-1.18
4.75	114.00	-0.93	12.00	288.00	-1.18
5.00	120.00	-0.94	12.25	294.00	-1.04
5.25	126.00	-0.96	12.50	300.00	-0.90
5.50	132.00	-0.97	12.75	306.00	-0.76
5.75	138.00	-0.98	13.00	312.00	-0.62
6.00	144.00	-0.99	13.25	318.00	-0.47
6.25	150.00	-1.01	13.50	324.00	-0.33
6.50	156.00	-1.02	13.75	330.00	-0.19
6.75	162.00	-1.03	14.00	336.00	-0.05
7.00	168.00	-1.04			

Table A.10 Combined restrained thermal and autogenous shrinkage strain at location A

Curve	**A**	
X	:	Time
Y	:	Restrained Strain

X (Days)	X (Hours)	Y (micron)	X (Days)	X (Hours)	Y (micron)
0.00	0.00	0.00	7.25	174.00	133.86
0.25	6.00	29.11	7.50	180.00	133.38
0.50	12.00	62.03	7.75	186.00	131.27
0.75	18.00	81.75	8.00	192.00	128.81
1.00	24.00	94.12	8.25	198.00	126.31
1.25	30.00	103.56	8.50	204.00	123.78
1.50	36.00	110.44	8.75	210.00	121.23
1.75	42.00	115.60	9.00	216.00	118.71
2.00	48.00	119.47	9.25	222.00	116.21
2.25	54.00	122.42	9.50	228.00	113.74
2.50	60.00	124.64	9.75	234.00	111.30
2.75	66.00	126.23	10.00	240.00	108.89
3.00	72.00	127.27	10.25	246.00	106.65
3.25	78.00	127.99	10.50	252.00	104.44
3.50	84.00	128.35	10.75	258.00	102.27
3.75	90.00	128.40	11.00	264.00	100.13
4.00	96.00	128.17	11.25	270.00	98.04
4.25	102.00	127.71	11.50	276.00	95.99
4.50	108.00	127.06	11.75	282.00	93.98
4.75	114.00	126.24	12.00	288.00	92.02
5.00	120.00	125.26	12.25	294.00	89.77
5.25	126.00	124.26	12.50	300.00	87.56
5.50	132.00	123.13	12.75	306.00	85.40
5.75	138.00	121.88	13.00	312.00	83.29
6.00	144.00	120.53	13.25	318.00	81.21
6.25	150.00	119.10	13.50	324.00	79.18
6.50	156.00	117.59	13.75	330.00	77.19
6.75	162.00	116.01	14.00	336.00	75.24
7.00	168.00	114.38			

Table A.11 Combined restrained thermal and autogenous shrinkage strain at location B

Curve	**B**	
X	:	Time
Y	:	Restrained Strain

X (Days)	X (Hours)	Y (micron)	X (Days)	X (Hours)	Y (micron)
0.00	0.00	0.00	7.25	174.00	-26.13
0.25	6.00	-2.20	7.50	180.00	-26.16
0.50	12.00	-6.07	7.75	186.00	-25.99
0.75	18.00	-10.01	8.00	192.00	-25.69
1.00	24.00	-13.65	8.25	198.00	-25.28
1.25	30.00	-17.28	8.50	204.00	-24.79
1.50	36.00	-20.46	8.75	210.00	-24.24
1.75	42.00	-23.17	9.00	216.00	-23.64
2.00	48.00	-25.44	9.25	222.00	-23.01
2.25	54.00	-27.29	9.50	228.00	-22.36
2.50	60.00	-28.76	9.75	234.00	-21.70
2.75	66.00	-29.90	10.00	240.00	-21.03
3.00	72.00	-30.74	10.25	246.00	-20.37
3.25	78.00	-31.25	10.50	252.00	-19.73
3.50	84.00	-31.54	10.75	258.00	-19.09
3.75	90.00	-31.65	11.00	264.00	-18.46
4.00	96.00	-31.60	11.25	270.00	-17.86
4.25	102.00	-31.42	11.50	276.00	-17.26
4.50	108.00	-31.13	11.75	282.00	-16.69
4.75	114.00	-30.76	12.00	288.00	-16.13
5.00	120.00	-30.32	12.25	294.00	-15.69
5.25	126.00	-29.84	12.50	300.00	-15.27
5.50	132.00	-29.31	12.75	306.00	-14.86
5.75	138.00	-28.74	13.00	312.00	-14.47
6.00	144.00	-28.15	13.25	318.00	-14.09
6.25	150.00	-27.54	13.50	324.00	-13.74
6.50	156.00	-26.92	13.75	330.00	-13.39
6.75	162.00	-26.29	14.00	336.00	-13.07
7.00	168.00	-25.66			

Table A.12 Combined restrained thermal and autogenous shrinkage strain at location C

Curve	**C**	
X	:	Time
Y	:	Restrained Strain

X (Days)	X (Hours)	Y (micron)	X (Days)	X (Hours)	Y (micron)
0.00	0.00	0.00	7.25	174.00	35.54
0.25	6.00	9.40	7.50	180.00	34.55
0.50	12.00	21.27	7.75	186.00	33.62
0.75	18.00	29.34	8.00	192.00	32.71
1.00	24.00	34.57	8.25	198.00	31.83
1.25	30.00	38.25	8.50	204.00	30.97
1.50	36.00	40.82	8.75	210.00	30.13
1.75	42.00	42.64	9.00	216.00	29.31
2.00	48.00	43.90	9.25	222.00	28.50
2.25	54.00	44.76	9.50	228.00	27.71
2.50	60.00	45.31	9.75	234.00	26.94
2.75	66.00	45.61	10.00	240.00	26.18
3.00	72.00	45.69	10.25	246.00	25.45
3.25	78.00	45.59	10.50	252.00	24.73
3.50	84.00	45.35	10.75	258.00	24.03
3.75	90.00	45.01	11.00	264.00	23.35
4.00	96.00	44.58	11.25	270.00	22.68
4.25	102.00	44.08	11.50	276.00	22.03
4.50	108.00	43.52	11.75	282.00	21.40
4.75	114.00	42.93	12.00	288.00	20.78
5.00	120.00	42.30	12.25	294.00	20.33
5.25	126.00	41.64	12.50	300.00	19.89
5.50	132.00	40.96	12.75	306.00	19.47
5.75	138.00	40.26	13.00	312.00	19.06
6.00	144.00	39.55	13.25	318.00	18.67
6.25	150.00	38.82	13.50	324.00	18.29
6.50	156.00	38.09	13.75	330.00	17.92
6.75	162.00	37.36	14.00	336.00	17.57
7.00	168.00	36.62			

Table A.13 Restrained total shrinkage strain at location A

Curve	**A**	
X	:	Time
Y	:	Restrained Strain

X (Days)	X (Hours)	Y (micron)	X (Days)	X (Hours)	Y (micron)
0.00	0.00	0.00	7.25	174.00	-0.99
0.25	6.00	-1.31	7.50	180.00	3.98
0.50	12.00	-2.61	7.75	186.00	8.94
0.75	18.00	-3.92	8.00	192.00	13.91
1.00	24.00	-5.23	8.25	198.00	18.34
1.25	30.00	-5.36	8.50	204.00	22.76
1.50	36.00	-5.49	8.75	210.00	27.19
1.75	42.00	-5.62	9.00	216.00	31.61
2.00	48.00	-5.76	9.25	222.00	36.03
2.25	54.00	-5.89	9.50	228.00	40.46
2.50	60.00	-6.02	9.75	234.00	44.88
2.75	66.00	-6.16	10.00	240.00	49.31
3.00	72.00	-6.29	10.25	246.00	53.18
3.25	78.00	-6.32	10.50	252.00	57.05
3.50	84.00	-6.36	10.75	258.00	60.93
3.75	90.00	-6.39	11.00	264.00	64.80
4.00	96.00	-6.43	11.25	270.00	68.68
4.25	102.00	-6.46	11.50	276.00	72.55
4.50	108.00	-6.49	11.75	282.00	76.42
4.75	114.00	-6.53	12.00	288.00	80.30
5.00	120.00	-6.56	12.25	294.00	83.33
5.25	126.00	-6.48	12.50	300.00	86.36
5.50	132.00	-6.41	12.75	306.00	89.39
5.75	138.00	-6.34	13.00	312.00	92.41
6.00	144.00	-6.26	13.25	318.00	95.44
6.25	150.00	-6.19	13.50	324.00	98.47
6.50	156.00	-6.11	13.75	330.00	101.50
6.75	162.00	-6.04	14.00	336.00	104.53
7.00	168.00	-5.96			

Table A.14 Restrained total shrinkage strain at location B

Curve	**B**	
X	:	Time
Y	:	Restrained Strain

X (Days)	X (Hours)	Y (micron)	X (Days)	X (Hours)	Y (micron)
0.00	0.00	0.00	7.25	174.00	1.11
0.25	6.00	0.35	7.50	180.00	1.09
0.50	12.00	0.70	7.75	186.00	1.07
0.75	18.00	1.05	8.00	192.00	1.05
1.00	24.00	1.39	8.25	198.00	1.03
1.25	30.00	1.33	8.50	204.00	1.01
1.50	36.00	1.27	8.75	210.00	1.00
1.75	42.00	1.21	9.00	216.00	0.98
2.00	48.00	1.14	9.25	222.00	0.96
2.25	54.00	1.08	9.50	228.00	0.94
2.50	60.00	1.02	9.75	234.00	0.92
2.75	66.00	0.96	10.00	240.00	0.90
3.00	72.00	0.89	10.25	246.00	0.88
3.25	78.00	0.91	10.50	252.00	0.86
3.50	84.00	0.93	10.75	258.00	0.84
3.75	90.00	0.95	11.00	264.00	0.82
4.00	96.00	0.96	11.25	270.00	0.80
4.25	102.00	0.98	11.50	276.00	0.78
4.50	108.00	1.00	11.75	282.00	0.75
4.75	114.00	1.02	12.00	288.00	0.73
5.00	120.00	1.03	12.25	294.00	0.62
5.25	126.00	1.05	12.50	300.00	0.51
5.50	132.00	1.06	12.75	306.00	0.40
5.75	138.00	1.07	13.00	312.00	0.28
6.00	144.00	1.08	13.25	318.00	0.17
6.25	150.00	1.09	13.50	324.00	0.06
6.50	156.00	1.10	13.75	330.00	-0.05
6.75	162.00	1.11	14.00	336.00	-0.16
7.00	168.00	1.12			

Table A.15 Restrained total shrinkage strain at location C

Curve	**C**	
X	:	Time
Y	:	Restrained Strain

X (Days)	X (Hours)	Y (micron)	X (Days)	X (Hours)	Y (micron)
0.00	0.00	0.00	7.25	174.00	-1.07
0.25	6.00	-0.21	7.50	180.00	-1.10
0.50	12.00	-0.42	7.75	186.00	-1.12
0.75	18.00	-0.62	8.00	192.00	-1.15
1.00	24.00	-0.83	8.25	198.00	-1.17
1.25	30.00	-0.83	8.50	204.00	-1.19
1.50	36.00	-0.83	8.75	210.00	-1.21
1.75	42.00	-0.82	9.00	216.00	-1.23
2.00	48.00	-0.82	9.25	222.00	-1.25
2.25	54.00	-0.82	9.50	228.00	-1.27
2.50	60.00	-0.82	9.75	234.00	-1.30
2.75	66.00	-0.81	10.00	240.00	-1.32
3.00	72.00	-0.81	10.25	246.00	-1.33
3.25	78.00	-0.83	10.50	252.00	-1.35
3.50	84.00	-0.84	10.75	258.00	-1.37
3.75	90.00	-0.86	11.00	264.00	-1.38
4.00	96.00	-0.88	11.25	270.00	-1.40
4.25	102.00	-0.89	11.50	276.00	-1.42
4.50	108.00	-0.91	11.75	282.00	-1.43
4.75	114.00	-0.93	12.00	288.00	-1.45
5.00	120.00	-0.94	12.25	294.00	-1.32
5.25	126.00	-0.96	12.50	300.00	-1.18
5.50	132.00	-0.97	12.75	306.00	-1.05
5.75	138.00	-0.98	13.00	312.00	-0.92
6.00	144.00	-0.99	13.25	318.00	-0.79
6.25	150.00	-1.01	13.50	324.00	-0.65
6.50	156.00	-1.02	13.75	330.00	-0.52
6.75	162.00	-1.03	14.00	336.00	-0.39
7.00	168.00	-1.04			

Table A.16 The net restrained strain at location A

Curve	**A**	
X	:	Time
Y	:	Restrained Strain

X (Days)	X (Hours)	Y (micron)	X (Days)	X (Hours)	Y (micron)
0.00	0.00	0.00	7.25	174.00	138.67
0.25	6.00	29.11	7.50	180.00	142.99
0.50	12.00	62.03	7.75	186.00	145.70
0.75	18.00	81.75	8.00	192.00	148.04
1.00	24.00	94.12	8.25	198.00	149.72
1.25	30.00	103.56	8.50	204.00	151.36
1.50	36.00	110.44	8.75	210.00	153.00
1.75	42.00	115.60	9.00	216.00	154.65
2.00	48.00	119.47	9.25	222.00	156.32
2.25	54.00	122.42	9.50	228.00	158.03
2.50	60.00	124.64	9.75	234.00	159.76
2.75	66.00	126.23	10.00	240.00	161.53
3.00	72.00	127.27	10.25	246.00	162.79
3.25	78.00	127.99	10.50	252.00	164.08
3.50	84.00	128.35	10.75	258.00	165.41
3.75	90.00	128.40	11.00	264.00	166.78
4.00	96.00	128.17	11.25	270.00	168.19
4.25	102.00	127.71	11.50	276.00	169.64
4.50	108.00	127.06	11.75	282.00	171.14
4.75	114.00	126.24	12.00	288.00	172.67
5.00	120.00	125.26	12.25	294.00	173.40
5.25	126.00	124.26	12.50	300.00	174.18
5.50	132.00	123.13	12.75	306.00	175.00
5.75	138.00	121.88	13.00	312.00	175.86
6.00	144.00	120.53	13.25	318.00	176.76
6.25	150.00	119.10	13.50	324.00	177.71
6.50	156.00	117.59	13.75	330.00	178.70
6.75	162.00	116.01	14.00	336.00	179.73
7.00	168.00	114.38			

Table A.17 The net restrained strain at location B

Curve	**B**	
X	:	Time
Y	:	Restrained Strain

X (Days)	X (Hours)	Y (micron)	X (Days)	X (Hours)	Y (micron)
0.00	0.00	0.00	7.25	174.00	-26.16
0.25	6.00	-2.20	7.50	180.00	-26.21
0.50	12.00	-6.07	7.75	186.00	-26.07
0.75	18.00	-10.01	8.00	192.00	-25.78
1.00	24.00	-13.65	8.25	198.00	-25.40
1.25	30.00	-17.28	8.50	204.00	-24.93
1.50	36.00	-20.46	8.75	210.00	-24.40
1.75	42.00	-23.17	9.00	216.00	-23.82
2.00	48.00	-25.44	9.25	222.00	-23.21
2.25	54.00	-27.29	9.50	228.00	-22.58
2.50	60.00	-28.76	9.75	234.00	-21.94
2.75	66.00	-29.90	10.00	240.00	-21.29
3.00	72.00	-30.74	10.25	246.00	-20.66
3.25	78.00	-31.25	10.50	252.00	-20.02
3.50	84.00	-31.54	10.75	258.00	-19.40
3.75	90.00	-31.65	11.00	264.00	-18.80
4.00	96.00	-31.60	11.25	270.00	-18.21
4.25	102.00	-31.42	11.50	276.00	-17.63
4.50	108.00	-31.13	11.75	282.00	-17.08
4.75	114.00	-30.76	12.00	288.00	-16.54
5.00	120.00	-30.32	12.25	294.00	-16.11
5.25	126.00	-29.84	12.50	300.00	-15.70
5.50	132.00	-29.31	12.75	306.00	-15.30
5.75	138.00	-28.74	13.00	312.00	-14.93
6.00	144.00	-28.15	13.25	318.00	-14.57
6.25	150.00	-27.54	13.50	324.00	-14.23
6.50	156.00	-26.92	13.75	330.00	-13.90
6.75	162.00	-26.29	14.00	336.00	-13.59
7.00	168.00	-25.66			

Table A.18 The net restrained strain at location C

Curve	**C**	
X	:	Time
Y	:	Restrained Strain

X (Days)	X (Hours)	Y (micron)	X (Days)	X (Hours)	Y (micron)
0.00	0.00	0.00	7.25	174.00	35.52
0.25	6.00	9.40	7.50	180.00	34.52
0.50	12.00	21.27	7.75	186.00	33.57
0.75	18.00	29.34	8.00	192.00	32.65
1.00	24.00	34.57	8.25	198.00	31.75
1.25	30.00	38.25	8.50	204.00	30.88
1.50	36.00	40.82	8.75	210.00	30.02
1.75	42.00	42.64	9.00	216.00	29.19
2.00	48.00	43.90	9.25	222.00	28.37
2.25	54.00	44.76	9.50	228.00	27.56
2.50	60.00	45.31	9.75	234.00	26.78
2.75	66.00	45.61	10.00	240.00	26.01
3.00	72.00	45.69	10.25	246.00	25.26
3.25	78.00	45.59	10.50	252.00	24.54
3.50	84.00	45.35	10.75	258.00	23.82
3.75	90.00	45.01	11.00	264.00	23.13
4.00	96.00	44.58	11.25	270.00	22.45
4.25	102.00	44.08	11.50	276.00	21.79
4.50	108.00	43.52	11.75	282.00	21.15
4.75	114.00	42.93	12.00	288.00	20.52
5.00	120.00	42.30	12.25	294.00	20.05
5.25	126.00	41.64	12.50	300.00	19.61
5.50	132.00	40.96	12.75	306.00	19.17
5.75	138.00	40.26	13.00	312.00	18.76
6.00	144.00	39.55	13.25	318.00	18.35
6.25	150.00	38.82	13.50	324.00	17.96
6.50	156.00	38.09	13.75	330.00	17.59
6.75	162.00	37.36	14.00	336.00	17.22
7.00	168.00	36.62			

Table A.19 Tensile strain capacity of the concrete

Curve	**TSC**	
X	:	Time
Y	:	Tensile Strain Capacity
X	X	Y
(Days)	(Hours)	(micron)
1.00	24.00	125.00
3.00	72.00	137.00
5.00	120.00	140.00
7.00	168.00	141.00
8.00	192.00	141.00
10.00	240.00	142.00
12.00	288.00	143.00
14.00	336.00	143.00

Appendix B

Analytical Results of Water Storage Structure

Table B.1 Predicted temperature of bottom slab using the proposed mix proportion, $T_{ini} = 32^{o}C$

Time (Hours)	Temp at A (°C)	Temp at B (°C)	Temp at C (°C)	Temp at D (°C)
0	32.00	32.00	32.00	32.00
6	51.65	47.71	49.25	48.77
12	55.89	47.85	49.95	49.74
18	57.39	47.05	49.14	49.17
24	57.81	46.16	48.12	48.26
30	57.84	45.41	47.22	47.42
36	57.69	44.80	46.47	46.69
42	57.43	44.28	45.84	46.06
48	57.12	43.84	45.29	45.51
54	56.77	43.46	44.82	45.04
60	56.40	43.13	44.41	44.62
66	56.01	42.84	44.05	44.25
72	55.61	42.57	43.71	43.91
78	55.19	42.33	43.41	43.60
84	54.78	42.11	43.14	43.32
90	54.36	41.91	42.89	43.06
96	53.94	41.72	42.65	42.82
102	53.28	38.49	39.17	39.80
108	52.36	38.31	38.76	39.34
114	51.41	38.24	38.61	39.11
120	50.50	38.21	38.52	38.95
126	49.68	38.18	38.46	38.83
132	48.93	38.17	38.41	38.74
138	48.25	38.15	38.38	38.67
144	47.62	38.14	38.34	38.61
150	47.03	38.13	38.32	38.56
156	46.49	38.12	38.29	38.52
162	45.99	38.11	38.27	38.48
168	45.52	38.10	38.26	38.45

Table B.2 Predicted restrained strain of bottom slab using the proposed mix proportion, $T_{ini} = 32^{o}C$

Time (Hours)	εres at B (°C)	εres at C (°C)	εres at D (°C)
0	0.00	0.00	0.00
6	27.51	14.95	18.97
12	53.74	36.49	38.53
18	67.45	50.24	50.40
24	75.03	58.92	58.08
30	79.37	64.47	63.18
36	81.84	68.04	66.57
42	83.09	70.27	68.73
48	83.51	71.54	70.00
54	83.33	72.12	70.60
60	82.74	72.19	70.70
66	81.81	71.86	70.42
72	80.63	71.21	69.82
78	79.25	70.32	68.98
84	77.73	69.25	67.96
90	76.11	68.04	66.80
96	74.40	66.72	65.52
102	88.41	82.03	77.23
108	81.90	77.64	73.14
114	75.95	72.52	68.67
120	70.65	67.72	64.41
126	65.88	63.30	60.40
132	61.52	59.22	56.64
138	57.53	55.44	53.11
144	53.83	51.93	49.82
150	50.42	48.67	46.74
156	47.28	45.65	43.87
162	44.36	42.85	41.21
168	41.66	40.24	38.72

Table B.3 Restrained strain (ε_{res}) due to thermal expansion of different nodes on the wall at location A

Curve	**A**
X :	Time
Y :	Restrained Strain

X (Hours)	Y (micron)	X (Hours)	Y (micron)	X (Hours)	Y (micron)
0.00	0.00	114.00	45.87	228.00	11.72
3.00	21.77	117.00	44.50	231.00	11.18
6.00	47.74	120.00	43.18	234.00	10.68
9.00	67.28	123.00	41.89	237.00	10.20
12.00	80.96	126.00	40.64	240.00	9.75
15.00	89.62	129.00	39.43	243.00	9.33
18.00	94.68	132.00	38.25	246.00	8.93
21.00	97.29	135.00	37.10	249.00	8.56
24.00	98.25	138.00	35.99	252.00	8.20
27.00	98.18	141.00	34.90	255.00	7.86
30.00	97.41	144.00	33.85	258.00	7.55
33.00	96.18	147.00	32.82	261.00	7.25
36.00	94.61	150.00	31.83	264.00	6.97
39.00	92.81	153.00	30.86	267.00	6.71
42.00	90.86	156.00	29.92	270.00	6.46
45.00	88.81	159.00	29.01	273.00	6.22
48.00	86.69	162.00	28.13	276.00	6.00
51.00	84.54	165.00	27.27	279.00	5.78
54.00	82.38	168.00	26.44	282.00	5.58
57.00	80.22	171.00	30.82	285.00	5.39
60.00	78.07	174.00	30.27	288.00	5.21
63.00	75.95	177.00	28.81	291.00	5.04
66.00	73.85	180.00	27.25	294.00	4.87
69.00	71.78	183.00	25.75	297.00	4.72
72.00	69.74	186.00	24.34	300.00	4.57
75.00	67.73	189.00	23.01	303.00	4.43
78.00	65.77	192.00	21.77	306.00	4.30
81.00	63.86	195.00	20.61	309.00	4.17
84.00	62.00	198.00	19.52	312.00	4.05
87.00	60.18	201.00	18.50	315.00	3.93
90.00	58.40	204.00	17.54	318.00	3.82

93.00	56.67	207.00	16.64	321.00	3.72
96.00	54.99	210.00	15.79	324.00	3.62
99.00	53.35	213.00	15.00	327.00	3.52
102.00	51.76	216.00	14.25	330.00	3.43
105.00	50.22	219.00	13.56	333.00	3.34
108.00	48.72	222.00	12.91	336.00	3.26
111.00	47.27	225.00	12.30		

Table B.4 Restrained strain (ε_{res}) due to thermal expansion of different nodes on the wall at location B

Curve	**B**
X :	Time
Y :	Restrained Strain

X (Hours)	Y (micron)	X (Hours)	Y (micron)	X (Hours)	Y (micron)
0.00	0.00	114.00	-26.65	228.00	-8.92
3.00	-5.23	117.00	-25.94	231.00	-8.52
6.00	-13.11	120.00	-25.25	234.00	-8.13
9.00	-20.91	123.00	-24.57	237.00	-7.77
12.00	-27.84	126.00	-23.91	240.00	-7.42
15.00	-33.50	129.00	-23.26	243.00	-7.10
18.00	-37.86	132.00	-22.63	246.00	-6.79
21.00	-41.07	135.00	-22.01	249.00	-6.50
24.00	-43.32	138.00	-21.41	252.00	-6.22
27.00	-44.82	141.00	-20.82	255.00	-5.96
30.00	-45.72	144.00	-20.24	258.00	-5.71
33.00	-46.18	147.00	-19.68	261.00	-5.48
36.00	-46.30	150.00	-19.13	264.00	-5.25
39.00	-46.15	153.00	-18.59	267.00	-5.04
42.00	-45.80	156.00	-18.07	270.00	-4.84
45.00	-45.30	159.00	-17.56	273.00	-4.66
48.00	-44.69	162.00	-17.06	276.00	-4.48
51.00	-44.00	165.00	-16.57	279.00	-4.31
54.00	-43.25	168.00	-16.10	282.00	-4.15
57.00	-42.45	171.00	-18.09	285.00	-4.00
60.00	-41.62	174.00	-18.71	288.00	-3.85
63.00	-40.76	177.00	-18.74	291.00	-3.71
66.00	-39.89	180.00	-18.44	294.00	-3.58
69.00	-39.01	183.00	-17.93	297.00	-3.46
72.00	-38.13	186.00	-17.30	300.00	-3.34
75.00	-37.24	189.00	-16.61	303.00	-3.23
78.00	-36.36	192.00	-15.89	306.00	-3.12
81.00	-35.48	195.00	-15.18	309.00	-3.02
84.00	-34.61	198.00	-14.47	312.00	-2.92
87.00	-33.75	201.00	-13.79	315.00	-2.83
90.00	-32.91	204.00	-13.14	318.00	-2.75

93.00	-32.07	207.00	-12.51	321.00	-2.66
96.00	-31.25	210.00	-11.91	324.00	-2.58
99.00	-30.45	213.00	-11.34	327.00	-2.51
102.00	-29.65	216.00	-10.80	330.00	-2.43
105.00	-28.88	219.00	-10.29	333.00	-2.36
108.00	-28.12	222.00	-9.81	336.00	-2.30
111.00	-27.38	225.00	-9.35		

Table B.5 Restrained strain (ε_{res}) due to thermal expansion of different nodes on the wall at location C

Curve	**C**
X :	Time
Y :	Restrained Strain

X (Hours)	Y (micron)	X (Hours)	Y (micron)	X (Hours)	Y (micron)
0.00	0.00	114.00	-2.59	228.00	-0.13
3.00	3.52	117.00	-2.48	231.00	-0.12
6.00	5.81	120.00	-2.38	234.00	-0.11
9.00	5.71	123.00	-2.28	237.00	-0.10
12.00	4.45	126.00	-2.18	240.00	-0.09
15.00	2.70	129.00	-2.09	243.00	-0.08
18.00	0.94	132.00	-2.00	246.00	-0.07
21.00	-0.63	135.00	-1.92	249.00	-0.07
24.00	-1.93	138.00	-1.84	252.00	-0.06
27.00	-2.96	141.00	-1.77	255.00	-0.05
30.00	-3.75	144.00	-1.70	258.00	-0.05
33.00	-4.34	147.00	-1.63	261.00	-0.05
36.00	-4.77	150.00	-1.56	264.00	-0.04
39.00	-5.07	153.00	-1.50	267.00	-0.04
42.00	-5.26	156.00	-1.44	270.00	-0.03
45.00	-5.38	159.00	-1.38	273.00	-0.03
48.00	-5.42	162.00	-1.33	276.00	-0.03
51.00	-5.41	165.00	-1.28	279.00	-0.03
54.00	-5.36	168.00	-1.23	282.00	-0.02
57.00	-5.28	171.00	-0.39	285.00	-0.02
60.00	-5.17	174.00	-0.38	288.00	-0.02
63.00	-5.04	177.00	-0.43	291.00	-0.02
66.00	-4.91	180.00	-0.45	294.00	-0.02
69.00	-4.76	183.00	-0.45	297.00	-0.02
72.00	-4.61	186.00	-0.44	300.00	-0.01
75.00	-4.45	189.00	-0.42	303.00	-0.01
78.00	-4.29	192.00	-0.39	306.00	-0.01
81.00	-4.13	195.00	-0.36	309.00	-0.01
84.00	-3.97	198.00	-0.33	312.00	-0.01
87.00	-3.81	201.00	-0.31	315.00	-0.01
90.00	-3.66	204.00	-0.28	318.00	-0.01

93.00	-3.51	207.00	-0.26	321.00	-0.01
96.00	-3.37	210.00	-0.24	324.00	-0.01
99.00	-3.23	213.00	-0.21	327.00	-0.01
102.00	-3.09	216.00	-0.19	330.00	-0.01
105.00	-2.96	219.00	-0.18	333.00	-0.01
108.00	-2.83	222.00	-0.16	336.00	-0.01
111.00	-2.71	225.00	-0.14		